C

CENTRAL RESEARCH LIBRARY
DOCUMENT COLLECTION

MARTIN MARIETTA ENERGY SYSTEMS LIBRARIES
3 4456 0350624 9

ORNL-2501 cy. 6
Physics and Mathematics
TID-4500 (13th ed. rev.)
February 15, 1958

# PHYSICS DIVISION
# SEMIANNUAL PROGRESS REPORT
# FOR PERIOD ENDING MARCH 10, 1958

**OAK RIDGE NATIONAL LABORATORY**
operated by
UNION CARBIDE CORPORATION
for the
U.S. ATOMIC ENERGY COMMISSION

CENTRAL RESEARCH LIBRARY
DOCUMENT COLLECTION
LIBRARY LOAN COPY
DO NOT TRANSFER TO ANOTHER PERSON
If you wish someone else to see this document, send in name with document and the library will arrange a loan.

Printed in USA. Price $2.25 cents. Available from the

Office of Technical Services
U. S. Department of Commerce
Washington 25, D. C.

LEGAL NOTICE

This report was prepared as an account of Government sponsored work. Neither the United States, nor the Commission, nor any person acting on behalf of the Commission:

A. Makes any warranty or representation, express or implied, with respect to the accuracy, completeness, or usefulness of the information contained in this report, or that the use of any information, apparatus, method, or process disclosed in this report may not infringe privately owned rights; or

B. Assumes any liabilities with respect to the use of, or for damages resulting from the use of any information, apparatus, method, or process disclosed in this report.

As used in the above, "person acting on behalf of the Commission" includes any employee or contractor of the Commission to the extent that such employee or contractor prepares, handles or distributes, or provides access to, any information pursuant to his employment or contract with the Commission.

ORNL-2501
Physics and Mathematics
TID-4500 (13th ed. rev.)
February 15, 1958

Contract No. W-7405-eng-26

# PHYSICS DIVISION
# SEMIANNUAL PROGRESS REPORT
## for Period Ending March 10, 1958

J. L. Fowler, Director
E. O. Wollan, Associate Director

DATE ISSUED

MAY 20 1958

OAK RIDGE NATIONAL LABORATORY
Oak Ridge, Tennessee
operated by
UNION CARBIDE CORPORATION
for the
U.S. ATOMIC ENERGY COMMISSION

MARTIN MARIETTA ENERGY SYSTEMS LIBRARIES

3 4456 0350624 9

## TABLE OF CONTENTS AND SUMMARY

*SPHERICAL MOMENTUM SPACE*

T. A. Welton ..... 1

A new formalism is described in some detail which allows the consistent introduction into relativistic quantum theory of a cutoff momentum without use of on arbitrary form factor.

*EFFECT OF ENVIRONMENTAL NUCLEI IN ELECTRON SPIN RESONANCE SPECTROSCOPY*

G. T. Trammell, H. Zeldes, and R. Livingston ..... 12

Occasionally an electron paramagnetic absorption line is accompanied by a satellite with a spacing which indicates the spin flip of a neighboring nucleus concurrent with that of the electron. Theoretical formulas covering this situation are developed and applied in this paper.

*COULOMB EXCITATION OF THE SECOND $2^+$ STATE IN W, Os, AND Pt NUCLEI*

P. H. Stelson and F. K. McGowan ..... 14

Information on the gamma-ray decay characteristics is obtained for the second $2^+$ states of W, Os, and Pt nuclei.

*TOTAL CROSS SECTIONS OF $C^{12}$ AND $C^{13}$ FOR FAST NEUTRONS*

H. B. Willard, J. K. Bair, and H. O. Cohn ..... 18

The total neutron cross section of $C^{12}$ has been remeasured with 5-kev energy resolution from 2.62 to 2.91 Mev. No resonances were observed. Measurements of the total cross section of $C^{13}$ were made between 0.2 and 4 Mev. Resonances were observed at 1.75, 2.43, and 2.45 Mev.

*RESONANCES IN THE TOTAL CROSS SECTION OF NEON*

H. O. Cohn and J. L. Fowler ..... 20

The total neutron cross section of neon in a gaseous form has been measured in the range 0.75 to 1.9 Mev. These data, together with previous differential measurements, allow parity and spin assignments for six resonance levels in $Ne^{21}$.

*CROSS SECTION AS A FUNCTION OF ENERGY FOR THE REACTION $S^{32}(n,\alpha)Si^{29}$*

H. W. Schmitt ..... 22

The $S^{32}(n,\alpha)Si^{29}$ cross section has been measured relative to the fission cross section of $U^{238}$ as a function of incident neutron energy in the range $1.3 < E_n < 3.8$ Mev. Results are given for $\sigma_{n,\alpha}/\sigma_f$ and for $\sigma_{n,\alpha}$ in this energy range.

*PULSED VAN DE GRAAFF AND FAST TIME-OF-FLIGHT STUDIES*

W. M. Good, J. H. Neiler, and J. H. Gibbons ..... 24

Total neutron cross sections of several separated isotopes have been measured in the kev energy range with a measured energy resolution of about 3%. Technical developments by which the anticipated resolution was achieved are discussed. The results on $Cu^{65}$ and $Fe^{57}$ are given as examples of the data being obtained and interpreted.

*FAST-CHOPPER TOTAL AND SCATTERING NEUTRON CROSS-SECTION MEASUREMENTS*

G. G. Slaughter, R. C. Block, and J. A. Harvey ..... 26

Total and scattering neutron cross sections of several elements have been measured with the new high-intensity time-of-flight spectrometer installed at the LITR. Parameters of resonances up to 300 ev are given for iodine and gold. The spin states of several resonances in $W^{183}$ and silver have been determined from scattering and total cross-section measurements.

*CROSS SECTIONS FOR (p,n) REACTIONS IN CADMIUM AND TELLURIUM ISOTOPES*

C. H. Johnson, A. Galonsky, and C. N. Inskeep ..... 29

Cross sections for $(p,n)$ reactions in cadmium and tellurium isotopes were measured from about 2.5 Mev to about 5.5 Mev. Over most of the energy range the cross sections of the isotopes of one element are in constant ratios, and the cross sections increase with mass number. The $Cd^{112}$ threshold was found to be 3.44 $\pm$ 0.02 Mev.

*ABSOLUTE (p,n) AND $(\alpha,n)$ CROSS SECTIONS FOR LIGHT NUCLEI*

R. L. Macklin and J. H. Gibbons ..... 33

Absolute cross sections have been measured for several $(p,n)$ and $(\alpha,n)$ reactions. Some further points of agreement with inverse reactions via the reciprocity relation are demonstrated. The absolute calibration of the flat-response neutron detector used agrees well with the NBS standard Ra-Be source.

*NEUTRON DIFFRACTION STUDY OF THE MAGNETIC PROPERTIES OF $MnI_2$*

J. W. Cable, M. K. Wilkinson, E. O. Wollan, and W. C. Koehler ..... 34

A neutron diffraction investigation of $MnI_2$ by using both powdered and single-crystal samples has been made. The results indicate that $MnI_2$ is antiferromagnetic, with a Néel temperature of 3.40°K. Structure domains are shown to exist in the single crystal, but the complex magnetic structure has not yet been determined.

*NEUTRON DIFFRACTION INVESTIGATIONS OF $MnCl_2$ IN EXTERNAL MAGNETIC FIELDS*

M. K. Wilkinson, J. W. Cable, E. O. Wollan, and W. C. Koehler ..... 37

The effects of an external magnetic field on the antiferromagnetic domain patterns and the transition temperatures associated with the two antiferromagnetic structures of $MnCl_2$ are described.

*NEUTRON DIFFRACTION OBSERVATIONS ON METALLIC CERIUM AND METALLIC NEODYMIUM*

W. C. Koehler, E. O. Wollan, H. R. Child, and M. K. Wilkinson ..... 40

Preliminary investigations concerning the low-temperature magnetic properties of metallic cerium and metallic neodymium are reported.

*SINGLE-CRYSTAL NEUTRON DIFFRACTION INVESTIGATIONS OF $CoCl_2$ AND $FeCl_2$*

M. K. Wilkinson, J. W. Cable, E. O. Wollan, and W. C. Koehler ..... 42

The size and orientation of the atomic magnetic moments existing in the antiferromagnetic structures of $FeCl_2$ and $CoCl_2$ have been determined from experiments on single crystals. The effects of an external magnetic field on these antiferromagnetic structures are described.

*ANTIFERROMAGNETIC PROPERTIES OF MANGANOUS TRIFLUORIDE*

E. O. Wollan, H. R. Child, W. C. Koehler, and M. K. Wilkinson ..... 48

The antiferromagnetic structure of $MnF_3$ has been determined and was found to be similar to that in $LaMnO_3$. The magnetic coupling properties are briefly discussed.

*INVESTIGATIONS ON THE ENERGY LEVELS OF THE CONFIGURATION $6p^2$ IN Hg I*

G. W. Charles ..... 49

Two lines have been found in the spectrum of a high-current arc in mercury which fit the transitions $6s6p\ {}^1P^\circ_1-6p^2\ {}^3P_0$ and $6s6p\ {}^1P^\circ_1-6p^2\ {}^3P_1$, confirming the assignments of the levels $6p^2\ {}^3P_{0,1}$ by Garton and Rajaratnam. Predictions of the position of the level $6p^2\ {}^3P_2$ have been made by extrapolation from Zn I and Cd I. The transition $6s6p\ {}^1P^\circ_1-6p^2\ {}^3P_2$ could not be definitely established.

*INFRARED SPECTRA OF THE DEUTERATED PHOSPHINE MOLECULES*

H. W. Morgan, P. A. Staats, and J. H. Goldstein ..... 51

The multiple-cell compensation technique developed for recording the infrared spectra of the isotopic ammonia molecules has been applied to the phosphine molecules $PH_2D$, $PHD_2$, and $PD_3$. The observed frequencies have been assigned to the normal modes of vibration. Calculated frequencies, based on a simple valence force field, agree satisfactorily with experimental values.

*COMPILATION OF DATA ON SOME SPECTRA OF THORIUM*

G. W. Charles ..... 58

A compilation has been made of available data on the spectra of Th IV, Th III, Th II, and Th I, including energy levels and classified lines with Zeeman effects and isotope shifts, as well as certain data on unclassified lines. The present status of knowledge of these spectra is discussed.

*THE ROLE OF SPECTROSCOPY IN THERMONUCLEAR RESEARCH*

J. R. McNally, Jr. ..... 55

The role of spectroscopy in thermonuclear research is reviewed briefly. The various techniques of observation and interpretation of spectra and some of the limitations are illustrated by appropriate tables and figures. The spectroscopist has available a unique, multipurpose, and yet unperturbing probe which can contribute significantly to the interpretation of the pressing problem besetting the thermonuclear scientists.

*ZEEMAN DATA REDUCTION. PART I*

K. L. Vander Sluis ..... 67

Previously reported preliminary experimental results have shown the feasibility of using Zeeman information quantitatively in the classification of atomic spectra. Oracle codes which make this approach practical as well as conceptually feasible have been written.

*SPHERICAL ELECTROSTATIC SPIN ROTATOR FOR ELECTRON POLARIZATION MEASUREMENTS*

H. B. Willard, A. Galonsky, H. O. Cohn, and N. H. Lazar ..... 68

A spherical electrostatic spin rotator is being used to study the polarization of electrons in beta decay. The spin rotator converts the polarization from longitudinal to transverse and allows the polarization to be determined from the degrees of asymmetry in the scattering of the transverse electrons from gold.

*BROAD-AREA GERMANIUM* p-n *JUNCTION COUNTERS*

J. W. T. Dabbs, F. J. Walter, and L. D. Roberts ..... 73

A germanium *p-n* surface barrier counter has been developed which is suitable for alpha-particle and fission-fragment counting between 1 and 77°K.

*SOME EVALUATIONS OF A NEW HIGH-INTENSITY ION SOURCE*

C. D. Moak, R. F. King, J. W. Johnson, and H. E. Banta ..... 75

The Duo-Plasmatron, a new ion source developed in Germany, is discussed. High gas efficiency and high ion current density are realized.

*CHARGE SPECTROMETRY*

A. H. Snell and F. Pleasonton ..... 77

Revisions have been made in the apparatus to increase the efficiency of collection for ions of low $e/m$, to improve the resolution, and to enable the detection of negative ions.

# PHYSICS DIVISION SEMIANNUAL PROGRESS REPORT

## SPHERICAL MOMENTUM SPACE

T. A. Welton

Several independent lines of evidence indicate the desirability of modifying the elementary fermion-boson interactions for large boson momenta. For example, the small Coulomb mass corrections for different $I$-spin states of the same elementary particle, as well as the short-range repulsive core in the nucleon-nucleon force, point in this direction. Up to the present, attempts to introduce modifications of the relativistic field theories for small distances and high momentum transfer have had a hopelessly phenomenological appearance, because of the necessary introduction of an arbitrary function to play the role of the spatial distribution of the source of the interaction. However, one possibility for avoiding the use of such an arbitrary function was suggested by Snyder[1] a number of years ago. In essence, Snyder proposed that a pseudospherical energy-momentum space be used instead of the Galilean (flat, with indefinite metric), which is customary. The "radius" of the sphere then sets an approximate limit to the momentum transfers, which yield reasonably conventional results. The four coordinates were introduced as noncommuting operators having the structure of angular-momentum operators, with the 5-axis singled out for special treatment. This noncommutability of the coordinate operators gave rise to an obvious limitation, analogous to the usual uncertainty principle for action, in the simultaneous measurement of two coordinates. In spite of these limitations, the general isotropy and homogeneity of space-time were retained, so that the elements of an elegant theory seemed to be present. On further study, however, Snyder[2] (and others) found that it was impossible to fit this operator concept of the coordinates into the existing structure of quantized field theory, where the coordinates played only the role of integration variables. The present work began when the author noticed that his previously reported[3] relativistic quantum theory without quantized fields appeared to be ideal for the consistent introduction of Snyder's idea. Certain modifications were necessary (or seemed desirable), but the basic ideas are quite recognizable.

Consider a five-dimensional Cartesian space with five rectangular coordinates: $z_1$, $z_2$, $z_3$, $z_4$, and $z_5$. Greek indices are assumed to range over 1, 2, 3, and 4, and the summation convention will be in force. No distinction is needed between covariant and contravariant quantities. Let $\kappa$ be a new natural constant with the dimensions of a reciprocal length (the customary units with $\hbar = c = 1$ will be used). The four-momentum operator for a particle will be taken as

$$p_\mu = \kappa z_\mu \ , \tag{1}$$

where the $z_\mu$ are restricted to lie on the surface of the unit hypersphere defined by

$$z_\mu z_\mu + z_5^2 \equiv z \cdot z = 1 \ . \tag{2}$$

---

[1] H. S. Snyder, *Phys. Rev.* **71**, 38 (1947).

[2] H. S. Snyder, *Phys. Rev.* **72**, 68 (1947).

[3] T. A. Welton, *Phys. Semiann. Prog. Rep. Sept. 10, 1955*, ORNL-1975, p 1.

The four coordinate operators for the particle will be taken as

(3) $$x_\mu = \frac{i}{\kappa}\left(z_5 \frac{\partial}{\partial z_\mu} - z_\mu \frac{\partial}{\partial z_5}\right) ,$$

so that the following commutation rules hold:

(4) $$\left[p_\mu, p_\nu\right] = 0 ,$$

(5) $$\left[x_\mu, p_\nu\right] = i z_5 \delta_{\mu\nu} ,$$

(6) $$\left[x_\mu, x_\nu\right] = \frac{1}{\kappa^2}\left(z_\mu \frac{\partial}{\partial z_\nu} - z_\nu \frac{\partial}{\partial z_\mu}\right) .$$

The commutation rule (Eq. 4) between momentum components allows simultaneous diagonalization of all four momentum components. Thus the momentum representation here, often used for convenience in the ordinary theory, will play a truly central role. If $z_5 \cong 1$, relation 5 reduces to the conventional commutation relation of quantum mechanics. It is relation 6 which most clearly marks the distinction between the new theory and the conventional approach. In general, $x_\mu$ and $x_\nu$ cannot be simultaneously exactly specified, unless the $\mu\nu$ component of angular momentum happens to vanish. Clearly, $1/\kappa$ is playing the role of a fundamental length.

The new theory has an obvious limit in the conventional theory. This "conventional limit" is characterized by momenta that are small compared with $\kappa$ and large compared with $1/\kappa$. In this limit, $z_5$ will be close to unity, and the curvature of the momentum space will not be apparent because only that part of the sphere will be in use which is close to the $z_5$ axis (the "north polar region").

A word is necessary as to the use of the definite metric. The energy-momentum space has an indefinite metric, and so must be related to the above, if at all, by a suitable analytic continuation to the imaginary axis of the $p_4$ variable. This continuation can be most conveniently deferred until the end of any computation, as will be seen. Such a procedure is justified only by its results, although this continuation is closely related to that which is ordinarily assumed possible, in consequence of the causal character of the conventional theory.

The simplest problems to discuss are those in which a fermion moves in a slowly varying field. The wave equation is

(7) $$i\dot{\psi} = \gamma p \psi + \epsilon \gamma A \psi ,$$

where

(8) $$\dot{\psi} \equiv \frac{\partial \psi}{\partial \tau} ,$$

(9) $$\gamma p \equiv \gamma_\mu p_\mu , \quad \gamma A \equiv \gamma_\mu A_\mu , \quad A_\mu = A_\mu(x) ,$$

(10) $$\gamma_\mu \gamma_\nu + \gamma_\nu \gamma_\mu = 2\delta_{\mu\nu} .$$

The variable $\tau$ is a fifth independent variable, related (as will be seen) to the proper-time parameter of conventional relativistic kinematics. Consider the kinematics of a wave packet as described by Eq. 7.

A second-order wave equation, with neglect of spin forces, is easily derived:

(11) $$-\ddot{\psi} = (p + \epsilon A)^2 \psi \ .$$

It is convenient to consider only solutions which are approximate eigenfunctions of $i(\partial/\partial\tau)$. Thus

(12) $$i\dot{\psi} \cong n\psi \ ,$$

where $n$ will be seen to be related to the rest mass of the particle; the "nearly equal" sign in Eq. 12 is required in order to form a packet localized in $\tau$.

From Eq. 11 it is seen reasonable to interpret

(13) $$\frac{1}{2in} \left\{\dot{\psi}^* \psi - \psi^* \dot{\psi}\right\}$$

as a "probability of presence" per unit volume, with an integral which is constant in $\tau$ and which can be taken to be unity. This integral, under condition 12, will further be very nearly equal to that of

(14) $$\psi^* \psi \ ,$$

so that this quantity can be used as the weighting function in any average over the packet.

The rate of change with $\tau$ of the mean $x_\mu$ and $p_\mu$ for the packet can now be easily calculated, with the following definitions:

(15) $$\left\langle x_\mu \right\rangle = \frac{1}{2in} \left\{(\dot{\psi}^* x_\mu \psi) - (\psi^* x_\mu \dot{\psi})\right\} \ ,$$

(16) $$\left\langle p_\mu \right\rangle = \frac{1}{2in} \left\{(\dot{\psi}^* p_\mu \psi) - (\psi^* p_\mu \dot{\psi})\right\} \ ,$$

(17) $$(\psi^* \psi) \equiv \int dx \ \psi^* \psi = 1 \ .$$

By differentiation with respect to $\tau$, and substitution from Eqs. 11, 15, and 16, the above can be rewritten as

(18) $$\left\langle \dot{x}_\mu \right\rangle = \frac{1}{2in} \left\{(\ddot{\psi}^* x_\mu \psi) - (\psi^* x_\mu \ddot{\psi})\right\}$$

$$= \frac{1}{2in} \left(\psi^* \left[x_\mu, (p + \epsilon A)^2\right] \psi\right) \ ,$$

(19) $$\left\langle \dot{p}_\mu \right\rangle = \frac{1}{2in} \left(\psi^* \left[p_\mu, (p + \epsilon A)^2\right] \psi\right) \ .$$

If $A$ is assumed to be a very slowly varying function of $x$, so that $1/\kappa$ can be neglected, the commutation relations 4 and 5 yield

(20) $$\left\langle \dot{x}_\mu \right\rangle = \frac{1}{n} \left\langle z_5 (p_\mu + \epsilon A_\mu) \right\rangle \ ,$$

(21) $$\left\langle \dot{p}_\mu \right\rangle = -\frac{\epsilon}{n} \left\langle z_5 \frac{\partial A_\nu}{\partial x_\mu} (p_\nu + \epsilon A_\nu) \right\rangle \quad .$$

For such a packet, $z_5$ will have a definite value, and fluctuations can be ignored. Thus an average of a product will be a product of the averages. By dropping the angular brackets, a pair of equations is obtained for the motion of the center of the packet:

(22) $$\dot{x}_n = \frac{1}{n} (p_\mu + \epsilon A_\mu) z_5 \quad , .$$

(23) $$\dot{p}_n = -\frac{\epsilon}{n} (p_\nu + \epsilon A_\nu) \frac{\partial A_\nu}{\partial x_\mu} z_5 \quad .$$

If the following substitutions are imagined,

(24) $$\begin{cases} iz_5 \, d\tau \to ds \quad , \\ in \to m \quad , \\ \epsilon \to e \quad , \\ ip_4 \to p_0 \quad , \\ ix_4 \to x_0 \quad , \end{cases}$$

the equations become formally equivalent to the conventional equations of motion in classical relativistic mechanics:

(25) $$\frac{dp_\mu}{ds} = -\frac{e}{m} (p_\nu + eA_\nu) \frac{\partial A_\nu}{\partial x_\mu} \quad ,$$

(26) $$\frac{dx_\mu}{ds} = \frac{1}{m} (p_\mu + eA_\mu) \quad .$$

As a consequence of Eq. 26,

(27) $$\frac{dx_\mu}{ds} \frac{dx_\mu}{ds} = \frac{(p + eA)^2}{m^2} = 1 \quad ,$$

which makes explicit the role of $s$ as proper time. By combining Eqs. 25 and 26, a second-order equation for $x_\mu$ is obtained:

(28) $$m \frac{d^2 x_\mu}{ds^2} = e \frac{dx_\nu}{ds} \left( \frac{\partial A_\mu}{\partial x_\nu} - \frac{\partial A_\nu}{\partial x_\mu} \right) \quad ,$$

which is more easily recognized as the Lorentz equation of motion in relativistic notation.

It has thus been shown that the classical motion of a particle in a slowly varying electromagnetic field, according to the new theory, will be identical with the conventional motion, even when $z_5$ is not equal to unity. Therefore no purely classical experiment will show any effect of the new constant, $\kappa$.

It is only in rapidly varying fields that $\kappa$-dependent effects will be expected to arise. In order to study such effects, the foregoing formalism must be considerably extended. A beginning can be made by using Eq. 7, with $A$ taken to be a specified force field. If $\kappa \to \infty$, a convenient form for $A_\mu$ is

$$A_\mu = \frac{1}{\sqrt{4\pi^3}} \int \frac{dk}{|k|} \mathcal{A}_\mu(k)\, e^{ikx} \quad , \tag{29}$$

with

$$\int_{-\infty} dk \equiv \int_{-\infty}^{\infty} dk_1 \int_{-\infty}^{\infty} dk_2 \int_{-\infty}^{\infty} dk_3 \int_{-\infty}^{\infty} dk_4 \quad , \tag{30}$$

$$|k| \equiv (k_1^2 + k_2^2 + k_3^2 + k_4^2)^{1/2} \quad , \tag{31}$$

$$kx \equiv k_1 x_1 + k_2 x_2 + k_3 x_3 + k_4 x_4 \quad . \tag{32}$$

The modification required for finite $\kappa$ consists of a redefinition of the domain of integration, a reinterpretation of the meaning of the exponential phase factor, and a change in form (for later convenience) of the normalizing factors. It is necessary to introduce a momentum sphere to replace the Cartesian $k$ space, and it is convenient to introduce polar variables for integration over the momentum space. Thus

$$\begin{aligned} k_1 &= \kappa \sin \alpha_k \sin \beta_k \sin \gamma_k \cos \delta_k \quad , \\ k_2 &= \kappa \sin \alpha_k \sin \beta_k \sin \gamma_k \sin \delta_k \quad , \\ k_3 &= \kappa \sin \alpha_k \sin \beta_k \cos \gamma_k \quad , \\ k_4 &= \kappa \sin \alpha_k \cos \beta_k \quad , \end{aligned} \tag{33}$$

$$dk_1\, dk_2\, dk_3\, dk_4 \to \kappa^4 \sin^3 \alpha_k \sin^2 \beta_k \sin \gamma_k\, d\alpha_k\, d\beta_k\, d\gamma_k\, d\delta_k = \kappa^4\, d\omega_k \quad , \tag{34}$$

$$|k| \to \kappa \sin \alpha_k \quad . \tag{35}$$

The vector potential can then be rewritten as

$$A_\mu = \frac{\kappa^3}{\sqrt{4\pi^3}} \int \frac{d\omega_k}{\sin \alpha_k} \mathcal{A}_\mu(\omega_k)\, e^{ikx} \quad . \tag{36}$$

If calculations are to be performed, the meaning of $e^{ikx}$ must be clarified. If the conventional flat momentum space is used, $e^{ikx}$ plays the role of a finite translation operator in the momentum space. Thus

$$pe^{ikx} = e^{ikx}(p + k) \quad ,$$

or

(37) $$e^{-ikx}\, pe^{ikx} = p + k \quad .$$

On the momentum sphere, $e^{ikx}$ will play the role of a *rotation* operator. This can be seen by noting that, from their definition (Eq. 3), the $x_\mu$ are proportional to the generating functions for four of the infinitesimal rotations. Thus

(38) $$x_\mu = \frac{1}{\kappa} L_{\mu 5} \quad ,$$

where the $L_{\mu 5}$ are four of the ten components of angular momentum about the origin of the $z$ space. If $\alpha_k \ll 1$, the four quantities, $k_\mu/\kappa$, will play the role of four small angles of rotation, and the exponential $e^{ikx}$ will correspondingly represent a special type of rotation through angle $\alpha_k$. If the angle $\alpha_k$ is not infinitesimal, the result must be obtained by compounding infinitesimal rotations, and is clearly defined even though it is less simple to write down. Note that successive rotations will not, in general, commute. This is in sharp contrast to the conventional theory obtained for $\kappa \to \infty$.

It is essential in practical computations to have a convenient method for compounding momentum vectors, analogous to the vector addition which suffices in the conventional theory. If a fermion momentum, with components $p_\mu$ , is augmented by definition of a fifth component,

(39) $$p_5 = \sqrt{\kappa^2 - p^2} \quad ,$$

the five-component quantity will be represented by $(p)$. If a boson momentum $k$ is compounded with this according to the above, the result will be written as $(p + k)$ and is related to $(p)$ by

(40) $$(p + k) = (e^{-ikx}\, pe^{ikx}) \quad .$$

On the other hand, the five components of $(p + k)$ must be some linear combinations of the components of $(p)$. Such a matrix representation of the rotation (the simplest, nontrivial, irreducible representation) can be written as

(41) $$(p + k) = R(k)\cdot(p) \quad ,$$

where the dot signifies a five-dimensional inner product on one repeated index.

The $5 \times 5$ matrix $R(k)$ has some simple properties. It is real and unitary, and therefore orthogonal. The natural definition of $(p - k)$ is

(42) $$(p - k) = R(-k)\cdot(p) = R^{-1}(k)\cdot(p) \quad ,$$

where $R^{-1}(k)$ is just equal to $\tilde{R}(k)$, the transpose of $R(k)$.

The evaluation of the components of $R(k)$ in terms of the angles $\alpha$, $\beta$, $\gamma$, $\delta$ (subscripts omitted) is a moderately complicated algebraic job. A straightforward procedure was suggested by Gordon.[4] First, perform a rotation $T(\beta,\gamma,\delta)$ in the 1, 2, 3, 4 subspace in order to make the desired rotation involve only the 4,5 axes. Second, perform a rotation through angle $\alpha$ in the 4,5 subspace. Third, perform the rotation

[4]Private communication.

inverse to $T$ in order to restore the axes to the original orientation. Thus

$$R(\alpha,\beta,\gamma,\delta) = T^{-1}(\beta,\gamma,\delta)\cdot S(\alpha)\cdot T(\beta,\gamma,\delta) \quad . \tag{43}$$

The $T$ matrix is not completely determined, but a convenient choice is obtained by considering the unit vector in the radial direction, in the four-dimensional subspace:

$$\vec{j}_4 = \vec{i}_1 \sin\beta \sin\gamma \cos\delta + \vec{i}_2 \sin\beta \sin\gamma \sin\delta + \vec{i}_3 \sin\beta \cos\gamma + \vec{i}_4 \cos\beta \quad , \tag{44}$$

where $\vec{i}_1$, $\vec{i}_2$, $\vec{i}_3$, $\vec{i}_4$ are unit vectors along the 1, 2, 3, 4 axes. A set of three unit vectors can be formed which are orthogonal to each other and to $\vec{j}_4$ by successively differentiating $\vec{j}_4$ with respect to $\beta$, $\gamma$, and $\delta$. Thus

$$\left\{\begin{aligned} \vec{j}_3 &= \frac{\partial \vec{j}_4}{\partial\beta} = \vec{i}_1 \cos\beta \sin\gamma \cos\delta + \vec{i}_2 \cos\beta \sin\gamma \sin\delta + \vec{i}_3 \cos\beta \cos\gamma - \vec{i}_4 \sin\beta \quad , \\ \vec{j}_2 &= \frac{1}{\sin\beta}\frac{\partial \vec{j}_4}{\partial\gamma} = \vec{i}_1 \cos\gamma \cos\delta + \vec{i}_2 \cos\gamma \sin\delta - \vec{i}_3 \sin\gamma \quad , \\ \vec{j}_1 &= \frac{1}{\sin\beta \sin\gamma}\frac{\partial \vec{j}_4}{\partial\delta} = -\vec{i}_1 \sin\delta + \vec{i}_2 \cos\delta \quad . \end{aligned}\right. \tag{45}$$

The transformation from the $i$'s to the $j$'s is orthogonal and closely related to a possible $T$ matrix. In fact, if

$$\vec{j}_i = \sum_{j=1}^{4} T_{ij}\,\vec{i}_j \quad (j = 1, \ldots, 4) \quad , \tag{46}$$

then the full $T$ matrix can be formed simply by augmenting $T_{ij}$ with zeros in the 15, 25, 35, 45, 51, 52, 53, 54 positions and with unity in the 55 position. Thus $T$ will be taken to be

$$T(\beta,\gamma,\delta) = \begin{pmatrix} -\sin\delta & \cos\delta & 0 & 0 & 0 \\ \cos\gamma\cos\delta & \cos\gamma\sin\delta & -\sin\gamma & 0 & 0 \\ \cos\beta\sin\gamma\cos\delta & \cos\beta\sin\gamma\sin\delta & \cos\beta\cos\gamma & -\sin\beta & 0 \\ \sin\beta\sin\gamma\cos\delta & \sin\beta\sin\gamma\sin\delta & \sin\beta\cos\gamma & \cos\beta & 0 \\ 0 & 0 & 0 & 0 & 1 \end{pmatrix} , \tag{47}$$

and $T^{-1}$ can be found simply by interchanging rows and columns. Finally, $S(\alpha)$ is simply

$$S(\alpha) = \begin{pmatrix} 1 & 0 & 0 & 0 & 0 \\ 0 & 1 & 0 & 0 & 0 \\ 0 & 0 & 1 & 0 & 0 \\ 0 & 0 & 0 & \cos\alpha & -\sin\alpha \\ 0 & 0 & 0 & \sin\alpha & \cos\alpha \end{pmatrix} . \tag{48}$$

It is easily verified by some elementary tests that $R$, as given by Eqs. 43, 47, and 48, has indeed the correct properties for small $\alpha$, and the result may be assumed valid in general.

From the basic wave equation (7), and with the potential as given in Eq. 36, stationary states and scattering processes can now be calculated. Such calculations are not particularly enlightening at this stage, and it is more important to complete the setting up of the formalism. One important question is the description of the interaction of two particles for the elucidation of the momentum conservation law in this novel formalism.

Thus far, only the motion of a single particle in a given field has been contemplated. Interaction can be treated by writing separate, simultaneous equations of the form given in Eq. 7 for a wave function which depends on the $\tau$ and $p$ variables for each particle and which is properly antisymmetrized. Compound transition probabilities for concurrent changes of state for two or more particles are easily defined. From such compound probabilities arise the interactions of particles, if the $\mathfrak{A}_\mu(k)$ are taken not as completely specified quantities but as statistically determined coefficients only. Thus the $\mathfrak{A}_\mu$ have specified magnitudes, but (classically) random phases, with averages over these phases given by

$$\left\langle \mathfrak{A}_\mu(k) \right\rangle = 0 \ , \qquad \left\langle \mathfrak{A}_\mu(k)\, \mathfrak{A}_\nu(k') \right\rangle = \delta_{\mu\nu}\, \delta(k + k') \ , \tag{49}$$

and similarly for products with more factors. An odd number of factors yields zero phase average, while an even number of factors yields a sum of terms, each obtained by pairing factors in some way and using the second relation of Eq. 49. This procedure is known to work for $\kappa = \infty$ (ref 5). For finite $\kappa$, $k$ and $k'$ are to be replaced by the angular variables $\omega_k$ and $\omega_{k'}$. The $\delta$ function in Eq. 49 must be replaced by a corresponding $\delta$ function on the surface of the sphere. A suitable form is

$$\delta(k + k') \rightarrow \frac{1}{\kappa^4}\, \Delta(\omega_k, \omega_{k'}) \ , \tag{50}$$

where $\Delta(\omega_k, \omega_{k'}) = 0$, unless

$$k_5 k_5' - kk' = \kappa^2 \ , \tag{51}$$

which is a single point on the surface of the $k$ sphere, if $k'$ is given. The singularity of $\Delta$ is defined by

$$\int \Delta(\omega_k, \omega_{k'})\, d\omega_k = 1 \ . \tag{52}$$

Interaction of two particles takes place by "addition" of a boson momentum, $k$, to the momentum, $p$, of one fermion and the concomitant "subtraction" of $k$ from the other fermion momentum, $P$. Thus, under collision,

$$(p) \rightarrow (p + k) \ , \qquad (P) \rightarrow (P - k) \ , \tag{53}$$

where the parentheses and the addition and subtraction signs have the meaning previously defined.

[5] T. A. Welton, *Phys. Semiann. Prog. Rep. Sept. 10, 1955*, ORNL-1975, p 1.

It is quite clear that momentum in the ordinary sense is not conserved. Thus

$$(p + k)_\mu \neq (p)_\mu + k_\mu \quad , \tag{54}$$

except for $\kappa \to \infty$, and it is *not* to be expected that

$$(p)_\mu + (P)_\mu = (p + k)_\mu + (P - k)_\mu \quad . \tag{55}$$

This apparent violation of conventional momentum conservation is so much at variance with experience that some change in procedure is essential, if the new formalism is to be saved. Fortunately, a simple reinterpretation will suffice. If the definitions given in Eqs. 41 and 42 are used, in conjunction with Eqs. 43, 47, and 48, it is seen by a straightforward (but lengthy) calculation that

$$\frac{p_i}{\sqrt{1 - (n^2/\kappa^2)}} + \frac{P_i}{\sqrt{1 - (N^2/\kappa^2)}} = \frac{p_f}{\sqrt{1 - (n^2/\kappa^2)}} + \frac{P_f}{\sqrt{1 - (N^2/\kappa^2)}} \quad , \tag{56}$$

where $i$ and $f$ refer to initial and final values, respectively. The addition signs now have their conventional meaning, and $n$ and $N$ satisfy

$$\begin{aligned} n^2 &= p_i^2 = p_f^2 \quad , \\ N^2 &= P_i^2 = P_f^2 \quad . \end{aligned} \tag{57}$$

It therefore appears that a "pseudomomentum," associated with a given particle and defined by

$$p = \frac{p}{\sqrt{1 - (n^2/\kappa^2)}} = \frac{p}{\sqrt{1 - (p^2/\kappa^2)}} \quad , \tag{58}$$

has the *conservation* properties of conventional momentum. Unfortunately, the pseudomomentum is *not* the quantity which would be identified as momentum by conventional kinematical and dynamical measurements in electromagnetic fields, according to the development which culminated in Eqs. 25 and 26. This apparent contradiction with experience can be removed by a new set of identifications to replace Eq. 24:

$$\begin{aligned} & iz_5\, d\tau \to ds \quad , \quad \frac{in}{\sqrt{1 - (n^2/\kappa^2)}} \to m \quad , \quad \frac{\epsilon}{\sqrt{1 - (n^2/\kappa^2)}} \to e \quad , \quad \frac{ip_4}{\sqrt{1 - (n^2/\kappa^2)}} \to p_4 \quad , \\ & \frac{\vec{p}}{\sqrt{1 - (n^2/\kappa^2)}} \to \vec{p} \quad , \quad ix_4 \to x_0 \quad , \quad \vec{x} \to x \quad . \end{aligned} \tag{59}$$

It is easily verified that this set of identifications will yield completely consistent results, and goes over into the previous ones (which were only preliminary guesses) for $\kappa \to \infty$. It is of considerable interest that the coupling constant, $\epsilon$, must be different for particles of different mass, if their apparent electrical charge is to be the same. In this connection it is necessary to verify that the *strength* of the electromagnetic interaction between two particles will be properly given, since $\epsilon$ has appeared thus far only to describe the *response* of a particle to a given field. This point is easily checked by writing

down the two-particle wave equation.[6] Consider the two separate wave equations for two particles, with parameters for the particles designated by small and capital letters, respectively:

$$(60)\qquad \begin{aligned} (n - \gamma p)\ \psi &= \epsilon\gamma\ A(x)\ \psi\ , \\ (N - \Gamma P)\ \psi &= \mathrm{E}\Gamma\ A(X)\ \psi\ . \end{aligned}$$

The elementary two-particle wave equation (ladder approximation) is derived by first multiplying the operators:

$$(61)\qquad (n - \gamma p)\ (N - \Gamma P)\ \psi = \epsilon \mathrm{E}\gamma_\mu \Gamma_\nu\ A_\mu(x)\ A_\nu(X)\ \psi\ ,$$

which can be justified by a little manipulation. If $\psi$ is then imagined to be expanded in a series of powers of the $\mathfrak{A}_\mu(\omega_k)$, a phase average can be performed:

$$(62)\qquad (n - \gamma p)\ (N - \Gamma P) \left\langle \psi \right\rangle = \epsilon \mathrm{E}\gamma_\mu \Gamma_\nu\ \left\langle A_\mu(x)\ A_\nu(X)\ \psi \right\rangle\ .$$

The ladder approximation (quite adequate for discussion of the hydrogen atom) is obtained by neglecting on each side all terms except that term in $\psi$ which is independent of $\mathfrak{A}_\mu(\omega_k)$. Denoting this term by $\Psi$, Eq. 62 becomes

$$(63)\qquad (n - \gamma p)\ (N - \Gamma P)\ \Psi = \epsilon \mathrm{E}\gamma_\mu \Gamma_\nu\ \left\langle A_\mu(x)\ A_\nu(X) \right\rangle \Psi\ .$$

By use of Eqs. 36, 49, 50, 51, and 52, this becomes

$$(64)\qquad (n - \gamma p)\ (N - \Gamma P)\ \Psi = \frac{\epsilon \mathrm{E}\kappa^2}{4\pi^3} \int \frac{d\omega_k}{\sin^2 \alpha_k}\, e^{ikx}\, e^{-ikX}\, \gamma\Gamma\Psi\ .$$

Finally, under the substitutions defined by Eqs. 59, the equation becomes

$$(65)\qquad (im - \gamma p)\ (iM - \Gamma P)\ \Psi = \frac{e^2 \kappa^2}{4\pi^3} \int \frac{d\omega_k}{\sin^2 \alpha_k}\, e^{ikx}\, e^{-ikX}\, \gamma\Gamma\Psi\ ,$$

which has the form of the conventional two-body equation, aside from the modification of the "potential" according to the new formalism. In particular, the interaction involves the conventional $e^2$ (or $-e^2$ if the particles have opposite sign), so that if only values of $k^2$ are important for which $k^2/\kappa^2 \ll 1$ (as is presumably the case in the hydrogen atom), the "conventional" limit will be applicable, with

$$\frac{\kappa^2 d\omega_k}{\sin^2 \alpha_k} \rightarrow \frac{dk}{k^2}\ .$$

This will be valid except for changes in electron momentum which are no longer small compared with $\kappa$.

The formalism is now basically complete for all processes which do not involve closed loops. These are to be included by a convergent method, previously described, which makes use of similar mathematical machinery (no quantized fields, use of a 4-space with *definite* metric, and analytic continuation to obtain physical results). The introduction of a pion field, coupled only to nucleons, is an

---

[6] E. E. Salpeter and H. A. Bethe, *Phys. Rev.* 84, 1232 (1951).

obvious extension of the foregoing, while if the pions are also to be coupled to the electromagnetic field, the required modification has also been given.[7] It is anticipated that recent developments in the description of the coupling between pions, nucleons, and the strange particles can be incorporated without serious trouble, although this remains to be done.

As a simple illustration of the use of the new formalism, consider the calculation of the electron mass correction in the lowest order. From Eq. 7, by use of standard Schrödinger perturbation theory,

$$\delta n = \left(0\left|\left\langle \delta N \right\rangle\right|0\right) , \tag{66}$$

where the parentheses refer to an expectation value for the unperturbed state. The operator $\delta N$ is given by

$$\delta N = \epsilon \gamma A + \epsilon^2 \gamma A \frac{1}{n - \gamma p} \gamma A + 0(\epsilon^3) . \tag{67}$$

The phase average causes the first term to vanish and simplifies the second term:

$$\begin{aligned} \left\langle \delta N \right\rangle &= \frac{\epsilon^2 \kappa^6}{4\pi^3} \int \frac{d\omega_{k'}}{\sin \alpha_{k'}} \int \frac{d\omega_k}{\sin \alpha_k} \gamma_\mu e^{ik'x} \frac{1}{n - \gamma p} e^{ikx} \gamma_\nu \left\langle \mathcal{A}_\mu (\omega_{k'}) \mathcal{A}_\nu (\omega_k) \right\rangle \\ &= \frac{\epsilon^2 \kappa^2}{4\pi^3} \int \frac{d\omega_k}{\sin^2 \alpha_k} \gamma_\mu e^{-ikx} \frac{1}{n - \gamma p} e^{ikx} \gamma_\nu . \end{aligned} \tag{68}$$

By use of Eq. 40, the expression simplifies to

$$\left\langle \delta N \right\rangle = \frac{\epsilon^2 \kappa^2}{4\pi^3} \int \frac{d\omega_k}{\sin^2 \alpha_k} \gamma_\mu \frac{1}{n - \gamma(p + k)} \gamma_\nu , \tag{69}$$

where the expression differs from the conventional one only in the altered volume element (and domain of integration) and in the new definition of the quantity $(p + k)$ as $R(k)\cdot(p)$. For small $k^2$, the integrand has the familar form, but for $k^2 \gtrsim \kappa^2$, it is drastically modified. It is therefore clear that $\delta n$ will be simply related to the conventional expression, with $\kappa$ appearing as an explicit upper cutoff in momentum. The procedure of mass renormalization is therefore no longer essential, but remains a convenient computational tool. A number of elementary processes are observably modified by the new formalism, and it is hoped that a reasonable value will be found for $\kappa$ from experiment, and that the validity of the formalism will be proved or disproved.

---

[7] T. A. Welton, *Phys. Semiann. Prog. Rep. Sept. 10, 1955*, ORNL-1975, p 1.

# EFFECT OF ENVIRONMENTAL NUCLEI IN ELECTRON SPIN RESONANCE SPECTROSCOPY[1]

G. T. Trammell H. Zeldes[2] R. Livingston[2]

In an earlier report[3] by two of the authors, attention was called to extra satellite absorption lines that appear in the paramagnetic resonance spectrum for atomic hydrogen produced in various acids at low temperatures by irradiation with gamma rays. Each of the two atomic hydrogen hyperfine lines had a pair of satellites. The frequency spacing from satellite to main line was close to the appropriate proton magnetic resonance frequency for the applied fields of 3000 and 8000 gauss. The satellite-to-main-line intensity ratio varied approximately as the inverse square of the applied fields. These observations were interpreted as being the result of the occasional concurrent spin flip of the electron and a nearby proton caused by their magnetic coupling. On the basis of this interpretation it was possible to compute an effective distance from the atomic hydrogen to its neighboring proton(s) from the observed intensity ratios, and a preliminary distance of 1.8 Å, assuming a single nearby proton, was reported.

More generally applicable formulas for the spacings and intensities have now been developed. For simplicity, it is assumed that there is a single unpaired electron, that spin orbital effects are absent (due either to quenching or to the electron being in an $s$ state), and that the applied magnetic field is sufficiently strong to make the coupling energy of the electron spin to the applied field large compared with its coupling to the various nuclei in its vicinity.

The appropriate spin-dependent part of the Hamiltonian is

$$(1)\quad \mathcal{H} = -\vec{\mu}_e\cdot\vec{H} - \sum_i (\vec{H} + \vec{b}_{ei})\cdot\vec{\mu}_i = g_e\beta_e S_{ez} H - \sum_i g_i\beta_N \vec{S}_i\cdot\left\{\vec{H} + g_e\beta_e\left[\frac{8\pi}{3}\vec{S}_e\delta^{(3)}(r_{ei}) - r_{ei}^{-3}(\vec{S}_e - 3r_{ei}^{-2}\vec{S}_e\cdot\vec{r}_{ei}\vec{r}_{ei})\right]\right\},$$

where $e$ and $i$ refer to the electron and the $i$th nucleus, respectively, $\vec{H}$ is the applied field (taken to be in the $Z$ direction), $g$ is the gyromagnetic ratio, $\beta_e$ and $\beta_N$ are the Bohr and nuclear magnetons, respectively, and $\vec{S}$ is the spin operator (in units of $\hbar$).

By taking $\mu_i\cdot(\vec{H} + \vec{b}_{ei}) \ll \vec{\mu}_e\cdot\vec{H}$, the zeroth order approximation to the stationary-state vectors may be written

$$(2)\quad \left|U_0\right) = \left|a\ ;\quad Me\ ;\quad \vec{\tau}_i(Me)\ ,\quad Mi\right)\ ,$$

where

$$\vec{\tau}_i(Me) = \frac{\vec{b}_{ei}(Me) + \vec{H}}{\left|\vec{b}_{ei}(Me) + \vec{H}\right|}\ ,$$

$$S_{ez}\left|U_0\right) = Me\left|U_0\right)\ ,\quad Me = \pm\tfrac{1}{2}\ ,$$

$$\vec{S}_i\cdot\vec{\tau}_i\left|U_0\right) = Mi\left|U_0\right)\ ,\quad Mi = S_i,\ S_i^{-1},\ \ldots,\ -S_i\ ,$$

$$\vec{b}_{ei}(Me) = Me\, g_e\beta_e\left[\frac{8\pi}{3}\left|\psi(r_e)_i\right|^2\vec{\tau}_z - \left\langle r_{ei}^{-3}\left(\vec{\tau}_z - \frac{3\, z_{ei}\,\vec{r}_{ei}}{r_{ei}^2}\right)\right\rangle\right],$$

in which $\vec{b}_{ei}$ is the magnetic field of the electron at the $i$th nucleus, $\psi(r_e)_i$ is the electron wave function evaluated at the $i$th nucleus, and the brackets, $\langle\ \rangle$, indicate that the expectation value is taken for the spatial part of the electron wave function. In the expression of $|U_0)$, $a$ represents the quantum numbers which serve to fix the spatial distribution of the electron.

The energies corresponding to the states $|U_0)$ are, to first order,

$$(3)\quad E(Me,Mi) = -g_e\beta_e\, MeH - \sum_i g_i\beta_N\, Mi\left|\vec{H} + \vec{b}_{ei}(Me)\right|\ .$$

In general, when the electron flips its spin $\vec{\tau}_i$, the quantization axis for the $i$th nucleus, will

[1] A more detailed report on this work has been submitted for publication in *The Physical Review*.

[2] Chemistry Division.

[3] H. Zeldes and R. Livingston, *Phys. Rev.* 96, 1702 (1954).

change, and one will have nonvanishing matrix elements between states with energies given by Eq. 3 and having different $Me$ and $Mi$. In particular, the transition probability from state $|Me,Mi)$ to state $|Me',Mi')$, where $Me'$ is different from $Mi$, is given by

$$(4)\quad T(M_e',M_i';\ M_e,M_i) = \frac{g_e^2\beta_e^2 H_w^2}{4w\hbar^2}\prod_i \left|D^{S_i}_{M_iM_i'}(\beta_i)\right|^2 ,$$

where $D^{S_i}$ is the rotation matrix for a particle of spin $S_i$, $\beta_i$ is the angle between $\vec{\tau}_i(Me)$ and $\vec{\tau}_i(M'e)$, and $2H_w$ is the strength of the sinusoidal magnetic field perpendicular to $H$ and oscillating with angular frequency $w = \hbar^{-1}\,[E(M') - E(M)]$.

One has

$$(5)\quad \cos\beta_i = \frac{H^2 - b_{ei}^2}{\left[\left(H^2 - b_{ei}^2\right)^2 + 4\,b_{i\perp}^2 H^2\right]^{1/2}} ,$$

and if, for example, $\beta_i$ is small,

$$(6)\quad D^S_{MM'}\,\alpha\beta_i^{|M-M'|} = \left|\frac{2\,b_{i\perp}H}{H^2 - b_{ei}^2}\right|^{|M-M'|} ,$$

and the most prominent transition is one for which $Mi = Mi'$, transitions involving a change in $Mi$ being reduced in intensity by a factor $|\beta_i|^{2|\Delta M|}$. Then $\vec{b}_{ei}(r_i)$ may be written as

$$(7)\quad \vec{b}_{ei}(\vec{r}_i) = Me\; g_e\beta_e\left[\frac{8\pi}{3}\left|\psi(r_e)_i\right|^2\vec{\tau}_z + \vec{\tau}_z\cdot\nabla\nabla\phi(r)\right]_{\vec{r}=\vec{r}_i} ,$$

where

$$\phi(\vec{r}) = \int \frac{\rho(r_e)}{\left|r - \vec{r}_e\right|}\, d^3r_e ,$$

$$\rho(\vec{r}_e) = \left|\psi(r_e)\right|^2 .$$

If the electron is on one atom, or if it visits several atom sites but spends negligible time between them, $\rho$ may be written as a sum of the several simple orbital distributions centered at the various sites, and the well-known spherical harmonic expansion for the electric potential, $\phi$, may be used.

An application of the formulas to the previously discussed[4] case of atomic hydrogens with only protons as magnetic neighbors shows that $b_{ei}/H$ was small at the neighbors; hence the spacing of satellites from main lines as given by Eq. 3 is $\pm g_i\beta_N H$. The intensity ratio for this case becomes

$$\frac{T_1}{2T_2} = \frac{9}{8}\sum_i \frac{g_e^2\beta_e^2}{H^2 r_i^6}\sin^2\theta_i\cos^2\theta_i ,$$

where $T_1$ is the intensity of either satellite, $2T_2$ is the intensity of the two central (unresolved) lines, $r_i$ is the distance from the atomic hydrogen proton to its $i$th neighbor, and $\theta_i$ is the angle this line makes with the applied field direction. For polycrystals or glassy solids, this equation must be averaged to give

$$\frac{\overline{T_1}}{\overline{2T_2}} = \frac{3}{20}\left\langle\sum_i \frac{g_e^2\beta_e^2}{H^2 r_i^6}\right\rangle ,$$

where $\langle\ \rangle$ indicates an average to account for the possibility of atomic hydrogens being present with different neighborhoods. Experimentally, $\overline{T_1}/2\overline{T_2} \cong 0.03$ for $H = 7982$ gauss, which gives $r_{\text{eff}} = 1.73$ Å as an effective single proton distance with

$$r_{\text{eff}} \equiv \left(\left\langle\sum_i \frac{1}{r_i^6}\right\rangle\right)^{-1/6} .$$

If observations should be made with a spectrometer of sufficient sensitivity, a second set of satellites ($1/r^{12}$ intensity, twice the spacing) could be observed, giving additional information concerning the environment of the unpaired electron.

[4] R. Livingston, H. Zeldes, and E. H. Taylor, *Discussions Farraday Soc.* 19, 166 (1955).

# COULOMB EXCITATION OF THE SECOND $2^+$ STATE IN W, Os, AND Pt NUCLEI

P. H. Stelson F. K. McGowan

## INTRODUCTION

The previously reported measurements of the weak Coulomb excitation of the second $2^+$ state in some medium-weight even-even nuclei provided information on the values of $B(E2)$ for the decay of the second $2^+$ state.[1] The upper cascade $B(E2)$ was, within experimental error, twice as large as the $B(E2)$ for the lower cascade transition. This was confirmation of the prediction of the vibrational model.

The heavy nuclei near platinum also exhibit levels which suggest vibrational motion. However, the previously reported measurement of the Coulomb excitation of the second $2^+$ state in $Pt^{194}$ showed that this nucleus had an upper cascade $B(E2)$ which was one-third that expected for the vibrational model.[2] This result, together with other characteristics to be discussed below, suggests that the platinum nuclei are not examples of fully developed vibrational-type nuclei.

Nuclei somewhat lighter than platinum (the rare-earth region) exhibit the rotational spectra of permanently deformed nuclei. In addition to these rotational states, information from radioactive decay measurements indicates the systematic occurrence of a high-lying (~1 Mev) $2^+$ state in the rare-earth nuclei. This state is interpreted as a vibrational state of the permanently deformed nuclei. The branching ratios for the decay of this state suggest that it is a gamma vibrational state. Scharff-Goldhaber[3] has emphasized that the states of the osmium nuclei are interesting because these nuclei bridge the gap from the rotational spectra (tungsten and below) and the quasi-vibrational nuclei of platinum. We wish to report some measurements of the weak Coulomb excitation of the second $2^+$ states of nuclei in this region.

[1] P. H. Stelson and F. K. McGowan, *Phys. Semiann. Prog. Rep. Sept. 10, 1957*, ORNL-2430, p 19.

[2] F. K. McGowan and P. H. Stelson, *Phys. Rev.* **106**, 522 (1957).

[3] G. Scharff-Goldhaber, p 447 in *Nuclear Structure, Proceedings of the University of Pittsburgh Conference, June 6–8, 1957*, ed. by S. Meshkov.

## EXPERIMENTAL RESULTS

**$W^{184}$ and $W^{186}$.** – The second $2^+$ states in $W^{184}$ and $W^{186}$ were studied by proton bombardment (4.0 to 5.0 Mev) of both a normal tungsten target and targets enriched in $W^{184}$ and $W^{186}$. Coincidence measurements of the cascade gamma rays were made by the use of the arrangement previously described.[1] In contrast to the situation for the medium-weight elements, the singles spectra were sufficiently clean to allow gamma-ray intensity measurements. Consequently the yields of the crossover transitions were determined. The singles and coincidence spectra for $W^{186}$ are shown in Fig. 1. The results for $W^{186}$ are consistent with the Coulomb excitation of a $2^+$ state at 730 ± 7 kev. Similarly, the results for $W^{184}$ indicate a $2^+$ state at 891 ± 9 kev.

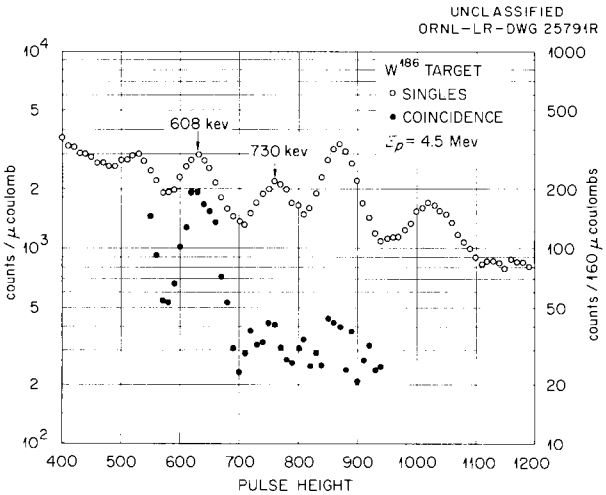


**Fig. 1. Singles and Coincidence Spectra for Coulomb Excitation of $W^{186}$.**

Poë[4] studied the levels in $W^{186}$ by measurements of the gamma rays resulting from the decay of 10-min $Ta^{186}$. He found nine gamma rays, two of which have energies of 730 and 610 kev, and these values agree well with our results. Poë's ratio cascade/crossover is 0.7, whereas we find 1.0. Similarly, Butement and Poë[5] studied the

[4] A. J. Poë, *Phil. Mag.* **46**, 1165 (1955).

[5] F. D. S. Butement and A. J. Poë, *Phil. Mag.* **46**, 482 (1955).

levels in $W^{184}$ by measurement of the gamma rays following the decay of 8.7-hr $Ta^{184}$. Here also they found nine different gamma rays. Two of these, having energies of 890 and 780 kev, agree well with our results. Their value for cascades/crossover is 0.2 and is considerably different from our value of 1.0.

Figure 2 shows level diagrams for $W^{184}$ and $W^{186}$ in which our results are summarized. The numbers accompanying the gamma-ray transition arrows are the measured enhancements of the $E2$ transitions. The enhancement is defined as

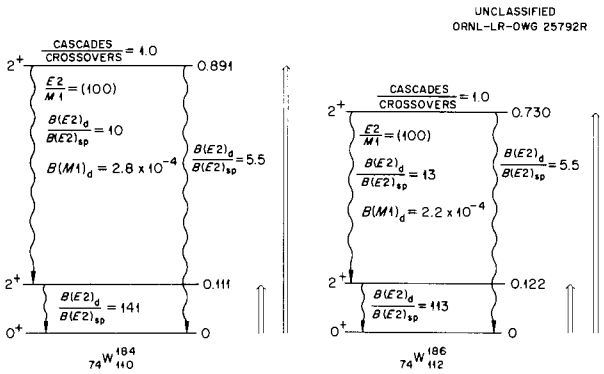


**Fig. 2. Level Diagrams for $W^{184}$ and $W^{186}$.**

$B(E2)_d/B(E2)_{sp}$, where $B(E2)_{sp}$ is $\frac{1}{4\pi}|\frac{3}{5}R_0^2|^2$. Unfortunately, the $E2/M1$ values for the upper cascade gamma rays are not yet known. However, it seems clear that the values for $B(M1)_d$ will be quite small. The experimental results are also summarized in Table 1.

**$Os^{188}$, $Os^{190}$, and $Os^{192}$.** – Separated isotopes of osmium are not yet available. However, the locations of the first $2^+$ states of $Os^{188}$ (155 kev), $Os^{190}$ (187 kev), and $Os^{192}$ (206 kev) are well known. Therefore, by coincidence measurements it was possible to identify and assign the corresponding second $2^+$ states. With this information available, it was then possible to identify the crossover transitions in the singles spectrum. The results of these measurements are summarized in Table 1.

Figure 3 contains the information obtained for $Os^{188}$. Considerable information on the levels of $Os^{188}$ is available from radioactive decay measurements.[6,7] Our result showing a second $2^+$

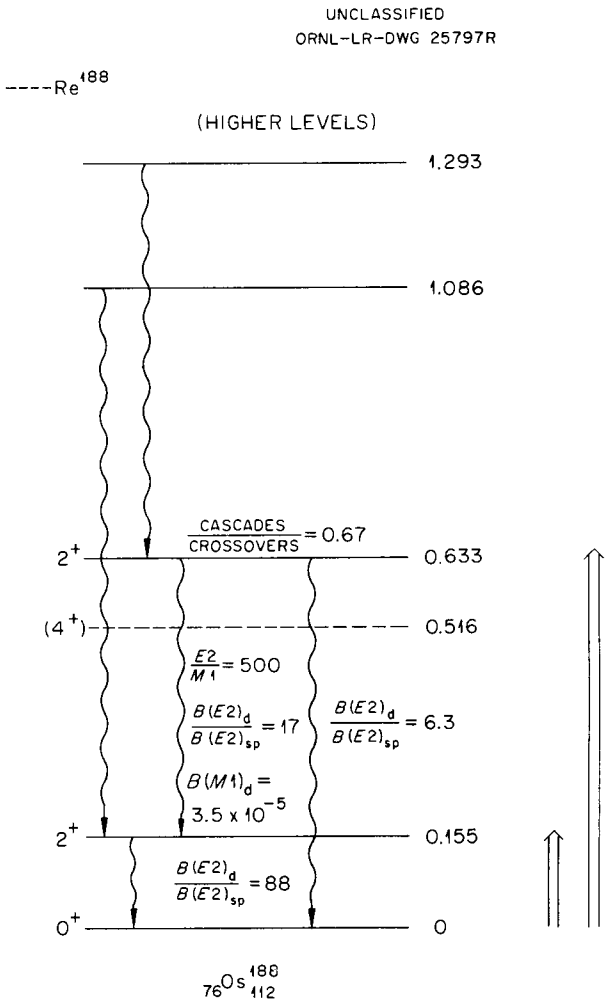


**Fig. 3. Level Diagram for $Os^{188}$.**

level at 633 kev is in good agreement with results from radioactive decay work. We have used the value for cascades/crossovers obtained from radioactive decay measurements.[6] A value for $E2/M1$ for the upper cascade gamma ray is available from gamma-gamma correlation measurements.[6] Taking this value of 500, one obtains the exceedingly small value of $3.5 \times 10^{-5}$ for $B(M1)_d$.

Figure 4 summarizes the results obtained for $Os^{190}$. The levels obtained from the measurements of the gamma rays following the decay of the high-lying 10-min isomer are also included.[8] These states exhibit a rotational spin sequence, although there is considerable departure from the expected level spacings for rotational levels.

[6] V. R. Potnis, *Phys. Rev.* **104**, 722 (1956).

[7] M. W. Johns *et al.*, *Can. J. Phys.* **34**, 69 (1956).

[8] G. Scharff-Goldhaber *et al.*, *Bull. Am. Phys. Soc.* **2**, Ser. II, 25, G10 (1957).

Table 1. Summary of Information Obtained from Coulomb Excitation

| Nucleus | $E_\gamma$ (kev) | $B(E2)_{ex}$ | Transition | $B(E2)_d$ | Cascades / Crossovers | $\alpha_T$ | $T_{1/2}$ (sec) | $B(E2)_d / B(E2)_{sp}$ | $B(E2,2' \to 2) / B(E2,2 \to 0)$ |
|---|---|---|---|---|---|---|---|---|---|
| $Pt^{196}$ | 358 | $(12.7 \pm 1.3) \times 10^{-49}$ | $2 \to 0$ | $2.53 \times 10^{-49}$ | | 0.0598 | | 37 | |
| | 330 | | | | | 0.074 | | | |
| | 688 | $< 1.3 \times 10^{-51}$ | $2' \to 0$ | $2.6 \times 10^{-52}$ | $> 2500$ | 0.0117 | | $< 3.8 \times 10^{-2}$ | |
| $Pt^{194}$ | 330 | $(19.4 \pm 2.0) \times 10^{-49}$ | $2 \to 0$ | $3.89 \times 10^{-49}$ | | 0.074 | | 58 | |
| | 292 | | $2' \to 2$ | $2.3 \times 10^{-49}$ | | 0.107 | | 34 | 0.59 |
| | 622 | $(8.7 \pm 2) \times 10^{-51}$ | $2' \to 0$ | $1.7 \times 10^{-51}$ | 3.3 | 0.016 | | 0.25 | |
| $Os^{192}$ | 206 | $(20.5 \pm 2.1) \times 10^{-49}$ | $2 \to 0$ | $4.1 \times 10^{-49}$ | | 0.313 | $2.83 \times 10^{-10}$ | 62 | |
| | $283 \pm 3$ | | $2' \to 2$ | $2.8 \times 10^{-49}$ | | 0.111 | | 42 | 0.68 |
| | $489 \pm 5$ | $(15 \pm 3) \times 10^{-50}$ | $2' \to 0$ | $3.0 \times 10^{-50}$ | 0.67 | 0.0246 | | 4.6 | |
| $Os^{190}$ | 187 | $(25.5 \pm 2.6) \times 10^{-49}$ | $2 \to 0$ | $5.1 \times 10^{-49}$ | | 0.434 | $3.47 \times 10^{-10}$ | 79 | |
| | $370 \pm 4$ | | $2' \to 2$ | $2.7 \times 10^{-49}$ | | 0.051 | | 41 | 0.53 |
| | $557 \pm 6$ | $(14 \pm 3) \times 10^{-50}$ | $2' \to 0$ | $2.8 \times 10^{-50}$ | 1.3 | 0.0179 | | 4.3 | |
| $Os^{188}$ | 155 | $(28.0 \pm 3.1) \times 10^{-49}$ | $2 \to 0$ | $5.60 \times 10^{-49}$ | | 0.82 | $6.2 \times 10^{-10}$ | 88 | |
| | $478 \pm 5$ | | $2' \to 2$ | $10.7 \times 10^{-50}$ | | 0.0263 | | 17 | 0.19 |
| | $633 \pm 6$ | $(20 \pm 6) \times 10^{-50}$ | $2' \to 0$ | $4.0 \times 10^{-50}$ | 0.67 | 0.0132 | | 6.3 | |
| $W^{186}$ | 122.5 | $(35.6 \pm 3.6) \times 10^{-49}$ | $2 \to 0$ | $7.12 \times 10^{-49}$ | | 1.75 | $9.85 \times 10^{-10}$ | 113 | |
| | $608 \pm 6$ | | $2' \to 2$ | $8.6 \times 10^{-50}$ | | 0.0133 | | 13 | 0.12 |
| | $730 \pm 7$ | $(17.4 \pm 3) \times 10^{-50}$ | $2' \to 0$ | $3.5 \times 10^{-50}$ | 1.0 | 0.0088 | | 5.5 | |
| $W^{184}$ | 111 | $(43.7 \pm 4.4) \times 10^{-49}$ | $2 \to 0$ | $8.74 \times 10^{-49}$ | | 2.59 | $1.02 \times 10^{-9}$ | 141 | |
| | $780 \pm 8$ | | $2' \to 2$ | $6.5 \times 10^{-50}$ | | 0.0075 | | 10 | 0.074 |
| | $891 \pm 9$ | $(17 \pm 5) \times 10^{-50}$ | $2' \to 0$ | $3.4 \times 10^{-50}$ | 1.0 | 0.0057 | | 5.5 | |

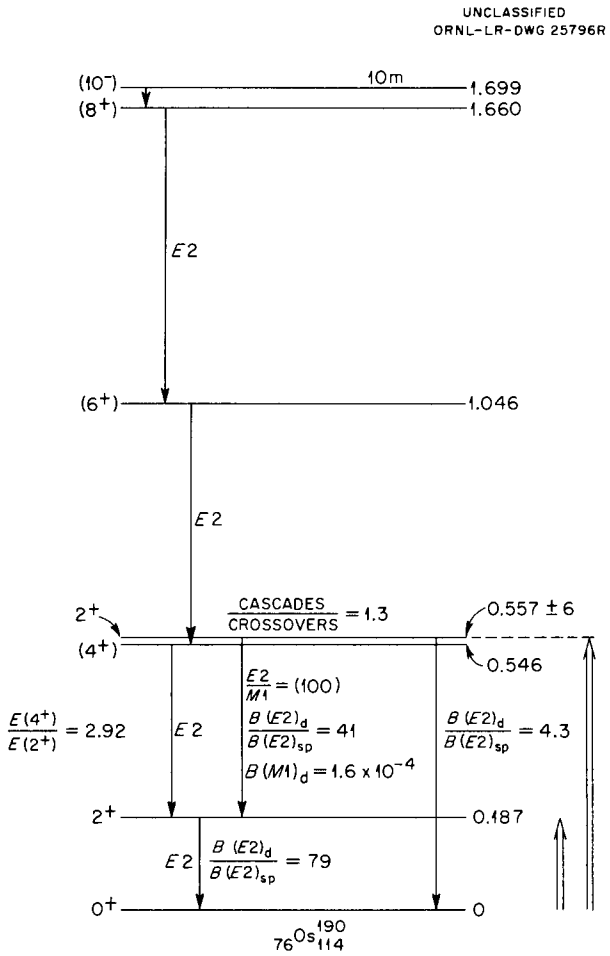


**Fig. 4. Level Diagram for $Os^{190}$.**

The second $2^+$ state is found to be quite close to the $4^+$ state.

Figure 5 summarizes the results for $Os^{192}$. We show also the level scheme proposed by Baggerly *et al.*[9] Measurement of the yield of the 283-kev gamma ray with variation in proton energy indicates that this gamma ray results from the excitation of a state at 489 kev rather than from one at 690 kev, as proposed by the level scheme of Baggerly *et al.* Recent radioactive decay work on the level scheme of this nucleus carried out at Brookhaven[10] also indicates that the second $2^+$

[9] L. L. Baggerly *et al.*, *Phys. Rev.* 100, 1364 (1955).

[10] Private communication, G. Scharff-Goldhaber.

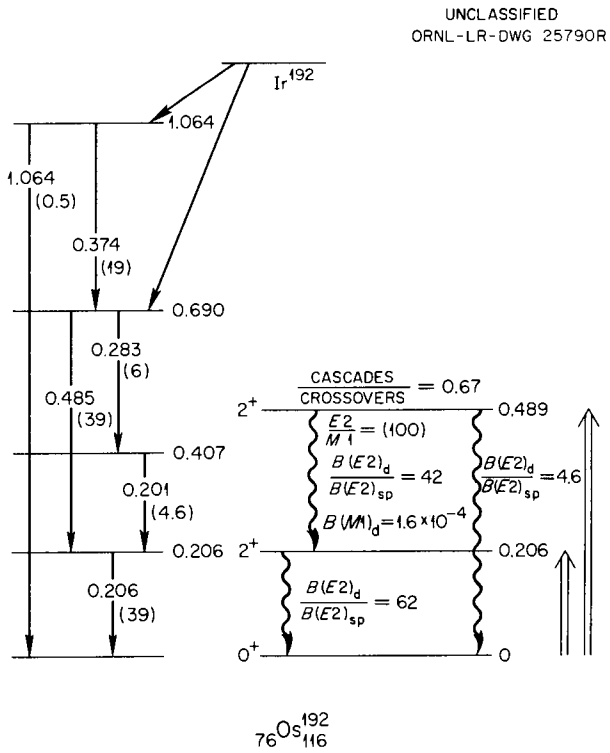


**Fig. 5. Level Diagram for $Os^{192}$.**

state is at 489 kev. Barloutaud *et al.*[11] have also measured the Coulomb excitation of the second $2^+$ state in $Os^{190}$ and $Os^{192}$. Our results are in reasonable agreement with theirs.

**$Pt^{196}$.** – From the study of the decay of $Au^{196}$ to $Pt^{196}$, Alburger[12] has set a limit for the ratio cascades/crossovers $\geq 2500$ for the decay of the second $2^+$ state in $Pt^{196}$. Taking this result, one finds that the assumption of a reasonable value for the cascade $B(E2)$ leads to a very small value for the crossover $B(E2)$. We have attempted to find evidence for the Coulomb excitation of the second $2^+$ state in $Pt^{196}$. A positive result was not obtained. Our result indicates that the $B(E2)$ for the crossover transitions is less than $1/25$ the Weisshopf single-particle estimate. The results for $Pt^{194}$ and $Pt^{196}$ are summarized in Fig. 6.

[11] R. Barloutaud, P. Lehmann, and A. Lévêque, *Compt. rend.* 245, 523 (1957).

[12] D. E. Alburger, *Phys. Rev.* 108, 812 (1957).

UNCLASSIFIED
ORNL-LR-DWG 25795R

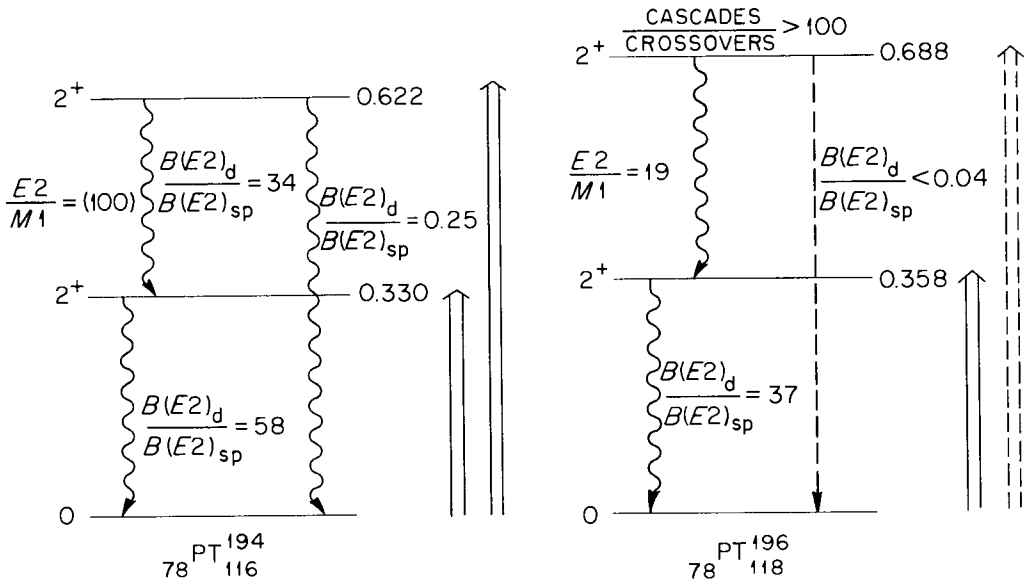


**Fig. 6. Level Diagrams for $Pt^{194}$ and $Pt^{196}$.**

---

## TOTAL CROSS SECTIONS OF $C^{12}$ AND $C^{13}$ FOR FAST NEUTRONS

H. B. Willard J. K. Bair H. O. Cohn

New energy levels of the nucleus $C^{13}$ have been observed in the $C^{12}(d,p)C^{13}$ reaction.[1] These states at 7.47- and 7.53-Mev excitation might appear as resonances in the total cross section of $C^{12}$ at 2.73- and 2.80-Mev neutran bombarding energy. Accordingly, good geometry measurements with 5-kev resolution were made between 2.62 and 2.91 Mev. The data (Fig. 1) show no deviations greater than ±0.2 barn in this region, the rise being due to the known level at 2.95 Mev. Thus it is concluded that the levels must be formed from neutrons of high orbital angular momentum.

Levels in $C^{14}$ have not previously been investigated by means of the $C^{13} + n$ interaction. Barium carbonate, enriched to 61.7% in $C^{13}$, was converted into elemental carbon. Samples sufficiently large for transmission measurements were prepared by pressing the amorphous carbon into a thin-walled nickel can. Total neutron cross sections from 0.2 to 4 Mev were obtained by experimental subtraction with a duplicate nickel can containing an equivalent amount of $C^{12}$. Both $Li^7(p,n)$ and $H^3(p,n)$ reactions were used as neutron sources, the resolution in the vicinity of resonances being about 7 kev, and elsewhere about 15 kev. A 5% contamination of water was present in the $C^{13}$ sample, and prolonged heating above 100°C failed to remove the water.

Measured data points are shown in Fig. 2. The resonance at 0.44 Mev is well known in $O^{16}$. Resonances were also observed at 1.75, 2.43, and 2.45 Mev. The dashed curve is the nonresonant total cross section corrected for the $H_2O$ contamination.

[1] J. N. McGruer, E. K. Warburton, and R. S. Bender, *Phys. Rev.* 100, 235 (1955).

Detailed studies of the individual resonances are shown in Figs. 3 and 4. The resonance at 1.75 Mev has a natural width of 19 kev, that at 2.43 Mev about 15 kev, and the interfering level at 2.45 Mev less than 10 kev. These states lie at excitation energies of 9.81, 10.44, and 10.46 Mev in $C^{13}$, in good agreement with levels observed in the $C^{13}(d,p)C^{14}$ reaction.[1]

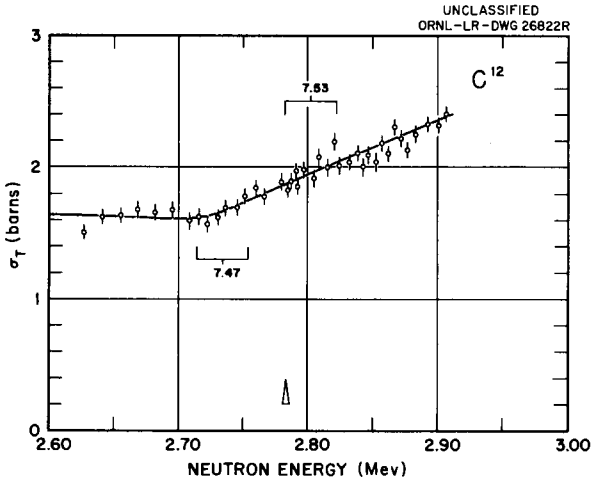


**Fig. 1. Total Cross Section of $C^{12}$. Resonances due to levels in $C^{13}$ at 7.47 and 7.53 Mev should appear at the indicated regions.**

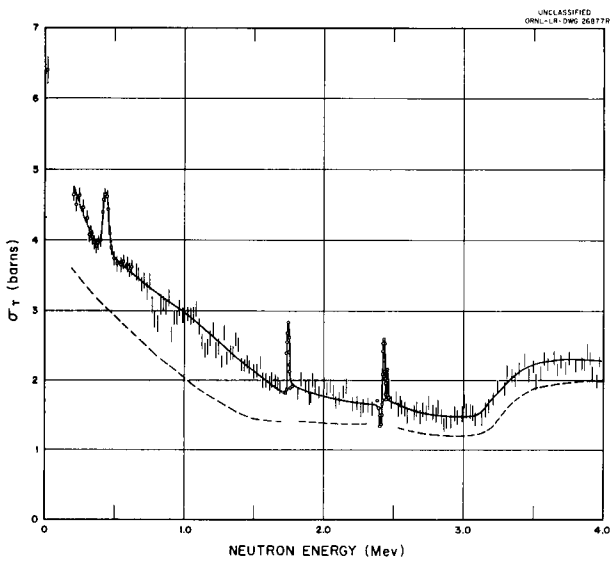


**Fig. 2. Total Cross Section of $C^{13}$ from 0.2 to 4 Mev. A dashed curve correcting for the $H_2O$ contamination is shown for the nonresonant region.**

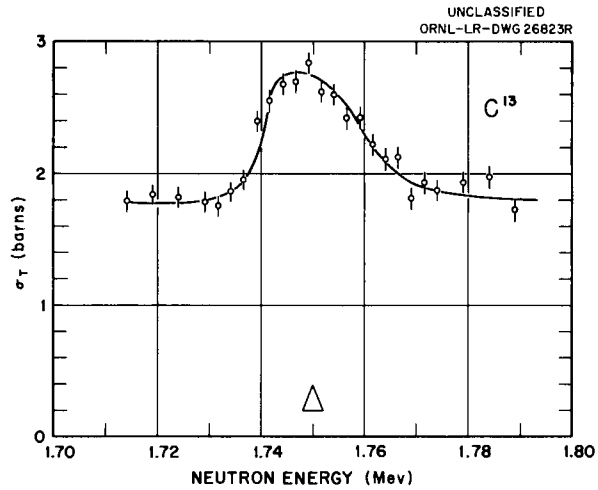


**Fig. 3. Total Cross Section of $C^{13}$ in the Region of the 1.75-Mev Resonance.**

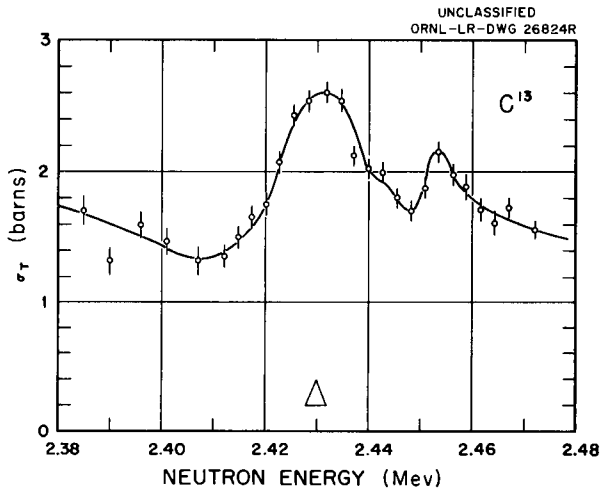


**Fig. 4. Total Cross Section of $C^{13}$ in the Region of the 2.43- and 2.45-Mev Resonances.**

## RESONANCES IN THE TOTAL CROSS SECTION OF NEON

H. O. Cohn J. L. Fowler

Elastic scattering of neutrons from zero-spin nuclei is of special interest. Since in such cases as $He^4$, $C^{12}$, $O^{16}$, and $Ne^{20}$ there is only one channel spin state, a unique phase-shift analysis of differential scattering data is possible.[1-4] In order to check such differential scattering measurements on $Ne^{20}$, as well as to more firmly fix resonance parameters, the total neutron cross section of neon in the range 0.8 to 1.9 Mev has been measured.

Figure 1 shows the geometry of the experiment. The sample was neon gas at 1200 psi contained in the 1-m-long stainless steel tube. A similar but evacuated tube was used to correct experimentally for the effect of the stainless steel. The Li($p,n$) reaction furnished the source of neutrons, with an energy spread of about 10 to 12 kev.

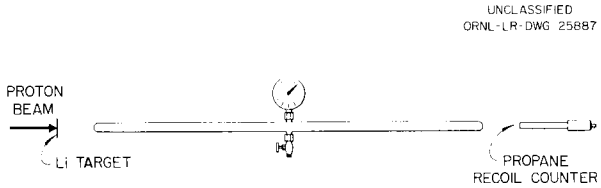


**Fig. 1. Apparatus for Neon Total-Cross-Section Measurements.**

Figure 2 shows the results of the measurements and gives the total cross section of neon. The data have been corrected for the second group of neutrons from the Li($p,n$) source, as well as for the effect due to background neutrons. In the region of measurements, seven prominent resonances are observed. From this data the three broad resonances can be identified as $J = 3/2$ at 0.91 Mev, $J = 1/2$ at 1.31 Mev, and $J = 3/2$ at 1.62 Mev. The curves shown here, taken in conjunction with differential measurements, allow one to assign the the parities for these levels as well as the $J$ value and parities of three of the other levels.

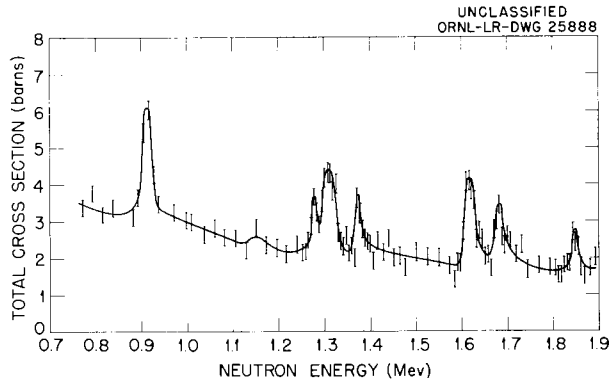


**Fig. 2. Total Neutron Cross Section of Neon.**

The differential cross sections have been measured by a technique described previously.[4] An anthracene crystal detects neutrons in coincidence with neon recoils which occur in a proportional counter. Direct source neutrons are shielded out by the combination of lithiated paraffin and lead shields. Since the crystal can be calibrated with the neutrons incident on the neon sample, the measurements give absolute differential cross sections.

Figure 3 shows the results of the differential measurements in the vicinity of the 0.91-Mev level. The vertical scale gives the differential cross section in barns per steradian in the center-of-mass system. The horizontal scale gives the cosine of the center-of-mass angle. Neutron energy is given on the skew scale. The solid lines are calculated by use of the Breit-Wigner resonance formalism from the set of parameters shown at the left of the drawing. Resonance width variation with energy and the effect of the experimental energy resolution are included in the theoretical curves. The theoretical curves fit the data quite

---

[1] E. Van der Spuy, *Nuclear Phys.* 1, 381 (1956).

[2] J. E. Wills Jr., *et al.*, *Phys. Rev.* 109, 891 (1958).

[3] J. L. Fowler and H. O. Cohn, *Phys. Rev.* 109, 89 (1958).

[4] H. O. Cohn and J. L. Fowler, *Bull. Am. Phys. Soc.* 1, Ser. II, 175, F6 (1956); and *Phys. Semiann. Prog. Rep. Sept. 10, 1957*, ORNL-2430, p 39.

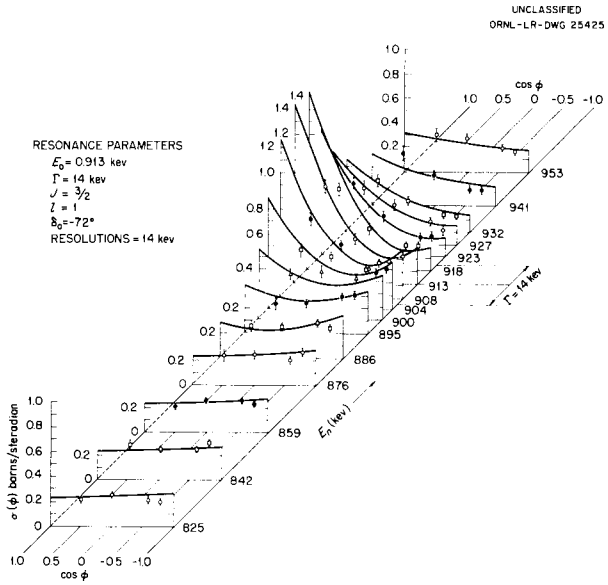


**Fig. 3. Differential Cross Sections of Neon in Vicinity of 0.91-Mev Level.** Data are in center-of-mass system.

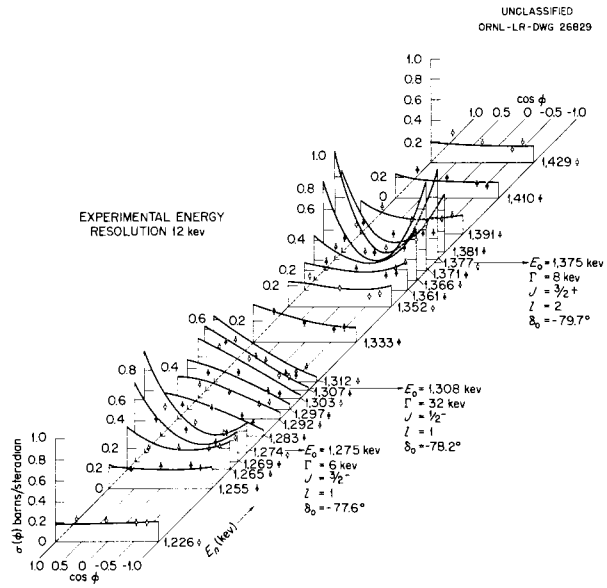


**Fig. 4. Differential Cross Section of Neon from 1.23 to 1.43 Mev in Center-of-Mass System.**

well, which indicates that the 0.91-Mev level is a $\frac{3}{2}$ level with a 14-kev width.

Figure 4 shows the situation in the vicinity of the 1.31-Mev level. Here one has three somewhat overlapping levels. The theoretical curves (shown as heavy lines) are calculated with the set of parameters given on the right. The effect of the tail of the $\frac{3}{2}$ level at 0.91 Mev is included. One calculates at each energy the effect of four phase shifts, where the *p*- and *d*-wave phase shifts are obtained from the resonance formalism. In the vicinity of the 1.37-Mev level, a somewhat better fit to the data could be found with a somewhat narrower resonance; perhaps Γ = 6 to 7 kev for this $\frac{3}{2}$+ level. Nevertheless, the agreement between the experimental points and the theoretical curves is such as to definitely fix the *J* value and parities as listed here

A similar analysis has been made in the vicinity of the 1.63- and 1.68-Mev levels. Table 1 summarizes the information available on the scattering of $Ne^{20}$, both for this work as well as for the work of Sikkema at Groningen, Netherlands.[5] Uncertainties of the level widths listed are indicated.

**Table 1. Resonance Levels for $Ne^{20}$ Neutron Scattering**

| $E_0$ (Mev) | Γ (kev) | *J* | *l* | π | |
|---|---|---|---|---|---|
| 0.91 | 14 ± 30% | $\frac{3}{2}$ | 1 | – | Present work |
| 1.27 | 6 ± 30% | $\frac{3}{2}$ | 1 | – | Present work |
| 1.31 | 32 ± 20% | $\frac{1}{2}$ | 1 | – | Present work |
| 1.37 | 8 ± 30% | $\frac{3}{2}$ | 2 | + | Present work |
| 1.62 | 29 ± 20% | $\frac{3}{2}$ | 1 | – | Present work |
| 1.68 | 10 ± 30% | $\frac{3}{2}$ | 2 | + | Present work |
| 1.85 | | | | | Present work |
| 1.94 | 20 ± 10 | $\frac{3}{2}$ | 2 | + | C. P. Sikkema |
| 2.00 | 50 ± 10 | $\frac{3}{2}$ | 1 | – | C. P. Sikkema |

Total angular momentum and parity assignments are reasonably definite.

It is of interest to examine this data in the light of what we know about neutron scattering from other light nuclei. In the case of $He^4$ and $O^{16}$, and to a lesser extent in the case of $C^{12}$, there are states observed by neutron elastic scattering which have large, almost single-particle, reduced

[5] C. P. Sikkema, *Nuclear Phys.* **3**, 375 (1957).

widths.[1-3] This is particularly true for even-parity states in $O^{17}$ and $C^{13}$ (ref 3). For neon the maximum reduced width is only of the order of 1% of the Wigner limit. In $Ne^{20}$, one is filling the 1*d* and 2*s* shells far from a closed shell. There is as a consequence a great deal of configuration mixing, and hence one observes a relatively large number of reasonably narrow resonances.

---

## CROSS SECTION AS A FUNCTION OF ENERGY FOR THE REACTION $S^{32}(n,\alpha)Si^{29}$

H. W. Schmitt

The measurements of the $S^{32}(n,\alpha)Si^{29}$ cross section reported previously[1] have been extended to include incident neutron energies up to 3.8 Mev. Data were taken in much the same manner as that described,[1] using a double back-to-back gridded ionization chamber. Fission fragments from $U^{238}$ neutron-induced fission were counted on one side; on the opposite side, alpha particles to the ground state of $Si^{29}$, whose pulse heights were displayed on a multichannel analyzer, were counted. Yield curves were obtained for the forward and back hemispheres and were converted to values of $\sigma_{n,\alpha}(0 \text{ to } 90 \text{ deg})/\sigma_f$ and $\sigma_{n,\alpha}(90 \text{ to } 180 \text{ deg})/\sigma_f$. These curves were added point by point to give the curve shown in Fig. 1.

A discussion of corrections applied in these measurements, together with uncertainties, has been given.[1] In the present experiment the mass of sulfur in each of the lead sulfide deposits was determined by means of a quantitative chemical analysis in which colorimetric techniques were

[1] H. W. Schmitt, *Phys. Semiann. Prog. Rep. Sept. 10, 1957*, ORNL-2430, p 42.

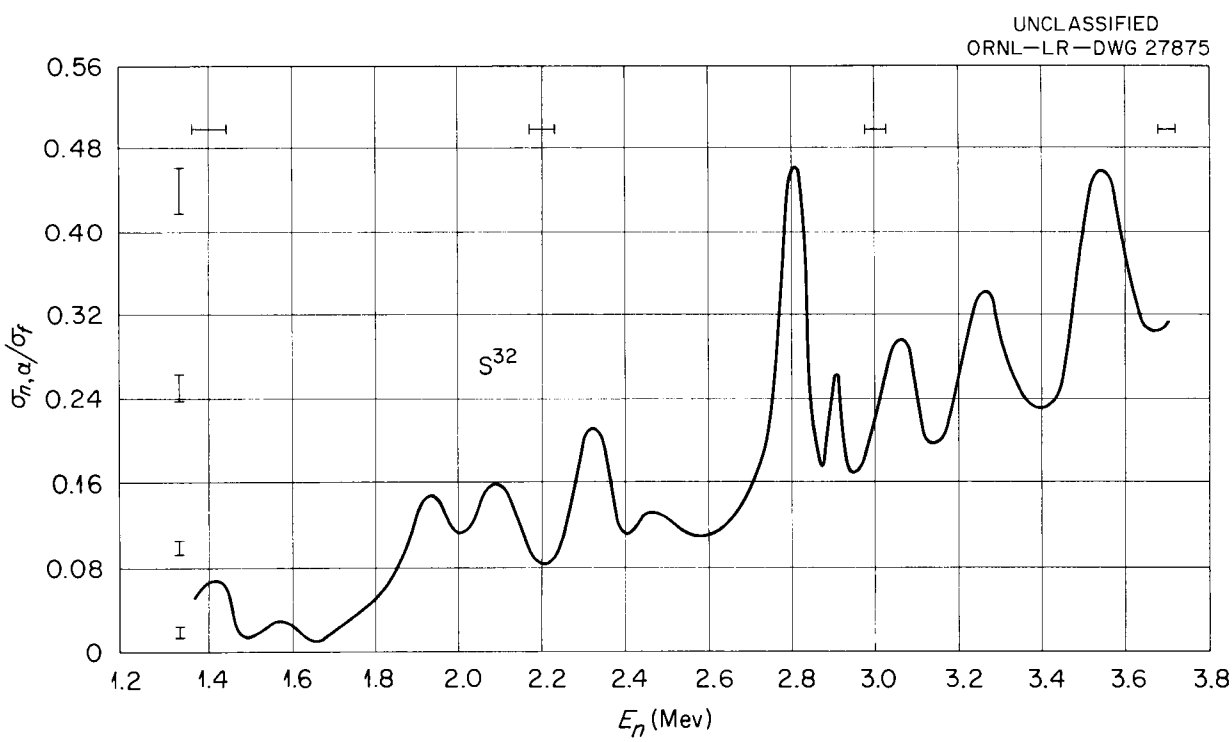


**Fig. 1. Ratio of $S^{32}(n,\alpha)Si^{29}$ Cross Section to $U^{238}$ Fission Cross Section.** Typical statistical uncertainties and neutron energy spreads are shown.

used.[2] A discrepancy between the mass determined in this way and the mass of sulfur deduced from careful weighing of the deposits has been attributed to free lead deposited on the platinum backing along with the lead sulfide. The foils used in the measurements reported[1] have been analyzed, and the results, which are included here, are corrected.

In Fig. 2 the $S^{32}(n,\alpha)Si^{29}$ cross section is given as a function of incident neutron energy. In both Figs. 1 and 2 typical statistical uncertainties are given, and typical neutron energy spreads are

[2]We gratefully acknowledge the assistance of P. Thomason of the Analytical Chemistry Division, who did these analyses.

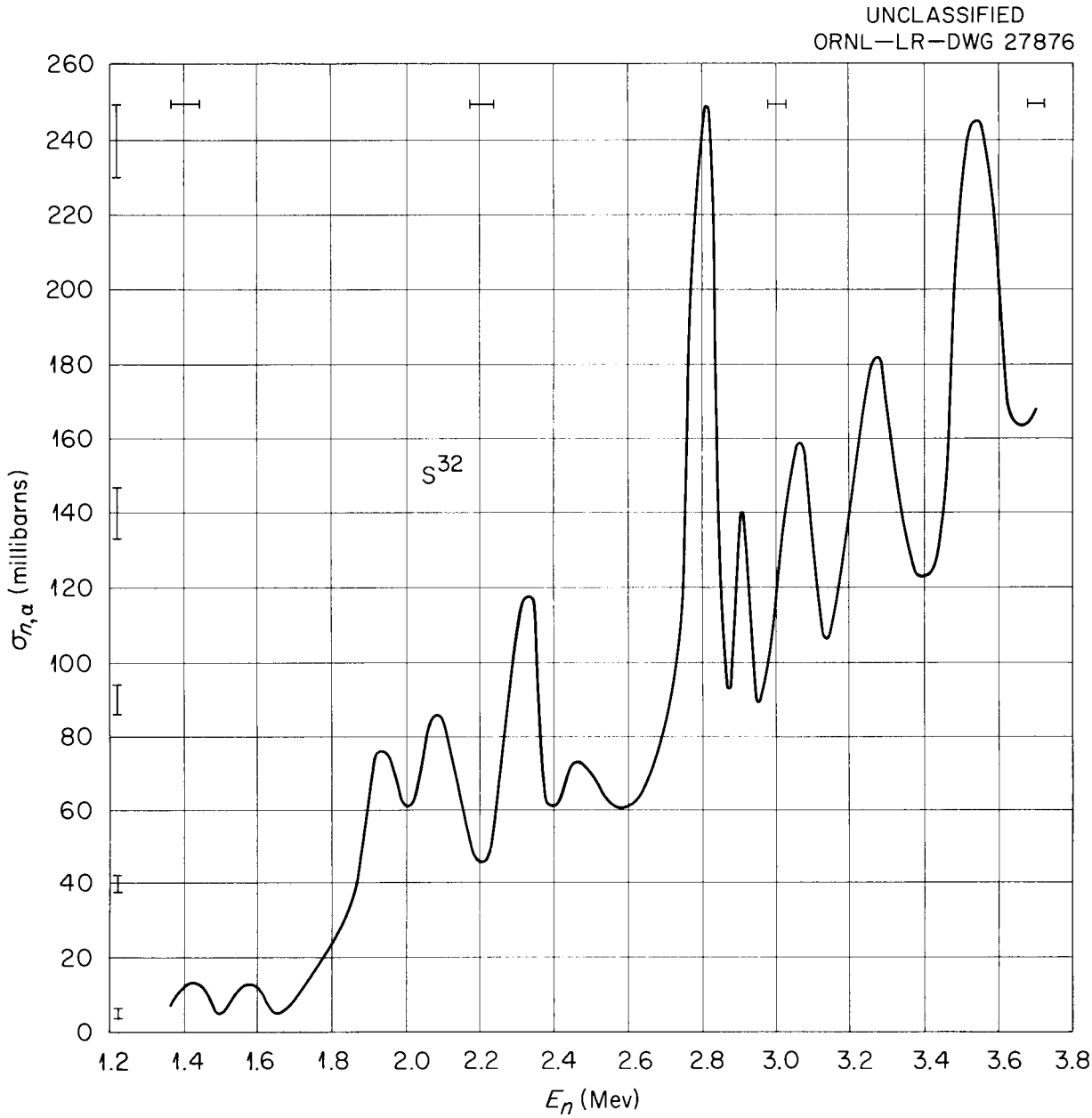


**Fig. 2. The $S^{32}(n,\alpha)Si^{29}$ Cross Section as a Function of Incident Neutron Energy.** To obtain $\sigma_{n,\alpha}$ from $\sigma_{n,\alpha}/\sigma_f$, values of $\sigma_f(E)$ given by R. L. Henkel [*Summary of Neutron-Induced Fission Cross Sections*, LA-2114 (May 1957)] were used.

shown at the top. The uncertainty in the absolute values of $\sigma_{n,\alpha}$ is ±9%. Agreement with the data of Hürlimann and Huber,[3] in the energy range of overlap, is satisfactory.

The peaks observed in these experiments are not resolved resonances but are groups of resonances, as shown in $Si^{29}(\alpha,n)S^{32}$ experiments (see "Absolute $(p,n)$ and $(\alpha,n)$ Cross Sections for Light Nuclei," this report). A preliminary Hauser-Feshbach[4] calculation predicts to within a factor of 2 a smooth, averaged cross section drawn through the results given in Fig. 2.

[3] T. Hürlimann and P. Huber, *Helv. Phys. Acta* 28, 33 (1955).

[4] W. Hauser and H. Feshbach, *Phys. Rev.* 87, 366 (1952).

## PULSED VAN DE GRAAF AND FAST TIME-OF-FLIGHT STUDIES

W. M. Good J. H. Neiler J. H. Gibbons

Progress has been made on several of the instrumental problems associated with beam pulsing and multichannel time analysis. The operating life of the ion source has been extended to ~100 hr at currents of ~500 μa. The beam spot size does not increase appreciably during this time, so that the beam pulse time resolution remains essentially constant. Several improvements have been made in the time-to-pulse-height converter.[1] The circuit diagram of the most recent version is given in Fig. 1. It was primarily designed to provide linear time-to-pulse-height conversion over the range 100 to 1500 mμsec while maintaining time resolution somewhat better than the 6 to 7 mμsec, which is the present limit of resolution of the NaI crystal for the 480-kev gamma ray from the $B^{10}(n,\alpha\gamma)Li^7$ reaction. When used with an A-8 linear amplifier[2]

[1] J. H. Neiler *et al.*, *Phys. Semiann. Prog. Rep. Sept. 10, 1955*, ORNL-1975, p 66.

[2] G. G. Kelley, *Phys. Semiann. Prog. Rep. March 10, 1957*, ORNL-2302, p 48.

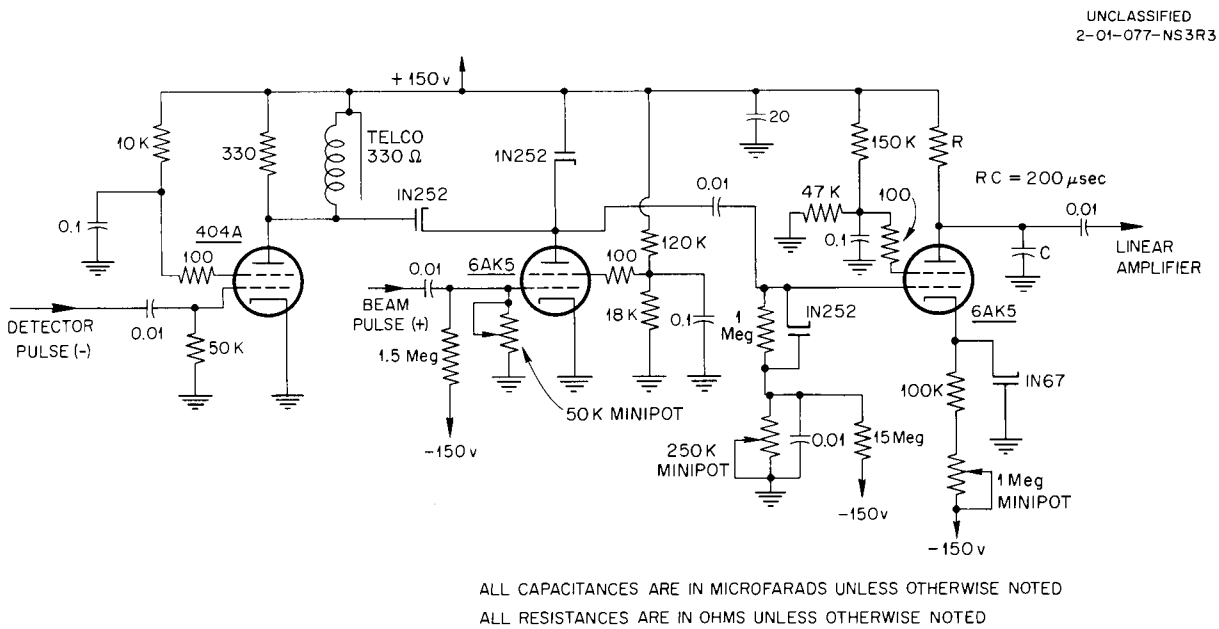


**Fig. 1. Circuit Diagram of Time-to-Pulse-Height Converter.**

with 2-$\mu$sec differentiation lines, this circuit produces a very stable signal which shows no counting rate shifts and has adequate time resolution over the entire range. The linearity of time-interval-to-pulse-height conversion is shown in Fig. 2.

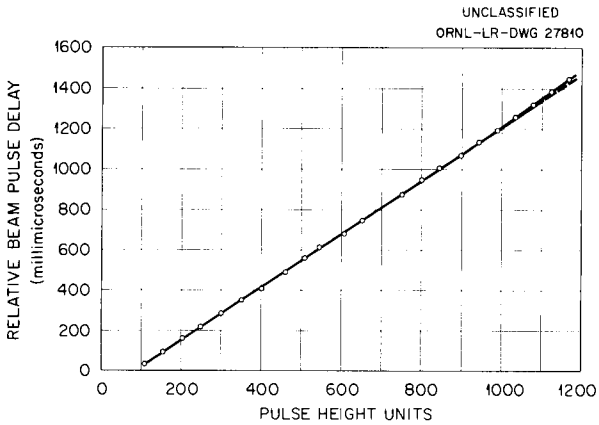


**Fig. 2. Pulse Height as a Function of Time Interval.**

The effects of these improvements may be seen in the results obtained during the most recent run, at which time the total cross sections for neutron energies in the range 2 to 20 kev were obtained for the following nuclides: $N^{14}$, $Cl^{35}$, $Ti^{48}$, $Ti^{49}$, $V^{51}$, $Fe^{56}$, $Fe^{57}$, $Cu^{65}$, $Rb^{85}$, $Rb^{87}$, $Sr^{86}$, and $Zr^{90}$. Representative results are shown in Figs. 3 and 4. In the case of $Cu^{65}$ the resonances are quite narrow, so that the widths shown are essentially the resolution width of the instrument at each energy. The resonances in $Fe^{57}$ are typical of those cases where the actual resonance width is greater than, or of the same order as, the instrumental resolutions. In this case, resonance parameters may be calculated from the results of area analysis or by unfolding the instrumental resolution. Mutual consistency of these two types of analysis yielded an instrumental resolution which agreed with that obtained from the narrow copper resonances. In addition, the observed resolution agreed with that obtained by assuming a time resolution for neutrons equal to the prompt-gamma time resolution and adding in detector thickness effects for the flight path used.

By virtue of the improved resolution and because separated isotopes are being used, considerable

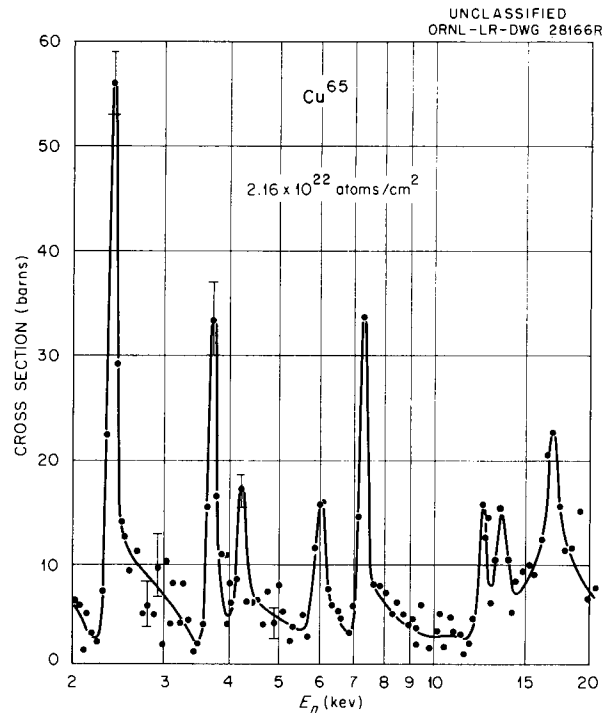


**Fig. 3. Total Cross Section of $Cu^{65}$. The small value of observed peak cross sections is indicative of the narrow natural widths of the observed resonances. Thus the observed widths are an approximate measure of the over-all experimental resolution.**

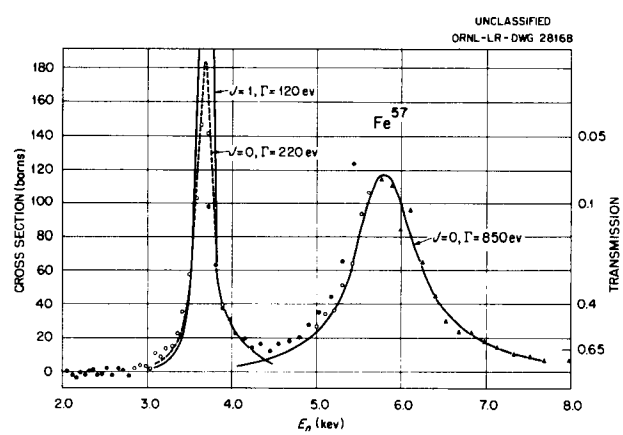


**Fig. 4. Two Resonances in the Total Cross Section of $Fe^{57}$. The solid curve represents an incoherent addition of two single-level Breit-Wigner fits to the data. Resonance widths ($\Gamma$) and spins ($J$) were determined both by shape and area analysis.**

new information is being obtained. The data obtained on the nuclides listed are being analyzed at this writing. The $Fe^{57}$ referred to is the most interesting of the isotopes analyzed so far. The data can be fitted (Fig. 4) by two Breit-Wigner single-level formulas, with the cross sections added incoherently. The apparent lack of resonance interference is surprising in view of the fact that both resonances appear to have the same $J$ and parity. The peak cross section of the 5.8-kev resonance turns out to be compatible only with $I = \frac{1}{2}$ for the ground state of $Fe^{57}$, thus removing uncertainty in the ground-state spin of that nucleus. Further confirmation of this $I$ assignment has recently been published.[3] The off-resonance $Fe^{57}$ cross section yields a value of the effective radius, $R'$, significantly lower than we expected.[4]

[3]N. S. Garif'ianov, M. M. Zaripov, and B. M. Kozyrev, *Soviet Physics, Doklady (Proc. Acad. Phys. Sci. U.S.S.R.)* 2, 195 (1957).

[4]K. K. Seth, *Conference on Neutron Physics by Time-of-Flight; Held at Gatlinburg, Tennessee, November 1 and 2, 1956*, ORNL-2309, p 8 (June 17, 1957).

## FAST-CHOPPER TOTAL AND SCATTERING NEUTRON CROSS-SECTION MEASUREMENTS

G. G. Slaughter R. C. Block J. A. Harvey

The new high-intensity, fast-chopper, time-of-flight neutron spectrometer has been utilized to make transmission and scattering measurements. This equipment, installed at the LITR, consists of an 18-in.-dia stainless steel rotor, a 45-m evacuated flight path, a bank of $BF_3$ proportional counters, a digital speed-control unit which maintains rotor speed to ±1 rpm, and a 256-channel magnetic-core time analyzer. This rotor has been spun up to 6000 rpm, at which the neutron resolution has been observed to be ~0.06 μsec/m. In the near future this rotor will be spun at a maximum design speed of 10,000 rpm to take advantage of the increase in resolution. The data from the time analyzer are punched out on teletype tape which is processed by the Oracle to yield neutron energies, transmissions, cross sections, and plots of transmission vs time-analyzer channel number.

The total cross sections of gold and iodine were measured by the transmission technique in order to determine the performance of this new spectrometer. Two metallic samples of gold, $5.96 \times 10^{21}$ and $2.49 \times 10^{22}$ atoms/cm$^2$ thick, were used in the neutron energy range from 70 to 800 ev. The output of the Oracle curve plotter for one of the gold runs is shown in Fig. 1. The ordinate of this plot is the background-corrected neutron transmission, and the abscissa is the time-analyzer channel number. These data indicate an increase in resolution by a factor of about 2 over that reported by Seidl *et al.*[1] The total cross section of iodine is plotted in Fig. 2. These data also show an increase in resolution by a factor of about 2 over that reported by Seidl *et al.* An elemental iodine sample $3.75 \times 10^{21}$ atoms/cm$^2$ thick and an NaI sample, in heavy water, which had an iodine thickness of $4.20 \times 10^{20}$ atoms/cm$^2$ were used for these measurements. These gold and iodine data have been analyzed for resonance parameters, and the results are listed in Table 1.

UNCLASSIFIED
PHOTO 43498

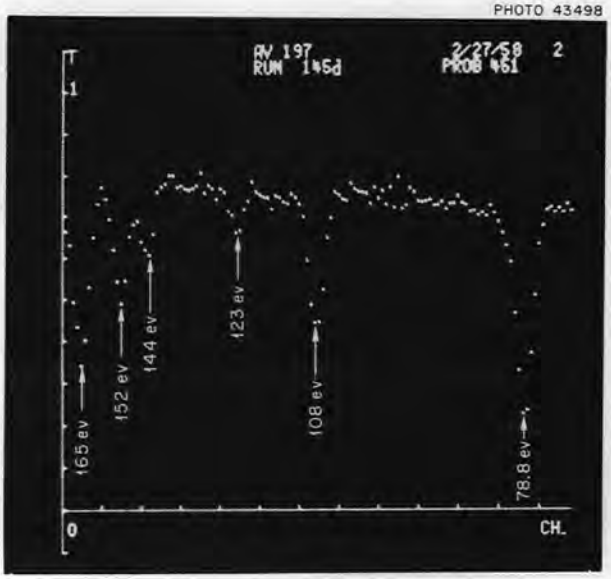


**Fig. 1. Curve Plot from Oracle of the Transmission of a 40-mil Gold Sample as a Function of Channel Number in the Energy Range 170 to 74 ev.**

[1]F. G. P. Seidl *et al.*, *Phys. Rev.* 95, 476 (1954).

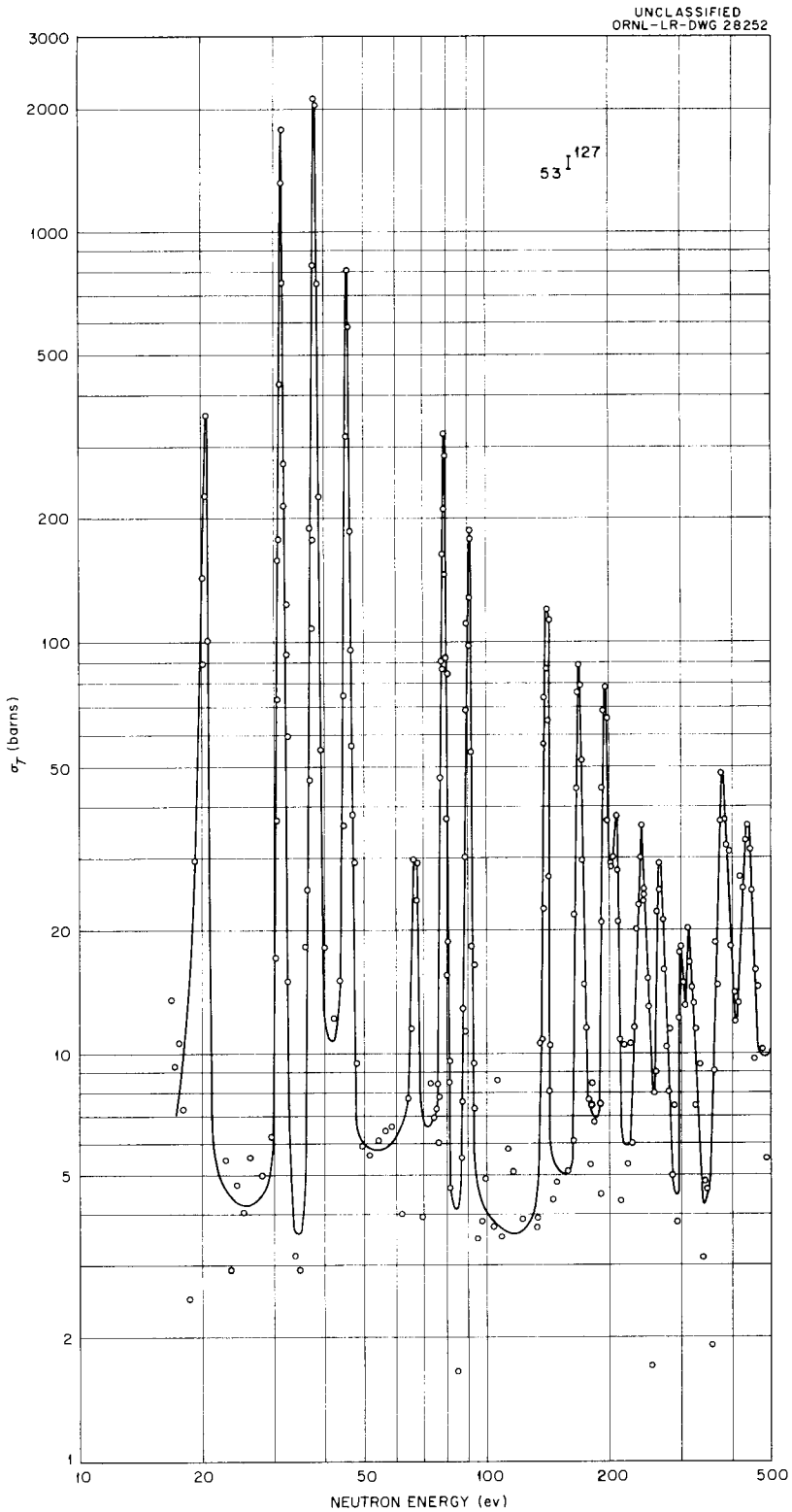


**Fig. 2. Total Neutron Cross Section of Iodine as a Function of Energy in the Energy Range 20 to 500 ev.**

Table 1. Neutron Resonance Parameters

| $Au^{197}$ | | | $I^{127}$ | | |
|---|---|---|---|---|---|
| $E_0$ (ev) | $2g\Gamma_n$ ($10^{-3}$ ev) | $2g\Gamma_n^0$ ($10^{-3}$ ev) | $E_0$ (ev) | $2g\Gamma_n$ ($10^{-3}$ ev) | $2g\Gamma_n^0$ ($10^{-3}$ ev) |
| 61.0 | 108 | 14 | 20.5 | 1.4 | 0.31 |
| 78.6 | 16 | 1.8 | 31.4 | 19 | 3.4 |
| 107.3 | 14 | 1.4 | 38.0 | 47 | 7.6 |
| 122.7 | 1.2 | 0.11 | 46.7 | 21 | 3.8 |
| 144.9 | 11 | 0.89 | 66.7 | 2.8 | 0.35 |
| 152.2 | 41 | 3.3 | 79.0 | 36 | 4.1 |
| 164.7 | 130 | 10 | 90.6 | 27 | 2.8 |
| 192.2 | 93 | 6.7 | 140.0 | 63 | 5.3 |
| 243 | 95 | 6.1 | 168.3 | 135 | 10 |
| 266 | 200 | 12 | 195.7 | 180 | 13 |

From these parameters, strength functions ($\overline{\Gamma}_n^0/D$) of $(1.2 \pm 0.3) \times 10^{-4}$ and $(1.3 \pm 0.3) \times 10^{-4}$, and average level spacings of $36 \pm 9$ and $36 \pm 10$ ev per spin state are assigned to gold and iodine, respectively.

Scattering measurements have been made with this spectrometer in order to determine the spin states of several resonances. For target nuclei with nonzero spin, the incident neutron can be absorbed or scattered by a resonance with its spin parallel or antiparallel to that of the target nucleus. For resonances which are predominantly scattering, the spin states can sometimes be determined from total cross-section measurements. However, if the scattering in a resonance is small, a scattering measurement must also be made in order to determine the spin state. This is because the scattering measurement determines $\Gamma_n/\Gamma$, whereas total cross-section measurements give $g\Gamma_n$ and $\Gamma$, where $\Gamma_n$ and $\Gamma$ are the neutron and total widths, and $g$ is the statistical weight. When the spin of the target nucleus is $\frac{1}{2}$, for $S$-wave neutrons the two values of $g$ are $\frac{1}{4}$ and $\frac{3}{4}$, and the spins of the states in the compound nucleus are 0 and 1. Total and scattering cross sections of natural tungsten have been measured with samples of various thicknesses in order to determine the spin states of several resonances in $W^{183}$. Resonances in $W^{183}$ were observed at energies of 7.6, 27.3, 46.5, 48.1, 102.4, 147, and 157 ev; the resonances in $W^{182}$, $W^{184}$, and $W^{186}$ which occur at energies of 18.9, 21.3, 115, 186, 219, and 252 ev were used for calibration, since $g = 1$ for these zero-spin target nuclei. The scattering at 90 deg and transmission of 300- to 15-ev neutrons from a 5-mil tungsten foil are shown in Fig. 3 as a function of time of flight. All the resonances shown in the transmission are also seen in the scattering cross-section curve. Calculations are being made in order to correct for any self-absorption of the scattered neutrons in getting out of the foil. Preliminary results indicate that the state corresponding to the 48.1-ev resonance has a spin of 0 and that those states corresponding to resonances at 27.3, 46.5, and 102.4 ev have spins of 1. Total and scattering measurements have also been made on several samples of silver, and the spin-state assignments agree with those measured at Harwell.[2]

[2] E. Bretscher, *Conference on Neutron Physics by Time-of-Flight, Held at Gatlinburg, Tennessee, November 1 and 2, 1956*, ORNL-2309, p 41 (June 17, 1957).

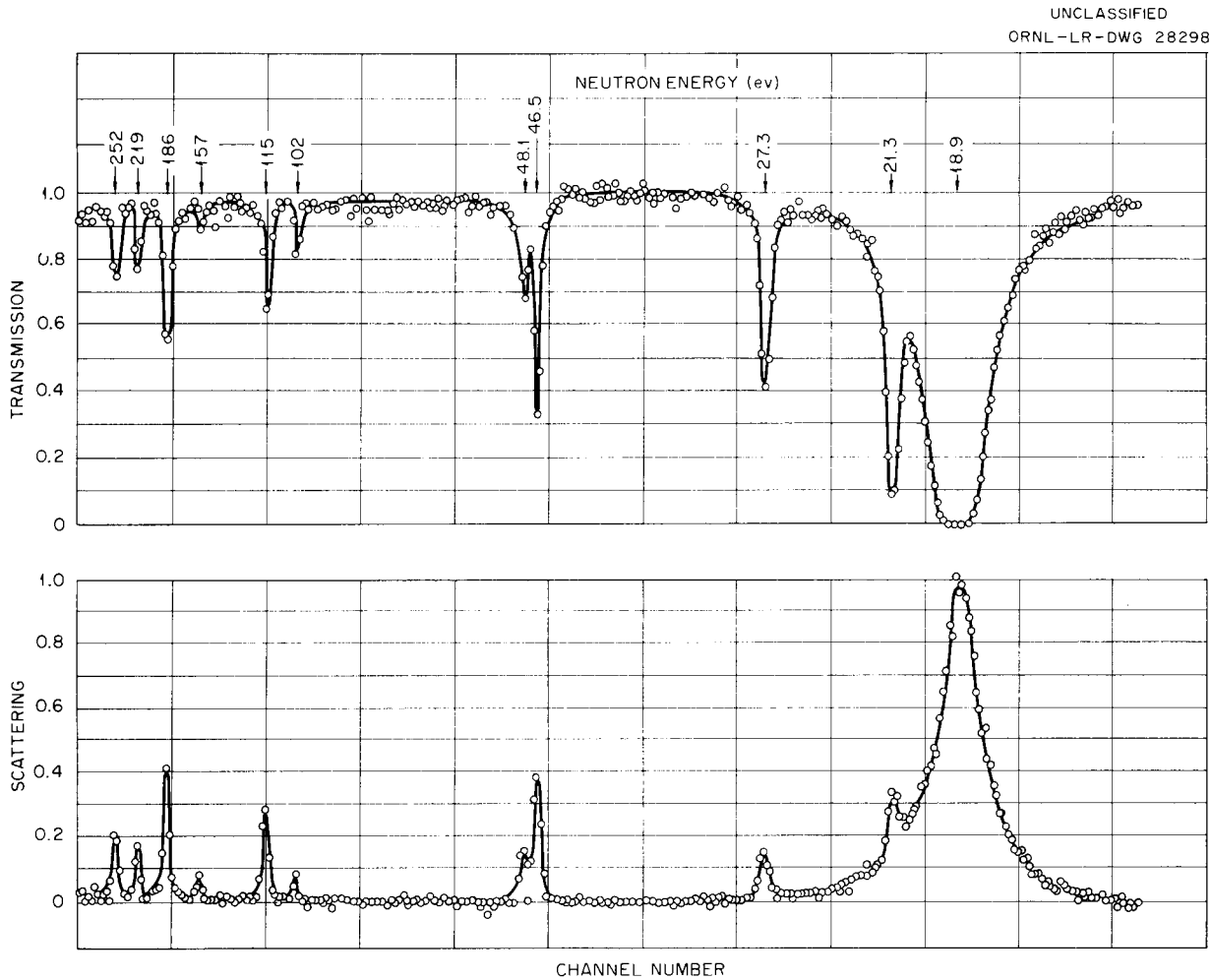


**Fig. 3. Transmission and Scattering Cross Section of a 5-mil Tungsten Foil as a Function of Time-of-Flight in the Energy Range 300 to 15 ev.**

---

## CROSS SECTIONS FOR $(p,n)$ REACTIONS IN CADMIUM AND TELLURIUM ISOTOPES

C. H. Johnson A. Galonsky C. N. Inskeep

The $(p,n)$ reaction cross section in a nucleus of intermediate mass is nearly equal to the cross section for forming the compound nucleus, providing that the proton energy is neither near the $(p,n)$ threshold nor near the top of the Coulomb barrier. In this energy region the proton sees a much larger barrier to emission from the compound nucleus than does the neutron, so that the compound nucleus, once formed, probably emits a neutron. If the formation of the compound nucleus is described by an average nuclear potential, the average $(p,n)$ cross section varies smoothly with proton energy, atomic weight, and atomic number. If this average potential were a very good approximation, isotopes of a single element would have nearly identical cross sections. The proton strength functions which depend essentially on the volume of the well would vary negligibly between adjacent isotopes, and the most significant isotope effect would be the relatively large change in Coulomb penetrability corresponding to the rather small change in radius with mass number.

Cross sections for $(p,n)$ reactions on five cadmium and four tellurium isotopes were measured from about 2.6 Mev, or from the $(p,n)$ threshold if greater than 2.6 Mev, to about 5.7 Mev. Protons were accelerated by the 5.5-Mv Van de Graaff. Separated isotopes of cadmium were electroplated on 10-mil platinum blanks by E. B. Olszewski of the Isotopes Division, and the tellurium isotopes were evaporated onto platinum blanks by B. J. Massey and J. C. Smith of the Isotopes Division. The properties of the targets are given in Table 1. The last column lists the expected $(p,n)$ thresholds as determined from Wapstra's tables.[1]

Neutrons produced in the target were detected by means of a 1.56-m-dia graphite sphere with $BF_3$ counters embedded near the surface.[2] This detector was chosen because it is a $4\pi$ detector and because it has nearly a flat response. The neutrons from the source will have energies up to the proton energy minus the threshold, that is, up to about 5 Mev for $Cd^{113}$. Macklin[2] has shown that the compensatory energy dependence of the fast leakage and thermal capture in the sphere produces a slow change in efficiency, so that the efficiency at 5 Mev is 93% of that at 25 kev. In our experiment the target holder flattened the curve by preferential absorption of low-energy neutrons. The ratio of efficiencies with and without the holder increased from 0.936 for a 25-kev Sb-Be neutron source at the center of the sphere to 0.958 for a 2.7-Mev (ref 3) Po-B source at the center. A crude linear extrapolation to 5 Mev indicates that the efficiency at 5 Mev is 97% of that at 25 kev. We assume an average efficiency for 0- to 5-Mev neutrons of 99% of that at 25 kev. Absolute calibration was made with the target in place by introducing an Sb-Be source at the center of the sphere. The source was standardized at the National Bureau of Standards and corrected for the antimony decay.[2]

Figure 1 gives a semilog plot of the cross section observed for $Cd^{116}$. Corrections have been made for the presence of other cadmium isotopes in the target. Backgrounds have been subtracted for neutrons produced by protons on the defining apertures and on the platinum target backing, and also for machine-independent counts. There remains a target contaminant which distorts the curve near 2 Mev. By comparison with preliminary cross sections which were obtained on 40 nuclei from $Cl^{37}$ to $Cs^{133}$, it is clear that the contaminant is

[1] A. H. Wapstra, *Physica* **21**, 385 (1955).

[2] R. L. Macklin, *Nuclear Instr.* **1**, 335 (1957).

[3] R. G. Cochran and K. M. Henry, *Rev. Sci. Instr.* **26**, 757 (1955).

**Table 1. Properties of the Cadmium and Tellurium Targets**

| Isotope | Abundance (at. %) | Areal Density ($mg/cm^2$) | Target Thickness at 3 Mev (kev) | Expected Threshold |
|---|---|---|---|---|
| $Cd^{111}$ | 89.9 | 1.10 | 56 | 1.68 |
| $Cd^{112}$ | 96.5 | 1.19 | 60 | 3.35 |
| $Cd^{113}$ | 87.3 | 1.82 | 90 | 0.64 |
| $Cd^{114}$ | 98.2 | 2.93 | 144 | 2.72 |
| $Cd^{116}$ | 93.8 | 1.92 | 94 | 1.43 |
| $Te^{125}$ | 65.5 | 0.389 | 18 Mev | 0.93 |
| $Te^{126}$ | 95.4 | 0.325 | 16 | 2.88 |
| $Te^{128}$ | 96.5 | 0.798 | 36 | 1.31 |
| $Te^{130}$ | 98.2 | 0.671 | 30 | 0.79 |

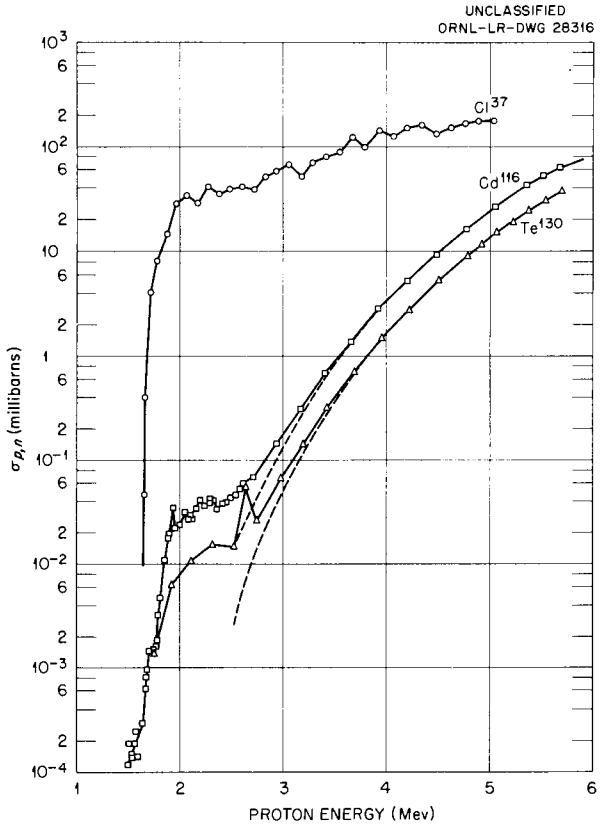


**Fig. 1. Cross Sections for $Cl^{37}$, $Cd^{116}$, and $Te^{130}$. The dashed curves for $Cd^{116}$ and $Te^{130}$ have been corrected for the Te background.**

$Cl^{37}$. Its cross section is also shown in Fig. 1. The general characteristics of the $Cl^{37}$ cross section and of the distortion to the $Cd^{116}$ curve are the same; the details differ because of differing target thicknesses. The corrected $Cd^{116}$ (dashed) curve was obtained by normalizing the curves near 2 Mev. Below 2.5 Mev the correction is too large to be meaningful.

Similar results were found for the four lighter cadmium isotopes. In each case the $Cl^{37}$ correction was less than for $Cd^{116}$, and it was negligible for $Cd^{114}$. The cross sections are so nearly the same that it is difficult to show the differences on a logarithmic plot. Instead, linear plots of the cross sections relative to the cross section of $Cd^{116}$ are shown in Fig. 2.

A threshold of 3.44 ± 0.02 Mev was observed for $Cd^{112}$, in good agreement with 3.35 Mev from

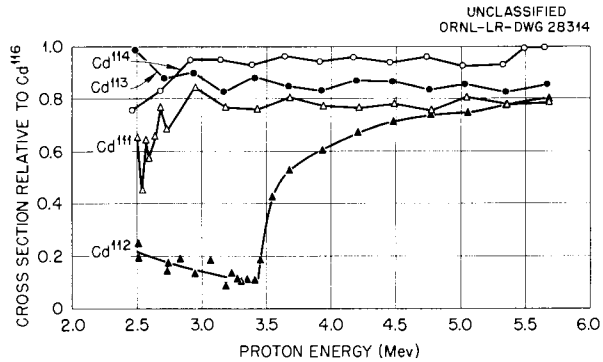


**Fig. 2. Cross Sections of $Cd^{111}$, $Cd^{112}$, $Cd^{113}$, and $Cd^{114}$ Relative to the Cross Section of $Cd^{116}$.**

Table 1. No evidence was found for a $Cd^{114}$ threshold near 2.7 Mev.

The yield below the $Cd^{112}$ threshold must be assigned to a target contaminant other than $Cl^{37}$. The spectroscopic analysis of the cadmium sample before electroplating showed high purity, so that the contaminant is probably a trace of a light element which is significant because of its large cross section. The likely impurities are potassium and copper. For either of these the background will be about 1% or less at 5.5 Mev. All five targets have similar chemical histories, so that all of them may have this impurity. The plot of ratios in Fig. 2 tends to cancel effects of impurities, but there remains some erratic behavior below 3 Mev.

For energies above 3 Mev the relative cross sections are in nearly constant ratios. The heavier isotopes, which are expected to have larger radii, show larger cross sections. The $Cd^{112}$ curve increases rapidly above its threshold and eventually crosses that of the $Cd^{111}$. These curves show that an average potential provides a very good description of the relative cross sections. Other effects, such as spin-orbit forces, are apparently quite weak.

These results disagree with those which Blaser *et al.*[4] obtained by using the activation method. Their $Cd^{112}$ curve is in rough agreement with ours; however, their $Cd^{111}$ curve is a factor of 2 higher and their $Cd^{114}$ curve is a factor of 3 lower.

[4] J. P. Blaser *et al.*, *Helv. Phys. Acta* **24**, 3 (1951).

Figure 1 also shows the cross section of $Te^{130}$. Here again a $Cl^{37}$ correction was required to give the final cross section (dashed curve). Since the $Te^{130}$ target was four times thinner than the NaCl target which was used for $Cl^{37}$, the $Cl^{37}$ yield in the $Te^{130}$ curve shows pronounced resonances.

Figure 3 shows the cross sections for $Te^{125}$, $Te^{126}$, and $Te^{128}$ relative to the cross section for $Te^{130}$ Above about 3 Mev, where the ratios become meaningful, the cross sections are nearly identical. Over most of the energy region the cross sections increase smoothly with mass number, just as is true for the cadmium isotopes.

Blaser *et al.*[4] also found the cross sections of $Te^{128}$ and $Te^{130}$ to be nearly identical; however, their cross sections lie about 40% below those in the present results.

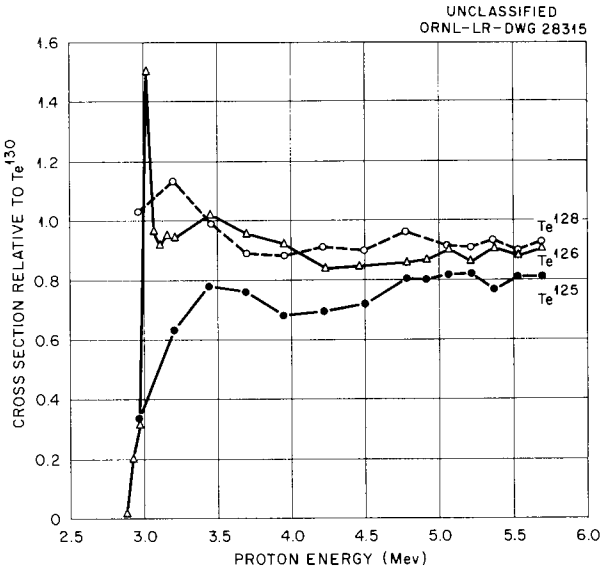


**Fig. 3. Cross Sections of $Te^{125}$, $Te^{126}$, and $Te^{128}$ Relative to the Cross Section of $Te^{130}$.**

## ABSOLUTE $(p,n)$ AND $(\alpha,n)$ CROSS SECTIONS FOR LIGHT NUCLEI

R. L. Macklin J. H. Gibbons

The graphite-sphere neutron detector, whose efficiency is known and is independent of neutron energy,[1] has been used to measure total cross sections for $(p,n)$ and $(\alpha,n)$ reactions in light nuclei. The lower-limit bombarding energies were chosen by reference to either the reaction threshold or to the lower limit of neutron-intensity detection. The upper limit on bombarding energy was bounded by a maximum neutron energy of about 4 Mev.

Reactions studied were $H^2(p,p')p,n$, $H^3(p,n)He^3$, $Be(p,n)B^9$, $B^{11}(p,n)C^{11}$, $C^{13}(p,n)N^{13}$, $C^{14}(p,n)N^{14}$, $F(p,n)Ne^{19}$, $Li^7(\alpha,n)B^{10}$, $Be(\alpha,n)C^{12}$, $B^{10}(\alpha,n)N^{13}$, $Si^{29}(\alpha,n)S^{32}$.

The $H^2(p,p')p,n$ reaction (Fig. 1) is very similar to the $H^2(n,p)n,n'$ reaction, for which calculations have been made.[2] Near threshold, Coulomb barrier effects are quite important, and a detailed comparison with the experiment should be instructive.

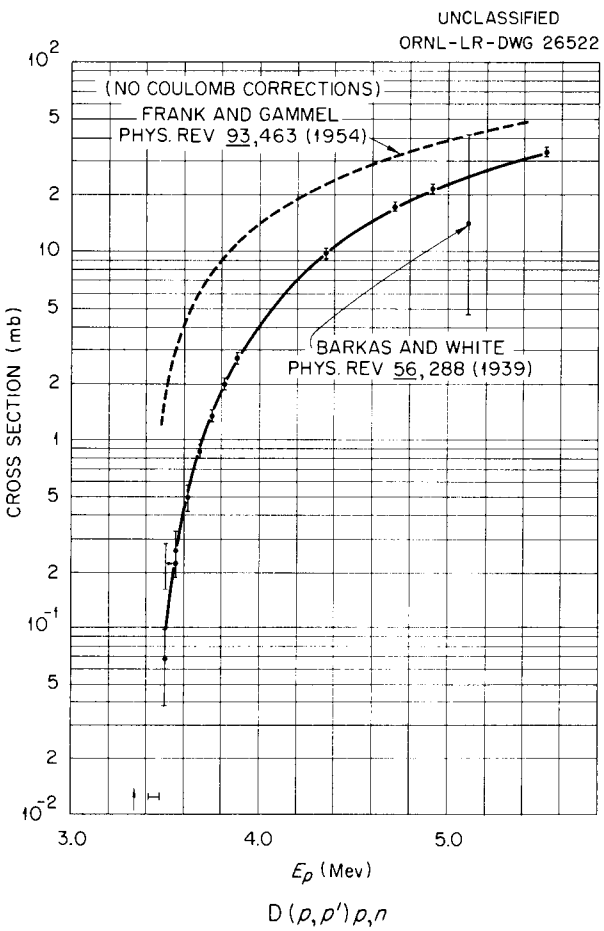


**Fig. 1. Cross Section for $H^2(p,p')p,n$ as a Function of Proton Energy. The difference between the measured cross section (solid line) and the calculated cross section (dotted line) is due to Coulomb effects, which were neglected in the calculation.[2]**

The $H^3(p,n)$ cross-section measurements have been extended to 5 Mev (Fig. 2). The $He^3(n,p)$ cross section derived from the reciprocity relation (Fig. 3) agrees quite well with directly measured values in the corresponding energy range.

The value of the cross section $N^{14}(n,p)C^{14}$ for 55-kev neutrons is an important number in calculations of heavy-element buildup in stars. The value of this cross section was determined by reciprocity from $C^{14}(p,n)N^{14}$ and was found to be 4 mb for $E_n = 55$ kev.

The $Li^7(\alpha,n)$ cross section (Fig. 4) has been compared with the inverse $B^{10}(n,\alpha)$ reaction up to the $Li^7(\alpha,n)B^{10*}$ threshold.

---

[1] R. L. Macklin, *Nuclear Instr.* 1, 335 (1957).

[2] R. M. Frank and J. L. Gammel, *Phys. Rev.* 93, 463 (1954).

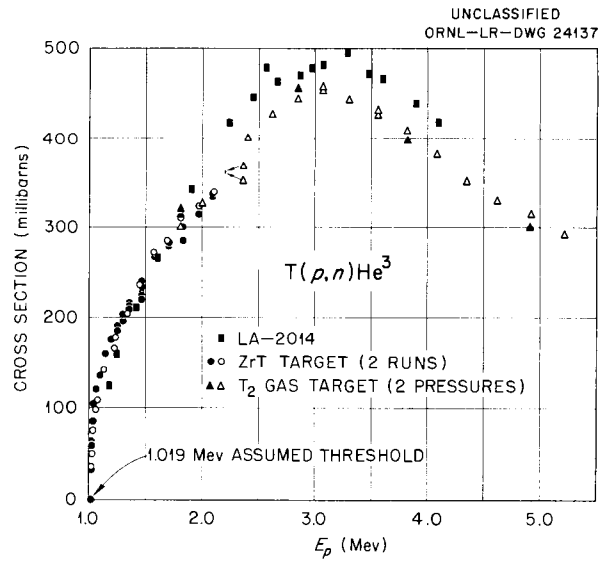


**Fig. 2. The $H^3(p,n)He^3$ Cross Section as a Function of Proton Energy.**

Results for $Si^{29}(\alpha,n)S^{32}$ show that the peaks observed in $S^{32}(n,\alpha)Si^{29}$ experiments[3,4] are groupings of several individual resonances.

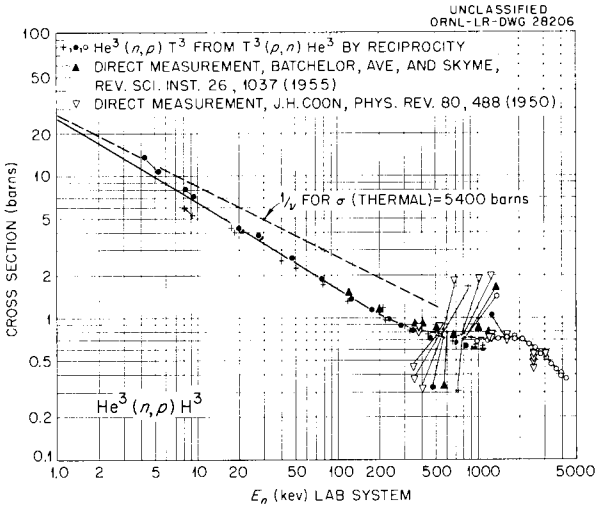


**Fig. 3. The $He^3(n,p)H^3$ Cross Section as a Function of Neutron Energy, as Determined from $H^3(p,n)He^3$ by Reciprocity. Agreement was also found between the directly measured value for thermal neutrons and the cross section computed by reciprocity from $H^3(p,n)$.**

An independent, absolute-intensity measurement of the NBS Ra-Be standard (No. 2) neutron source agrees, within 2%, with the NBS value.

[3]T. Hürlimann and P. Huber, *Helv. Phys. Acta* **28**, 33 (1955).

[4]H. W. Schmitt, *Bull. Am. Phys. Soc.* **3**, 37 (1958).

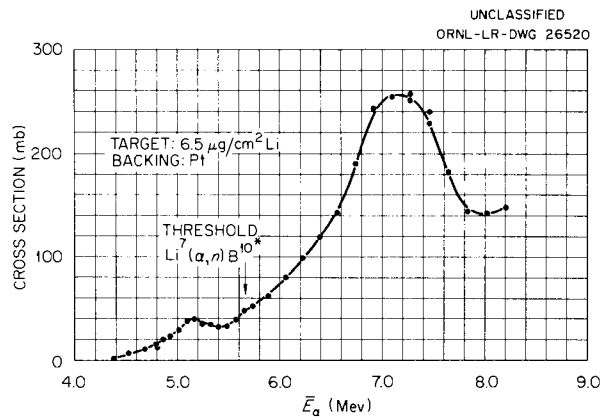


**Fig. 4. The $Li^7(\alpha,n)B^{10}$ Cross Section as a Function of Energy.**

## NEUTRON DIFFRACTION STUDY OF THE MAGNETIC PROPERTIES OF $MnI_2$

J. W. Cable M. K. Wilkinson E. O. Wollan W. C. Koehler

### INTRODUCTION

Anhydrous $MnI_2$ crystallizes in the hexagonal $CdI_2$ type of structure containing one molecule per unit cell. The $Mn^{++}$ ions occupy the (000) positions, and the two $I^-$ ions are located at $\pm(\frac{1}{3}\ \frac{2}{3}\ u)$, in which $u \cong 0.25$, $A_0 = 4.146$ Å, and $C_0 = 6.829$ Å. Neither specific-heat nor magnetic-susceptibility data at low temperatures have been reported for the compound. Nevertheless, antiferromagnetic order was expected to occur at helium temperatures by analogy with the isomorphous system $MnBr_2$, which orders antiferromagnetically below 2.16°K (ref 1). It was felt that a comparison of the magnetic order obtained in the two systems would lead to a better understanding of the types of magnetic interactions involved. The investigation was started with a powdered sample, but it soon became apparent that single-crystal studies would be required.

### EXPERIMENTAL RESULTS

#### Powdered Sample

This investigation was carried out on the anhydrous powder by using a neutron wavelength of 1.222 Å. The sample was enclosed in a cylindrical cell which also served as the bottom of the liquid-helium container. This placed the sample in direct contact with the bath and ensured temperature equilibrium for the system. Diffraction patterns

[1]E. O. Wollan, W. C. Koehler, and M. K. Wilkinson, *Phys. Semiann. Prog. Rep. Sept. 10, 1957*, ORNL-2430, p 56.

were taken at 298, 4.18, and 1.32°K. The room-temperature pattern is characteristic of a paramagnetic substance and consists of the nuclear reflections superimposed on a background which decreases in intensity with increasing scattering angle. In the pattern taken at 4.18°K the background no longer exhibits this form-factor dependence. Instead there are broad diffuse peaks, one extending from 3 to 8 deg in scattering angle, and another from 15 to 28 deg. These peaks are shown in curve *a* of Fig. 1, in which is presented the difference in scattered intensity from the sample at 4.18°K and at room temperature. This so-called "critical" scattering is characteristic of systems in which short-range order exists, and in this case indicates the presence of short-range antiferromagnetic order. The width of the peak at the 5.5-deg scattering angle corresponds to clusters of ordered spins with an average diameter of about 22 Å.

In the 1.32°K pattern, Bragg reflections are observed at superlattice positions, indicating that at this temperature long-range antiferromagnetic order has been attained. These reflections are shown in the 1.32-298°K difference pattern in curve *b* of Fig. 1. Also evident in this pattern is a decrease in the paramagnetic scattering, which is shown by the negative background in the difference pattern. This paramagnetic scattering level corresponds to a magnetic moment of 4.6 Bohr magnetons or a spin of 2.3, in good agreement with the expected value of $\frac{5}{2}$ for the $Mn^{++}$ ion. The intensity of the largest of the reflections at small scattering angles was taken as a function of temperature – a calibrated carbon resistance suspended into the pumped helium bath being used to measure the temperature. The resulting curve shows that the transition from a state of short-range order to that of long-range order is unusually sharp, with an indicated transition temperature of 3.48°K. This transition temperature is only approximate, since the variation of the critical scattering with temperature has not been determined. The peaks in this pattern, especially at large scattering angles, are unresolved and could not be indexed on any simple cell. It was decided to continue the investigation by using a single crystal.

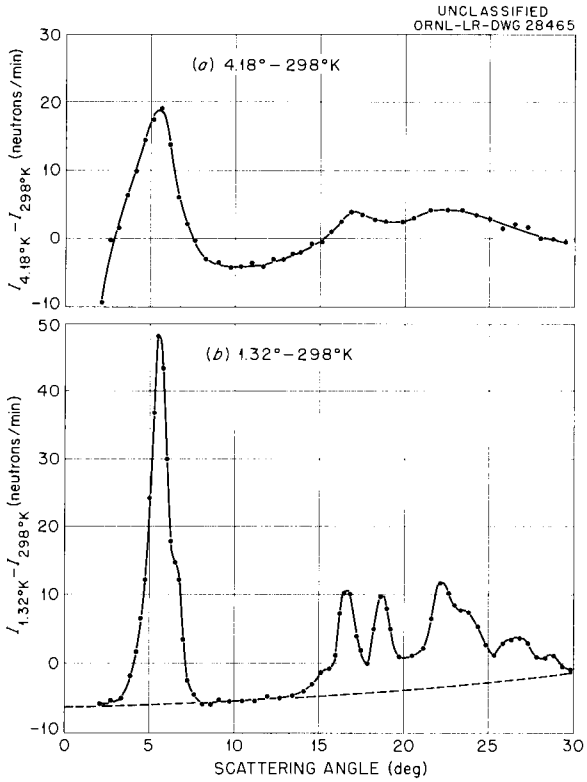


**Fig. 1. Temperature Difference Patterns from $MnI_2$ Powdered Sample.**

## Single Crystal

The $MnI_2$ single crystal was grown from a melt of the anhydrous material. The sample specimen was cut in the shape of a flat disk $\frac{5}{16}$ in. in diameter and $\frac{1}{8}$ in. thick, with (00*l*) planes forming the top and bottom of the disk. The specimen was mounted in the low-temperature goniometer[2] with the *c* axis parallel to the horizontal rotation axis. By using this goniometer, any set of crystal planes can be brought into position for Bragg reflection by the proper combination of rotations about the vertical and horizontal axes. The rotation about the vertical axis ($\alpha$) necessary to bring an (*hkl*) plane into the reflection position is directly related to the angle that the plane makes with the *c* axis, while the rotation required about the horizontal axis ($\beta$) depends on the angular position of the plane about the *c* axis of the crystal. The geometrical location in the crystal lattice of the reflecting plane can thus be directly determined from the values of $\alpha$, $\beta$, and the *d* spacing observed for that plane.

[2] E. O. Wollan *et al.*, *Phys. Semiann. Prog. Rep. Sept. 10, 1956*, ORNL-2204, p 49.

The magnetic reflection observed in the powder pattern at a scattering angle of 5.5 deg was the first to be studied. The intensity of this reflection is shown as a function of temperature in Fig. 2. As in the powder data, a very sharp transition is observed, with a Néel temperature of 3.40°K. The dashed curve in Fig. 2 is the square of a Brillouin function which has been normalized to fit the data below 3.3°K. The departure of the observed curve from the squared Brillouin curve may be interpreted as a delay in the spontaneous sublattice magnetization, but the reason for this delay is not understood. This effect has previously been observed only in the case of $MnBr_2$ and is undoubtedly associated with the large amount of short-range order observed in these materials.

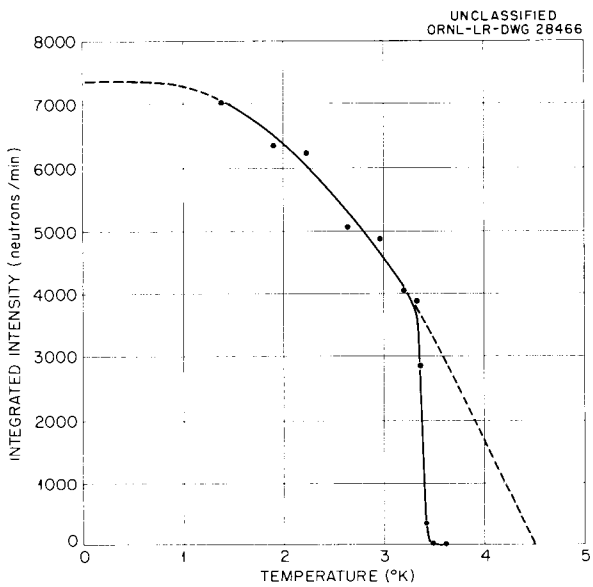


**Fig. 2. Temperature Dependence of the Largest Magnetic Reflection from an $MnI_2$ Single Crystal.**

This reflection was found to have a $\beta$ angle corresponding to the $(h0l)$ nuclear reflections and to be repeated in 120-deg intervals about the $c$ axis. Several other reflections with the same $\beta$ angle were found at larger scattering angles, and they also exhibited threefold symmetry. Another series of reflections with $\beta$ angles corresponding to $(0kl)$ nuclear reflections was found, and these reflections also showed threefold symmetry about the $c$ axis. Such apparent threefold symmetry was found, in the case of $MnI_2$ and $MnCl_2$, not to be the symmetry of the magnetic unit cell but instead the symmetry of the domains in which the magnetic unit cells possessed onefold symmetry. In such cases it is necessary to apply a magnetic field to the sample in order to determine whether the observed symmetry is that of the magnetic unit cell or of the structure domains. In antiferromagnets the magnetic moments tend to be aligned perpendicularly to an applied magnetic field. In the structure domain situation the application of a magnetic field favors that domain with moments most nearly perpendicular to the field. With increasing field this domain grows at the expense of the others, until at saturation the entire crystal consists of a single domain. If this single domain were to remain frozen in after removal of the field, then the threefold symmetry would no longer be observed. In the case of a magnetic unit cell with threefold symmetry, an increased intensity can also be obtained by application of a magnetic field along the scattering vector of a reflecting plane. This is due to the dependence of the intensity on $q^2 = 1 - (\overline{\epsilon}\cdot\overline{\kappa})^2$, where $\overline{\epsilon}$ is the unit scattering vector, and $\overline{\kappa}$ is a unit vector parallel to the moment orientation. This reorientation does not, however, destroy the threefold symmetry as it does in the structure domain case.

In zero field those reflections with threefold symmetry about the $c$ axis ($\beta$ = 355, 115, 235 deg) were of equal intensity. On application of the field along the scattering vector of, for example, the 235-deg reflection, the intensity increased with increasing field, reaching saturation at 6.6 kilogauss with three times the zero field intensity. Approximately 90% of this increased intensity was retained after removal of the field. With the moments effectively frozen into this aligned state and the field removed, the other two planes (355 and 115 deg) were rotated into their reflecting positions and were found to be a factor of 10 less intense than the 235-deg reflection. This result is incompatible with a magnetic unit cell of threefold symmetry and is attributed to unit cells of onefold symmetry and structure domains which grow (in zero field) with equal probability along three of the hexagonal crystal axes.

The field-induced single-domain crystal was used in scanning for additional reflections and in checking reflections predicted by the unit cell models. The two small scattering-angle magnetic reflections have $\beta$ angles corresponding to $(h0l)$ and $(0kl)$ nuclear reflections, and in zero field repeat in

120-deg intervals in $\beta$. Once the single-domain crystal has been prepared, each reflection has only onefold symmetry, and the two reflections occur 180 deg apart in $\beta$, for example, at 235 and 55 deg. If the lattice vector of the magnetic unit cell which is directed perpendicular to the hexagonal [0*k*0] direction is called $a_2$, then these reflections are of the (0*kl*) and (0$\bar{k}l$) type, respectively. The *d* spacings and $\alpha$ angles of four reflections of this type yield reflecting planes which can best be indexed as the (031) and (0$\bar{3}$1) of a cell containing 16 atoms in projection along the $a_2$ axis. A triclinic cell, with lattice vectors

$$a_1 = A_1 \ ,$$

$$a_2 = 8A_1 + 16A_2 \ ,$$

$$a_3 = 2A_1 + 3A_2 + C_0 \ ,$$

has been devised on the basis of which a total of 36 observed magnetic reflections, including 20 of the (*hkl*) type, has been successfully indexed. Assignment of moment orientations, as well as verification that this cell is the basic repeating unit, must await additional quantitative data.

---

## NEUTRON DIFFRACTION INVESTIGATIONS OF $MnCl_2$ IN EXTERNAL MAGNETIC FIELDS

M. K. Wilkinson
J. W. Cable
E. O. Wollan
W. C. Koehler

Neutron diffraction measurements[1] made on single crystals of $MnCl_2$ at temperatures as low as 1.38°K have confirmed the existence of the two antiferromagnetic ordering transitions which were suggested by earlier measurements of the specific heat[2] and magnetic susceptibility.[3] The diffraction data in the absence of an external magnetic field show a Néel temperature of 1.96°K and suggest that the transition from one antiferromagnetic structure to the other takes place over a small temperature interval (about 0.03°K) with an average value of 1.82°K. Both magnetic structures consist of large complex unit cells which grow with equal probability as structure domains along axes within the base plane of the hexagonal chemical unit cell.

Reflections from the high-temperature structure have been explained by use of an orthorhombic unit cell which forms domains along three of the hexagonal directions. The reflections from the low-temperature structure require a more complex domain pattern that has two very similar monoclinic unit cells, each of which grows along these three hexagonal directions. The magnetic structures which have been suggested from the neutron diffraction results have similar characteristics in that both have the atomic magnetic moments arranged in bands of ferromagnetism which are tilted at an angle of about 57 deg with respect to the hexagonal *c* axis. The widths of these bands are almost exactly the same for the two structures, and the primary difference appears to be the direction of the antiferromagnetic axis within the layers of manganese atoms.

The existence of antiferromagnetic structure domains has been clearly demonstrated[4] in $MnBr_2$ by the transformation of the domain pattern in an external magnetic field, and a similar behavior is observed for the high-temperature structure of $MnCl_2$. Figure 1 shows the variation in intensity of one of the (013) magnetic reflections from $MnCl_2$ at 1.85°K when an external magnetic field is applied. The sketches within the figure illustrate the manner in which the domains must change with field to enable explanation of these results. In zero field the crystal is divided almost equally into the three types of domains, and the intensity of the (013) reflection from each of these domains is about equal to that shown for domain (c).

---

[1] M. K. Wilkinson *et al.*, *Phys. Semiann. Prog. Rep. Sept. 10, 1957*, ORNL-2430, p 65.

[2] R. B. Murray, *Phys. Rev.* 100, 1071 (1955).

[3] R. B. Murray and L. D. Roberts, *Phys. Rev.* 100, 1067 (1955).

[4] E. O. Wollan, W. C. Koehler, and M. K. Wilkinson, *Phys. Rev.* (in press).

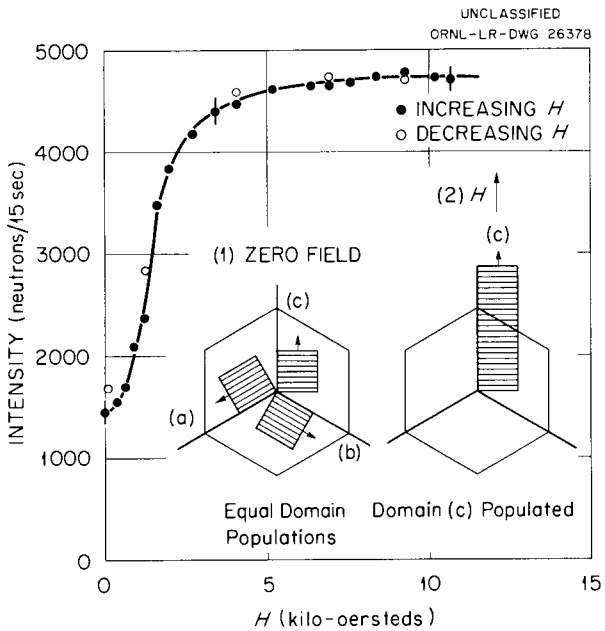


**Fig. 1. Variation of the (013) Magnetic Reflection from $MnCl_2$ at 1.85°K with an External Magnetic Field.**

However, when an external field is applied parallel to the scattering vector of the (013) reflecting planes in domain (c), the intensity of this reflection is increased by a factor of about 3. This intensity increase is interpreted as a transformation of the entire crystal into a domain of this type. Such a transformation would take place because the field direction is perpendicular to the axis of antiferromagnetism in domain (c), thereby making this particular domain stable under these conditions.

Unlike the case of $MnBr_2$, it is not possible to "lock in" the structure produced by the external field, and the intensity decreases to about the original zero-field value when the external field is removed. Since the single domain cannot be maintained in zero field and since experimental conditions permit the magnetic field to be applied only in a direction closely parallel to the scattering vector of the reflecting planes under observation, it is not possible to examine reflections from the domains which are diminished. Hence the complete behavior of the domain pattern cannot be examined, and the interpretation which has been described arises from a correlation of the observed data with the known transformation which occurs in $MnBr_2$.

The domain pattern in the low-temperature magnetic structure also is changed when an external magnetic field is applied, but the details of this transformation are not understood. Figure 2 shows the intensity variation of one of the (013) magnetic reflections from the low-temperature structure when an external magnetic field is applied nearly parallel to the scattering vector. The intensity of this reflection increases somewhat more than by a factor of 3, and then it suddenly drops to zero. When the field is removed, the intensity remains almost twice as high as the original intensity in zero field, which indicates that part of the domain transformation which occurred for small external fields still remains. A systematic investigation has been performed to determine this domain behavior by measuring the relative intensities of the (013) reflections from all domains before and after the magnetic field was applied at various angles with respect to the crystal. These experiments suggest either a very complex domain behavior or a magnetic structure which is somewhat different from the one which is indicated from the zero-field measurements. Unfortunately, the experiments do not

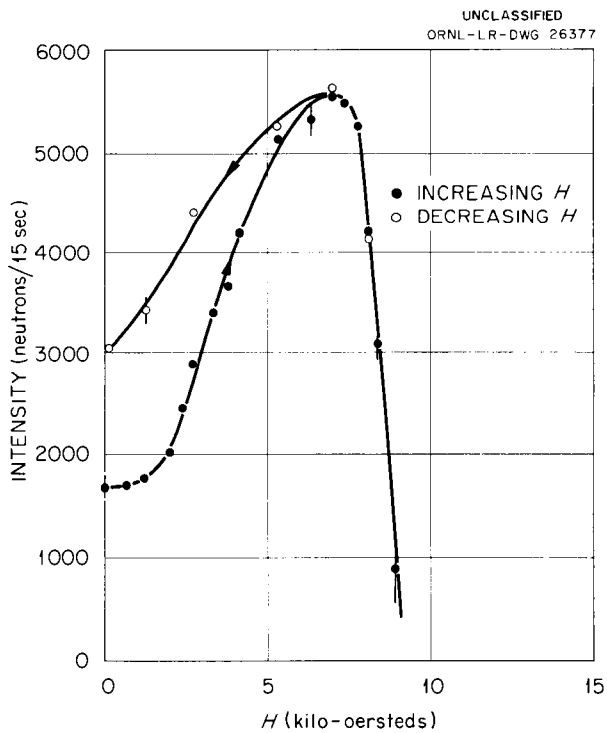


**Fig. 2. Variation of the (013) Magnetic Reflection from $MnCl_2$ at 1.38°K with an External Magnetic Field.**

appear to be conclusive with respect to either possibility.

The sudden decrease in the intensity of the (013) reflection from the low-temperature structure with an applied field of about 8 kilo-oersteds, as shown in Fig. 2, is accompanied by a sudden increase of intensity at the proper angular position for the (013) reflection of the high-temperature structure. This, of course, indicates that the high-temperature structure can be stabilized below 1.82°K in the presence of an external magnetic field. In order to check this possibility, the geometry of the apparatus was adjusted, exactly as described previously for measuring the transition temperatures,[1] and these temperatures were determined with different values of an external magnetic field. The effects of the field in stabilizing the high-temperature structure are shown in Fig. 3, and it is apparent that the low-temperature transition is depressed considerably when a magnetic field is applied. Furthermore, there is a slight change in the Néel temperature for the high-temperature structure under these conditions. In zero field this Néel temperature is 1.96°K, while for the three values of the magnetic field which were used, it has increased to 1.98°K.

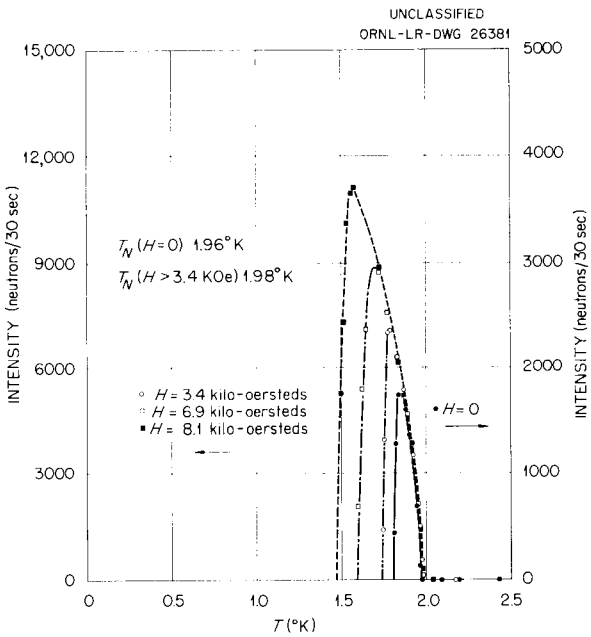


**Fig. 3. Temperature Variation of the (013) Magnetic Reflection from the High-Temperature Magnetic Structure of $MnCl_2$ in External Magnetic Fields.**

In Fig. 3 the ordinate scale is so adjusted that neutron intensities taken for data with an external field are three times those for data with zero field, since the external field stabilizes a single domain of this structure.

From these experiments it is possible to obtain a magnetic phase diagram for $MnCl_2$ in the region of available magnetic fields and sample temperatures. This phase diagram is shown in Fig. 4, where the values of magnetic field correspond to fields applied parallel to the scattering vector of the (013) reflecting planes. The solid lines represent the experimental data, and the dashed lines do not have any significance, but merely suggest possible extrapolations of the measurements. The transition from the paramagnetic state to the high-temperature antiferromagnetic structure was always sharply defined, but the transition from one magnetic structure to the other appeared to take place over a temperature interval which became large for higher values of the magnetic field. The geometry of the apparatus does not permit a similar investigation to determine the change in transition temperature with the direction of applied field, since the field direction is restricted. However, experiments performed on other types of (*hkl*) magnetic reflections suggested that the magnetic field which was important in stabilizing the high-temperature structure below 1.82°K was the component parallel to the *b* axis of the high-temperature orthorhombic magnetic cell (parallel to the *a* axis of the hexagonal chemical cell). Therefore, magnetic fields applied in this direction would have been only about 54% of the values shown in the figure.

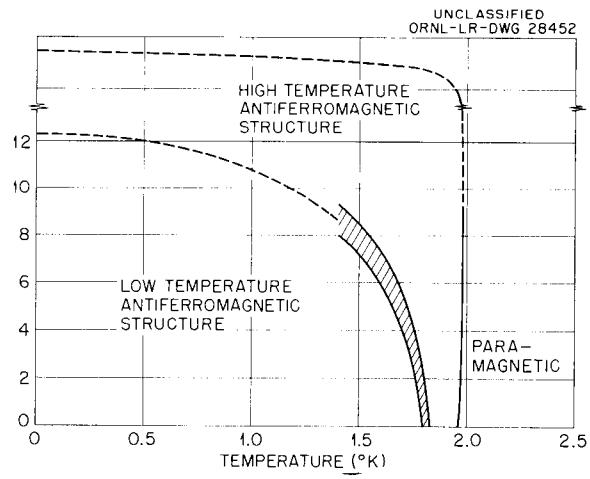


**Fig. 4. Magnetic Phase Diagram for $MnCl_2$.**

# NEUTRON DIFFRACTION OBSERVATIONS ON METALLIC CERIUM AND METALLIC NEODYMIUM

W. C. Koehler E. O. Wollan H. R. Child M. K. Wilkinson

In recent years, following the development of methods for the extraction of pure rare-earth salts[1] and for the preparation of pure rare-earth metals,[2] these elements have become available in such sufficient quantities that their properties are now being studied in a systematic and detailed manner.[3] With each new measurement it is becoming increasingly apparent that these materials are extremely complex.

Certain of the rare-earth metals, namely, those with reasonable capture cross sections for thermal neutrons, are amenable to study by neutron diffraction methods. So far only metallic erbium has been investigated in detail by these techniques.[4] This report is concerned with some observations, on the metals cerium and neodymium, which must as yet be considered as only preliminary.

## METALLIC CERIUM

The magnetic and thermal properties of metallic cerium are among the most singular of those of the rare-earth metals, and are evidently intimately related to its equally singular structural properties. It has been known for some time that cerium exists in a number of crystallographic states, but until recently little has been known about the detailed nature of these states or of the kinetics of their transformations. A study of these problems has now been initiated.[5]

Briefly, three crystallographic forms have been found in the temperature range from 77 to 450°K, the relative concentrations of which, at a given temperature, are markedly dependent upon the previous thermal history of the sample. At room temperature a face-centered cubic phase with $a_0$ = 5.15 Å is stable in a previously uncooled annealed sample. Just below 273°K a transformation to a double-hexagonal close-packed structure sets in, and at still lower temperatures the remainder of the face-centered cubic phase transforms into a collapsed face-centered cubic phase with $a_0$ = 4.85 Å at 77°K.

The several transitions are characterized by broad hysteresis. For example, the start of the f.c.c.-to-h.c.p. transformation occurs at 263 ± 5°K. For the reverse transformation the corresponding temperature is found to be 363 ± 5°K. Similarly, the f.c.c.–to–$\alpha$-f.c.c., where $\alpha$ denotes the collapsed phase, starts at 103 ± 5°K, and the reverse transformation starts at 170 ± 5°K. At 77°K all three phases were present in the above-mentioned annealed sample. If a sample containing only the face-centered cubic phase at room temperature is cold-worked and then cooled, the transition to the hexagonal phase is suppressed or even in some cases eliminated, at least at temperatures down to 77°K.

The specific heat[6,7] and magnetic susceptibility[8] of metallic cerium have been shown to exhibit anomalies which are strongly dependent on the previous thermal history and probably also on impurity concentration. In some specimens there is observed a broad high-temperature anomaly which is attributed to the transformation to the collapsed phase. A suggestion has been made that this transformation is associated with the promotion of $4f$ electrons to a $5d$ valence band. At low temperatures, at about 12.5°K, in some specimens, a second anamoly is observed which has been attributed by Lock[8] to a transition to an antiferromagnetically ordered arrangement of cerium ion moments.

---

[1] F. H. Spedding and J. E. Powell, *J. Metals* 6, 1131 (1954).

[2] F. H. Spedding and A. H. Daane, *J. Metals* 6, 504 (1954).

[3] See, for example, the recent review article "Some Physical Properties of the Rare Earth Metals," by F. H. Spedding *et al.*, in *Progress in Low Temperature Physics*, vol II, Interscience, New York 1957.

[4] W. C. Koehler and E. O. Wollan, *Phys. Rev.* 97, 1177 (1955).

[5] C. J. McHargue, H. L. Yakel, Jr. and L. K. Jetter, ORNL-2422, p 207 (Nov. 29, 1957) (classified).

[6] D. H. Parkinson, F. E. Simon, and F. H. Spedding, *Proc. Roy. Soc. (London)* 207A, 137 (1951).

[7] D. H. Parkinson and L. M. Roberts, *Proc. Phys. Soc. (London)* 70B, 471 (1957).

[8] J. M. Lock, *Proc. Phys. Soc. (London)* 70B, 566 (1957).

In view of these interesting results we have begun a neutron diffraction study of metallic cerium in collaboration with McHargue, Yakel, and Jetter,[9] to whom we are indebted for the preparation of carefully controlled specimens. The neutron diffraction method is advantageous in this case, since the magnetic scattering properties can be investigated under conditions in which the crystallographic makeup of the sample is continuously monitored.

One sample, previously annealed and uncooled, has now been studied at temperatures ranging from room temperature to 4.2°K and over two cycles. At room temperature only the normal f.c.c. phase is observed, the nuclear intensities being superimposed upon a characteristically angularly dependent paramagnetic scattering background. When first cooled to 77°K, nearly all the normal f.c.c. phase was observed to have transformed into the h.c.p. and $\alpha$-f.c.c. phases, in agreement with the x-ray results of McHargue, Yakel, and Jetter. The major phase is the h.c.p. with an estimated concentration of 70%. A slight diminution of the diffuse scattering level was also observed which would be expected if a fraction, about 20%, of the cerium atoms had transformed to the $5d$ configuration. On further cooling to 4.2°K the unexpected result was found that the concentration of the collapsed cubic phase had increased to about 60%, with a corresponding reduction in the concentration of the h.c.p. phase. At neither of these two temperatures was there any evidence for a collapsed hexagonal phase.

At the lowest temperature the background scattering level was markedly decreased, corresponding to the promotion of a higher percentage of $4f$ electrons to the $5d$ valence band. At this temperature, which is well below that of the low-temperature anomaly, evidence for long-range magnetic ordering was sought, but no superstructure reflections with measurable intensity were observed. It is not possible at this stage of the investigation to make definite statements concerning the existence or nonexistence of antiferromagnetism in this specimen. It appears, however, that magnetic ordering, if any, should occur between atoms in the h.c.p. phase, which at this temperature is present to about 35%. In addition, one may expect that the free atom ground state $4f^1(^2F_{5/2})$ will be split by crystalline field interactions, and if the lowest state in the field is a "low-spin" state as is the case for a cubic field,[10] the magnetic intensities may be too small to be detected.

When the specimen was warmed to 77°K the diffraction pattern remained essentially unchanged, indicating a very broad hysteresis in the transformation of collapsed cubic to hexagonal phases, and the low background scattering level suggests that roughly the same proportion of ions have a $4f$ configuration at this temperature as at 4.2°K. On further warming to room temperature the collapsed cubic phase transformed to h.c.p. and to normal f.c.c., with an attendant increase in the paramagnetic scattering level. In a second cycle the pattern at 77°K was essentially the same as it had been in the first cooling, but at 43°K the concentration of the h.c.p. phase was found to be reduced to about 55%.

In summary it is tentatively concluded that for a previously unannealed specimen the transformation to the $\alpha$-f.c.c. phase starts first at the expense of the residual normal f.c.c. phase and proceeds at lower temperatures, but not to completion, at the expense of the h.c.p. phase. It is further suggested that the antiferromagnetic anomaly observed by Lock might be associated with, in his samples, an appreciable concentration of normal f.c.c. metal. To test this, work is now in progress on a severely cold-worked specimen.

As we have already mentioned, it has been shown that cold work suppresses the f.c.c.-to-h.c.p. transformation, and it is indicated by Lock's results that repeated thermal cycling tends to suppress the f.c.c.–to–$\alpha$-f.c.c. transformation. With such a cold-worked and thermally cycled specimen one may hope to retain at low temperatures the f.c.c. phase with which the antiferromagnetic state is presumed to be associated.

### NEODYMIUM

The neutron diffraction experiments on metallic neodymium must also be considered to be in an early stage of development, even though the problem has been attacked at intervals extending over some four years. The difficulties introduced by crystallographic phase transformations are not

[9]Metallurgy Division.

[10]T. Murao and T. Matsubara, *Progr. Theoret. Phys. (Kyoto)* 18, 215 (1957).

present for this material. At room temperature, neodymium crystallizes in the double-hexagonal close-packed structure, which is retained to 4.2°K as evidenced by the neutron diffraction data. Specific heat measurements[6] on neodymium had shown two peaks occurring at 19°K and at 7.5°K, and although these results could be qualitatively interpreted in terms of a crystal field splitting and subsequent level repopulation, the nature of the anomalies were such as to suggest a cooperative phenomenon.

Our early neutron diffraction data, and those of subsequent experiments, have revealed the existence of an antiferromagnetically ordered state at 4.2°K. The magnetic intensities were very weak, and only a few reflections were observable in the patterns. With these limited data, however, a possible structure in which the moments are parallel in the hexagonal layers with alternation in the sequence ++−− in adjacent layers was suggested.[11]

Subsequently, a single crystal of metallic neodymium, on which magnetic measurements had been made,[12] was made available to us by F. H. Spedding. Study of this crystal confirmed the existence of an antiferromagnetic state, but the magnetic structure, as yet unsolved, is much more complex than the simple layer structure first suggested. Unfortunately, even with the single crystal, the magnetically scattered intensities are so low that the complete investigation of this problem with the neutron flux presently available presents formidable difficulties. In view of the availability in the near future of much higher fluxes, the further study of this problem has been deferred until the ORR is in operation.

[11] W. C. Koehler and E. O. Wollan, *Pittsburgh Diffraction Conference, 1953.*

[12] D. R. Berhendt, S. Legvold, and F. H. Spedding, *Phys. Rev.* 106, 723 (1957).

## SINGLE-CRYSTAL NEUTRON DIFFRACTION INVESTIGATIONS OF $CoCl_2$ AND $FeCl_2$

M. K. Wilkinson J. W. Cable E. O. Wollan W. C. Koehler

### INTRODUCTION

Neutron diffraction measurements[1] made on powdered samples of $FeCl_2$ and $CoCl_2$ at temperatures as low as 4.2°K have established the antiferromagnetic structures existing in these compounds below about 25°K. In both compounds the magnetic moments within a metal layer are coupled ferromagnetically, and adjacent layers have the moments aligned antiparallel. In $CoCl_2$ the moments were found to be within or nearly within the layers, whereas in $FeCl_2$ they were oriented parallel to the *c* axis of the hexagonal unit cell. Furthermore, small-angle neutron-scattering investigations[2] at sample temperatures near the Néel transitions have shown that the ferromagnetic interaction between atomic moments within a layer is much larger than the antiferromagnetic interaction between atoms in adjacent layers. However, the plate-like structure of the small particles caused considerable preferred orientation in the powdered specimens which prevented a good determination of the value of the atomic magnetic moments from the coherent reflections. Similarly, it was not possible to establish, closer than almost 30 deg, the orientation of the moments in $CoCl_2$ with respect to the plane of the layers. Consequently, one purpose of the single-crystal measurements was to better determine the size and orientation of the magnetic moments existing in these structures.

A second reason for these investigations was the need to study the behavior of these antiferromagnetic structures in an external magnetic field. Magnetic measurements made on powdered samples of $FeCl_2$ and $CoCl_2$ by Starr, Bitter, and Kaufmann[3]

[1] M. K. Wilkinson and J. W. Cable, *Phys. Semiann. Prog. Rep. March 10, 1956*, ORNL-2076, p 44.

[2] M. K. Wilkinson and J. W. Cable, *Phys. Semiann. Prog. Rep. Sept. 10, 1956*, ORNL-2204, p 53.

[3] C. Starr, F. Bitter, and A. R. Kaufmann, *Phys. Rev.* 58, 977 (1940).

showed that the magnetization values below the transition temperatures are inconsistent with the normal behavior of antiferromagnetic materials. For both compounds, magnetic fields of only about 15,000 oersteds were required to attain a large fraction of the expected saturation magnetization, whereas the exchange field to be expected in antiferromagnetic materials with a Néel temperature near 25°K is a much larger value. Recent susceptibility measurements[4] made on single-crystal specimens are in good qualitative agreement with these early results on powders, but, in addition, they show that the large values of magnetization in relatively small fields can only be achieved when the field is applied parallel to the $c$ axis of $FeCl_2$ and perpendicular to the $c$ axis of $CoCl_2$. These results suggest a large value of the magnetic anisotropy constant, and they can be interpreted in terms of the molecular field treatment of Néel.[5] We were interested in determining whether neutron diffraction measurements could establish additional details concerning the manner in which the ferromagnetic structures were produced. In addition, it was of interest to make definite observations concerning the existence of antiferromagnetic domains in these compounds.

## DETERMINATION OF THE ATOMIC MAGNETIC MOMENTS

### Experimental Method

In the single-crystal investigations, the specimens were mounted on the low-temperature single-crystal goniometer which was designed and constructed at this Laboratory.[6] The crystals were cut in the form of flat cylinders with the axis of the cylinder parallel to the hexagonal $c$ axis, and they were mounted in the apparatus with this axis parallel to the horizontal axis of rotation of the goniometer. All measurements were taken at 4.2°K with the sample completely immersed in liquid helium.

The measurements were analyzed according to the method first used in single-crystal neutron diffraction experiments by Peterson and Levy.[7] In this method the entire crystal is irradiated by the neutron beam, and the integrated intensities, $E_{hkl}$, of the Bragg reflections are given by

$$E_{hkl} = \frac{I_0 \lambda^3 N^2 V}{\omega} \frac{|F_{hkl}|^2}{\sin 2\theta} A_{hkl} ,$$

where $I_0$ is the incident intensity, $\lambda$ is the wavelength, $\omega$ is the angular velocity of rotation of the crystal, $N$ is the number of unit cells per unit volume, $V$ is the volume of the specimen, $F_{hkl}$ is the structure amplitude per unit cell, $\theta$ is the Bragg angle, and $A_{hkl}$ is the absorption coefficient. For an experiment with a particular crystal in which data are obtained in the same manner for all reflections, this expression, of course, reduces to

$$E_{hkl} = \frac{K I_0 |F_{hkl}|^2}{\sin 2\theta} A_{hkl} ,$$

where $K$ is a constant of the experiment. In order to normalize the magnetic intensities so that values of the atomic magnetic moments could be determined, it was first necessary to determine the scale factor, $KI_0$. This determination was made from measurements on the nuclear reflections where the structure amplitudes could be calculated from known values of the nuclear coherent scattering cross sections of Fe, Co, and Cl. Absorption coefficients were calculated by the procedure established by Busing and Levy,[8] which uses the Oracle. The inherent imperfection of these crystals allowed the use of fairly large specimens without involving appreciable extinction corrections, but the effects of extinction were determined by making the investigations on crystals of different size and examining the relative intensities of the strong and weak reflections.

Both these compounds crystallize in the rhombohedral structure characteristic of $CdCl_2$, with the metal atoms located at 000 and the two chlorine atoms at $uuu$ and $\bar{u}\bar{u}\bar{u}$, where $u$ had been previously determined to be 0.25 ± 0.01. An

[4] H. Bizette, C. Terrier, and B. Tsai, *Compt. rend.* **243**, 895, 1295 (1956).

[5] L. Néel, *Report to 10th Solvay Congress, September, 1954.*

[6] E. O. Wollan *et al.*, *Phys. Semiann. Prog. Rep. Sept. 10, 1956*, ORNL-2204, p 49.

[7] S. W. Peterson and H. A. Levy, *J. Chem. Phys.* **20**, 704 (1952).

[8] W. R. Busing and H. A. Levy, *Acta Cryst.* **10**, 180 (1957).

analysis of the calculated structure amplitudes for the nuclear reflections shows that many of the weak reflections are extremely sensitive to the value of the chlorine parameter, even within the limit of accuracy which had been measured. Therefore it was necessary to establish a more accurate value of $u$ at the same time that a determination was made of the scale factor. This was done by plotting the experimentally determined values of $KI_0$ as a function of $u$ for several nuclear reflections, and Fig. 1 shows this plot for one of the $CoCl_2$ crystals which was examined. All these reflections are indexed on the basis of the pseudohexagonal cell which contains three $CoCl_2$ molecules. The (101), (003), (009), and (107) reflections which are sensitive to the value of the parameter have intensities that are weak or medium. The other group contains reflections which are insensitive to the value of $u$, and these reflections have much stronger intensities. Since both these groups of reflections give very similar average values for $KI_0$, the extinction effects in this crystal must be relatively unimportant. The value of the chlorine parameter in $CoCl_2$ was determined from these results to be 0.2558 ± 0.0007. A similar determination gave a value of 0.2543 ± 0.0005 for $u$ in $FeCl_2$.

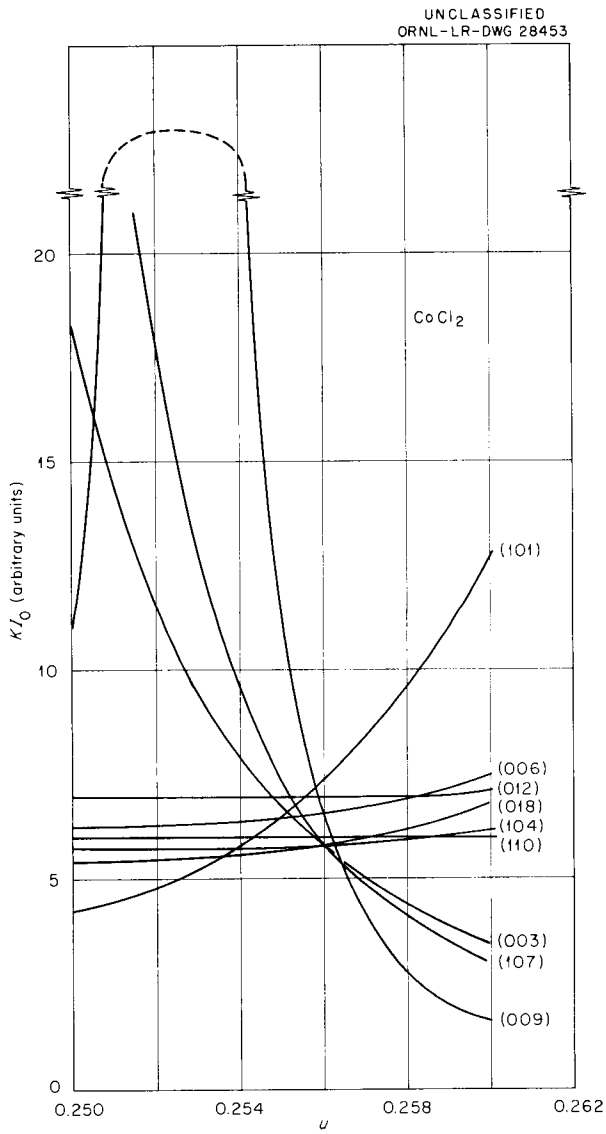


**Fig. 1. Determination of Scale Factor, $KI_0$, and Chlorine Parameter, $u$, in $CoCl_2$.**

With the scale factor determined from the nuclear intensities, an analysis was made of the magnetic reflections which occurred at relatively small values of the scattering angle. Measurements were limited to those reflections with a scattering angle less than 35 deg [$(\sin\theta)/\lambda = 0.28$] because of the position of the magnet pole pieces around the sample. Eight magnetic reflections were examined from $CoCl_2$ and six from $FeCl_2$. These magnetic reflections have been indexed for the magnetic hexagonal cell in which the value for the $c$ axis is twice that in the hexagonal nuclear cell and in which the $a$ axis is unchanged.

In determining the integrated intensities of antiferromagnetic reflections from single crystals, it is necessary to consider the possibility of antiferromagnetic domains in which the axis of antiferromagnetism can be oriented along equivalent crystallographic directions. In $CoCl_2$ the presence of such domains was actually observed by the differences in intensities of equivalent ($h0l$) reflections. Such intensity differences, of course, indicate that in zero external magnetic field the crystal was not divided equally into the domains with equivalent moment directions. This condition could presumably be caused by strains or stacking faults which exist in the crystal. In the case of $FeCl_2$, where the axis of antiferromagnetism is directed along the unique $c$ axis of the hexagonal cell, no such domain effect was observed. However, the integrated intensities of the magnetic reflections from both $CoCl_2$ and $FeCl_2$ that were used in calculations of the magnetic moments were average values of intensities observed from all reflections with equivalent indices. This method cancels any effect due to an inequality in the size of antiferromagnetic domains.

### Magnetic Moment Values

Since the form factor for the magnetic scattering from $Co^{++}$ was not known, an iterative process was used to determine both the magnetic moment value and the form factor. The best value for the atomic moment was calculated to be 3.15 ± 0.30 Bohr magnetons. The magnetic form factor fitting the data most satisfactorily was one which was slightly higher than the Steinberger-Wick form factor at the largest values of $(\sin \theta)/\lambda$. In order to determine a significant difference, however, results must be obtained for magnetic reflections at much larger values of the scattering angle, and this experiment will be performed at a later date. It will be important to make an accurate determination of the magnetic form factor in order to establish whether the atomic moment has an orbital contribution. The value of 3.15 Bohr magnetons, of course, agrees satisfactorily with a spin-only moment corresponding to $S = 3/2$, but other magnetic investigations on diluted cobalt compounds suggest that such an agreement is fortuitous. The single-crystal measurements also showed that the atomic moments must be very nearly within the layers of cobalt atoms, and experiments with an external magnetic field restricted the angle of possible deviation to about 5 deg.

A similar analysis was performed on the magnetic intensities from $FeCl_2$. These data were found to fit the Steinberger-Wick form factor satisfactorily and gave a value of 4.20 ± 0.40 Bohr magnetons for the atomic magnetic moment of the $Fe^{++}$ ions. This value also corresponds quite well to the spin-only moment that would be present for $S = 4/2$.

## EXPERIMENTS IN AN EXTERNAL MAGNETIC FIELD

### Effects of an External Field on the Magnetic Structure of $CoCl_2$

It has been mentioned previously that the single-crystal measurements on $CoCl_2$ in the absence of an external magnetic field had indicated the existence of antiferromagnetic domains because the intensities of equivalent magnetic $(h0l)$ reflections were different. This interpretation was confirmed in the experiments with an external field applied to the sample. Figure 2 shows the change in intensity of the (101) reflection when magnetic fields up to 10.8 kilo-oersteds were applied parallel to the scattering vector, and the sketches within the figure explain these results according to the domain behavior. Although the sketches show that the magnetic moments within the layer are directed along the hexagonal axes, this direction is not known definitely, and it is not necessary in confirming the existence of antiferromagnetic domains. The explanation of the data requires only that in zero field the moments are directed along equivalent directions in the base plane of the hexagonal cell. The intensities of the (101), $(\bar{1}11)$, and $(0\bar{1}1)$ were actually found to vary about 25% in the absence of a magnetic field, but this was not included in the sketch which shows equal population of the domains when $H = 0$. When an external field was applied, the moment orientation perpendicular to the field direction was the most stable, and the domain pattern changed until the crystal was transformed into one domain with a field of about 1.8 kilo-oersteds. Within statistical accuracy the data showed no additional change in intensity, up to the highest value of magnetic field which could be obtained with the particular geometry used in this

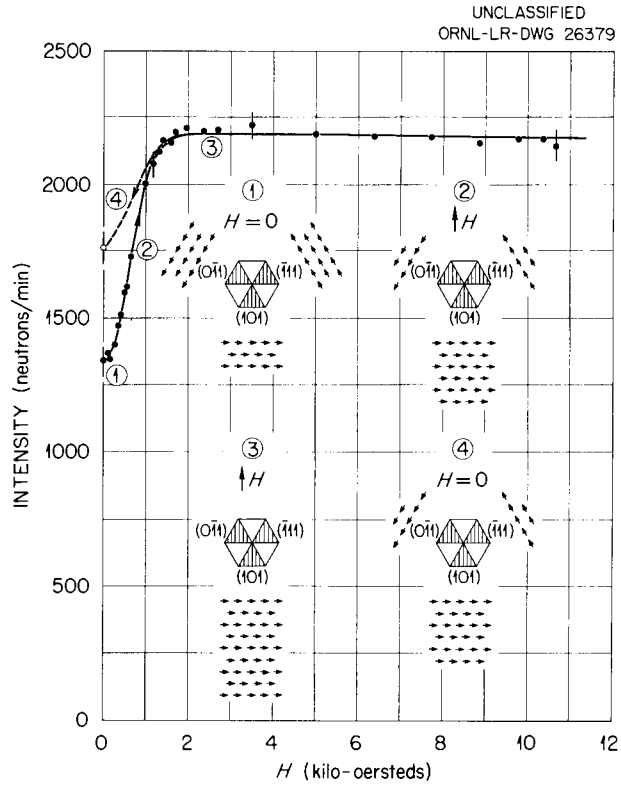


**Fig. 2. Variation of the (101) Antiferromagnetic Reflection from $CoCl_2$ in an External Magnetic Field.**

experiment. When the field was removed, the intensity remained higher than the original zero-field value, indicating that part of the domain transformation had remained. This was confirmed by intensity measurements of the $(\bar{1}11)$ and $(0\bar{1}1)$ reflections, which were much smaller than the original values.

The increase in intensity which is observed with the application of an external magnetic field is not so large as the threefold increase observed for the reflections from $MnBr_2$ (ref 9) and $MnCl_2$ (see "Neutron Diffraction Investigations of $MnCl_2$ in External Magnetic Fields," this report). This different intensity variation is associated with the difference in the types of domains. In $MnBr_2$ and $MnCl_2$ the domains are structure domains, in which the arrangement of parallel and antiparallel moments within the crystal is associated with the axis of magnetization within a domain, and only one domain contributes intensity to a particular reflection. However, in $CoCl_2$, where the difference in antiferromagnetic domains is nothing more than a rotation of the axis of the magnetic moments, all domains contribute an intensity determined by $q^2$, the fraction of intensity allowed by the relative orientations of the atomic magnetic moments and the scattering vector. In fact, effective values of $q^2$ for each reflection can be determined experimentally from the ratio of the intensity in zero field to that when the moments are all perpendicular to the scattering vector in an applied field.

Table 1 shows experimental determinations of $\overline{q^2}_{exp}$, which are average values for groups of reflections with equivalent indices. In order to eliminate domain effects, the values represent the ratio of the average intensity from a group of reflections in zero field to a similar average value in an applied field of 6 kilo-oersteds. Calculated values, $\overline{q^2}_{calc}$, are also given which represent average values for the same groups of reflections if the magnetic moments lie within the base plane of the hexagonal cell. The exact direction of the moments within the plane cannot be determined from such an experiment. Experiments have been performed in which the intensity changes of the (101) reflection were investigated after a magnetic field was applied at various angles within the base plane and then removed. The results of these measurements suggest moment directions along the hexagonal axes as shown in Fig. 2, but the experiments do not allow a definite interpretation.

There is no suggestion from the data in Fig. 2 that magnetic fields up to 10.8 kilo-oersteds can cause appreciable magnetization values, and this might seem to be inconsistent with the magnetic measurements. However, a small field first turns all the moments perpendicular to the axis of the field, and larger fields which produce the magnetization must rotate these moments into the field direction. Since the changes in intensity of the (101) reflection will be proportional to $(\mu \cos \phi)^2$, where $\mu$ is the atomic magnetic moment, and $\phi$ is the angle between the moment and field, the experiment is not sensitive to small rotations. The reports on the single-crystal experiments[10] do not give magnetization values for $CoCl_2$ as a function of the field, but calculations based on the measurements on powdered samples[11] show that the intensity of this reflection should have decreased less than 5% for the largest magnetic fields which were used. The data in Fig. 2 actually show this trend, but it is not significant within the statistical accuracy.

[9] E. O. Wollan, W. C. Koehler, and M. K. Wilkinson, *Phys. Rev.* (in press).

Table 1. Comparison of Observed and Calculated Values of $\overline{q^2}$ for Groups of Reflections with Equivalent Indices

| Reflections Averaged | $\overline{q^2}_{exp}$ | $\overline{q^2}_{calc}$ |
|---|---|---|
| 101, $\bar{1}11$, $0\bar{1}1$ | 0.513 | 0.504 |
| 015, $\bar{1}15$, $\bar{1}05$ | 0.602 | 0.581 |
| 107, $\bar{1}17$, $0\bar{1}7$ | 0.639 | 0.637 |
| 0111, $1\bar{1}11$, $\bar{1}011$ | 0.737 | 0.742 |

## Effects of an External Field on the Magnetic Structure of $FeCl_2$

In a magnetic material such as $FeCl_2$, where the axis of antiferromagnetism is along a unique crystallographic direction, effects on neutron diffraction intensities due to domains would not

[10] H. Bizette, C. Terrier, and B. Tsai, *Compt. rend.* 243, 895, 1295 (1956).

[11] C. Starr, F. Bitter, and A. R. Kaufmann, *Phys. Rev.* 58, 977 (1940).

be anticipated, and they were not observed. There was no increase in the intensity of the antiferromagnetic reflections when the magnetic field was applied. This behavior is shown in Fig. 3 at low field values, while the effects at high fields are associated with the onset of a net magnetization in the crystal.

The lower part of Fig. 3 represents the data taken for three magnetic reflections with the field applied either parallel or nearly parallel to the scattering vectors of the reflecting planes. The top part of the figure shows the same data plotted against the component of magnetic field parallel to the *c* axis of the crystal. These results therefore confirm the susceptibility measurements made on single crystals which showed that external fields applied in this direction produced large magnetization values at relatively low field values. Moreover, the numerical values of the field necessary for the onset of this condition are also in satisfactory agreement.

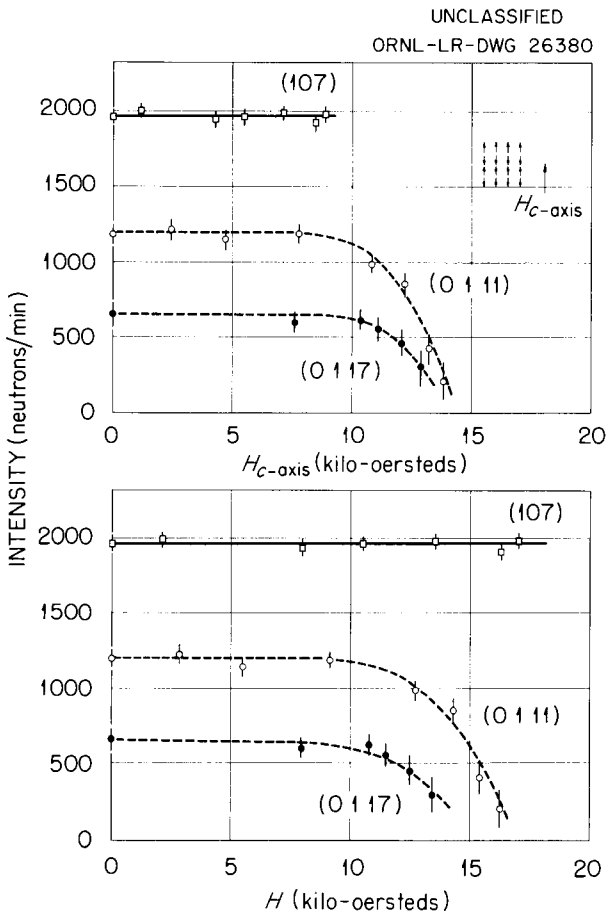


**Fig. 3. Variation of Antiferromagnetic Reflections from $FeCl_2$ with an Applied Magnetic Field.**

Earlier investigations of this effect which were made on another crystal showed that the crystal can be seriously damaged in an experiment of this type. When the component of the magnetic field along the *c* axis is sufficient to cause a net magnetization, and simultaneously there is a large component of the field perpendicular to the *c* axis, the magnetic forces seem to cause a displacement of the atomic layers, which fractures the crystal. When this occurs, there is a sudden decrease in the intensity of the reflections, of course, but both magnetic and nuclear reflections are affected, and since the process is irreversible, the intensities remain low when the field is removed. In order to avoid these fractures, the field was applied as closely parallel to the *c* axis as was permitted by the geometry of the apparatus. For the (0111) and (0117) reflections shown in Fig. 3, the field made angles of about 14 and 18 deg with respect to the scattering vectors. The results were completely reproducible as the intensity of the magnetic field was varied, and no effect was observed on nuclear reflections which were studied under similar geometrical conditions.

In the molecular field treatment of Néel,[12] two methods are described for parallel alignment of the atomic moments when a magnetic field is applied along the axis of antiferromagnetism. In one method, small fields first flip the axis of antiferromagnetism to a direction perpendicular to the field, after which the moments are rotated into the field direction as the field strength is increased. The other method merely requires that the moments which are antiparallel to the field flip into the field direction when the field exceeds a critical value. If the first method were correct in the case of $FeCl_2$, strong (00*l*) antiferromagnetic reflections would be observed at the first indication of a net magnetization. The position corresponding to a (003) antiferromagnetic reflection was carefully scanned as the magnetic field was applied parallel to the *c* axis, and no intensity was observed for fields up to 17,000 oersteds. Hence the parallel alignment of the moments in $FeCl_2$ is produced by the reversal in direction of those magnetic moments which are antiparallel to the direction of the applied field.

[12] L. Néel, *Report to 10th Solvay Congress, September, 1954.*

## ANTIFERROMAGNETIC PROPERTIES OF MANGANOUS TRIFLUORIDE

E. O. Wollan H. R. Child W. C. Koehler M. K. Wilkinson

In the last semiannual[1] a report was given on the antiferromagnetic structure properties of $CrF_3$, $FeF_3$, and $CoF_3$ as determined by neutron diffraction measurements. The other member of this series ($MnF_3$) has now been investigated. Manganous trifluoride also shows the growth of superlattice reflections at low temperatures ($T_N$ = 43°K), but the antiferromagnetic structure which develops in this compound is different from that in the other trifluorides of this group. The situation is identical to that observed in the corresponding perovskite-type compound, $LaMnO_3$.

A low-temperature powder pattern (4.2°K) for $MnF_3$ is reproduced in Fig. 1. The cross-hatched areas represent the magnetic contributions to the pattern. The small contributions which lie underneath strong nuclear reflections were again determined by taking the difference between the coherent contributions in patterns taken above and below the Néel temperature ($I_{4.2°K} - I_{300°K}$).

Although the crystal structure of $MnF_3$ is monoclinic, with 12 molecules per unit cell, the basic antiferromagnetic structure can most easily be described in terms of an idealized cubic form. The antiferromagnetic structure consists of ferromagnetic layers in which the spins in alternate layers are oppositely oriented. The antiferromagnetic cell is then the tetragonal one shown in Fig. 2, in which the arrows represent the spins of the magnetic ions. This antiferromagnetic cell gives rise to the reflections shown in the second column of Table 1. The high intensity observed for the first line (001) of this structure (Fig. 1) corresponds to the spins lying in or nearly in the plane of the ferromagnetic sheets. The observed magnetic intensities from this pattern are listed in the last column of Table 1. The corresponding intensities calculated on the basis of the true monoclinic cell, and for the spins in the ferromagnetic sheets, are shown in the third column of this table. The agreement is good except for the first reflection, for which the difference seems to be somewhat greater than the apparent experimental uncertainty. The magnetic moment of the $Mn^{+++}$ ion is also equal within experimental error to the spin-only value of 2 Bohr magnetons.

Of all the trifluorides, only the ones involving manganese would be expected to show distinctly different antiferromagnetic properties. The previously published results on the $LaMnO_3$-$CaMnO_3$ perovskite-type system were shown to have some

[1] H. R. Child *et al.*, *Phys. Semiann. Prog. Rep. Sept. 10, 1957*, ORNL-2430, pp 87–91.

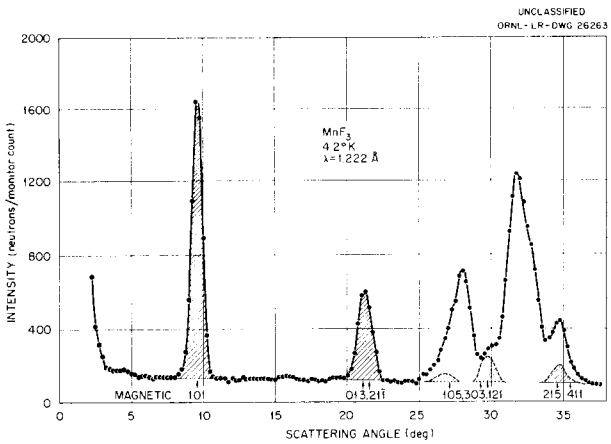


**Fig. 1. Neutron Powder Pattern for $MnF_3$.** Cross-hatched areas represent magnetic superlattice reflections.

**Table 1. $MnF_3$ Magnetic Intensities**

Spins parallel to (101) monoclinic planes

| Indices | | $P_{hk}$ (calc) ($S = 2$) | $P_{hk}$ (obs) |
|---|---|---|---|
| Monoclinic | Cubic Cell Doubled Along $c$ Axis | | |
| 101 | 001 | 1530 | 1402 |
| 013<br>$2\bar{1}1$ | 101 | 571 | 587 |
| $10\bar{5}$ | | 65 | 70 |
| | 111 | | |
| 121<br>303 | 003 | 180 | 190 |
| 215<br>411 | 103 | 134 | ~125 |

very striking correlations with the ordering of orbitals on the basis of Goodenough's hybridized orbital system. All these results carry over to the *d* orbitals of the ligand field theory, with the additional advantage of having a mechanism for magnetic exchange coupling. In the case of the $LaMnO_3$ compound it was necessary to infer the direction of antiferromagnetic coupling relative to the distortions of the crystal, because this direction could not be distinguished in the neutron pattern. In the present case of $MnF_3$ the antiferromagnetic cell could be determined in relation to the x-ray-determined crystal parameters, and this fact has an important bearing on the interpretation of the antiferromagnetic lattice in terms of orbital ordering.

To simplify the interpretation of the antiferromagnetic properties of the system, the pseudotetragonal antiferromagnetic cell has been extracted from the more complicated monoclinic crystallographic cell. In so doing, however, the relation of the antiferromagnetic structure to the fluorine parameters, which appear to bear an important relationship to the antiferromagnetic properties, has been maintained. This tetragonal antiferromagnetic cell is represented in Fig. 2, in which the staggering and spacings of the fluorine ion positions are also represented. Along the long axis of the cell the fluorine ions are half way between antiferromagnetic layers, which position suggests overlap of fluorine ion *p* orbitals with identical magnetic ion *d* orbitals on both sides, and this is the situation for which antiferromagnetic coupling would be expected. The ordered arrangement of long and short fluorine parameters within the ferromagnetic layers suggests an ordering of the magnetic ion orbitals such that a *p* orbital overlaps a filled cation orbital on one side and an empty cation orbital on the other. This is just the situation for which one would expect ferromagnetic coupling within the layers.

UNCLASSIFIED
ORNL-LR-DWG 26310R

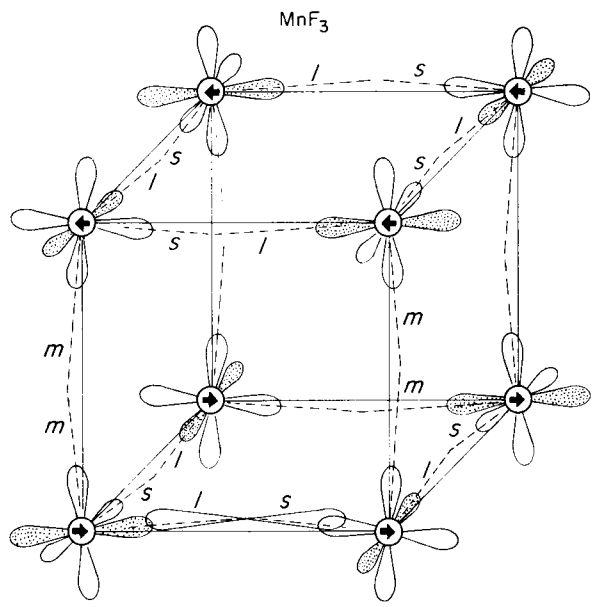


**Fig. 2. Antiferromagnetic Structure of $MnF_3$. See text for discussion of magnetic coupling in terms of orbitals shown.**

## INVESTIGATIONS ON THE ENERGY LEVELS OF THE CONFIGURATION $6p^2$ IN Hg I

G. W. Charles

Garton and Rajaratnam have recently reported[1] the discovery of the energy levels $4p^2\,{}^3P_2$ of Zn I and $5p^2\,{}^3P_2$ of Cd I. In the same paper, these authors tentatively suggested a revision of Sawyer's[2] assignment of the level $6p^2\,{}^3P_0$ to Hg I, while confirming his assignment of $6p^2\,{}^3P_1$. Recent measurements of spectrograms by the author have yielded two lines which are taken to be the transitions $6s6p\ {}^1P^o_1-6p^2\,{}^3P_0$ and $6s6p\ {}^1P^o_1-6p^2\,{}^3P_1$, adding some further evidence in favor of the assignments of Garton and Rajaratnam.

The spectrograms were made on a Hilger E-1 Littrow spectrograph at the University of Oklahoma. The source was a low-pressure mercury-arc lamp such as the type used for observations of the Raman effect. The lines in question were found when the tube, carrying 15 amp, was observed end-on for periods of about 1 min. Spectrograms were measured on a Gaertner comparator at ORNL. Table 1 shows the lines of the transition $6s6p-6p^2\,{}^3P_{0,1}$.

[1] W. R. S. Garton and A. Rajaratnam, *Proc. Phys. Soc. (London)* **68A**, 1107 (1955).

[2] R. A. Sawyer, *J. Opt. Soc. Am.* **13**, 431 (1926).

Table 1. The Transition $6s6p-6p^2\ {}^3P_{0,1}$ of Hg I

| Intensity | λ (Å) | σ (cm$^{-1}$) | Transition | Upper Level (cm$^{-1}$) |
|---|---|---|---|---|
| | 1775.20[a] | 56332.$_1$ | $6s6p\ {}^3P^\circ_0-6p^2\ {}^3P_1$ [b] | 93975.$_4$ |
| | 1832.74[a] | 54563.$_1$ | $6s6p\ {}^3P^\circ_1-6p^2\ {}^3P_1$ [b] | 93976.$_8$ |
| 200 *HR* | 1972.96[c] | 50685.$_3$ | $6s6p\ {}^3P^\circ_1-6p^2\ {}^3P_0$ [d] | 90097.$_6$ |
| 200 *H* | 2002.70[c] | 49932.$_6$ | $6s6p\ {}^3P^\circ_2-6p^2\ {}^3P_1$ [b] | 93975.$_6$ |
| 20 *b* | 2505.00[c] | 39908.$_1$ | $6s6p\ {}^1P^\circ_1-6p^2\ {}^3P_1$ | 93976.$_9$ |
| 150 *H* | 2774.80[c] | 36028.$_0$ | $6s6p\ {}^1P^\circ_1-6p^2\ {}^3P_0$ | 90096.$_8$ |

[a]Measurements from E. W. H. Selwyn, *Proc. Phys. Soc.* (*London*) 41, 392 (1929).
[b]Classification from R. A. Sawyer, *J. Opt. Soc. Am.* 13, 431 (1926).
[c]Measurements by the author.
[d]Classification from W. R. S. Garton and A. Rajaratnam, *Proc. Phys. Soc.* (*London*) 68A, 1107 (1955).

The discovery of the ${}^3P_2$ levels of Zn I and Cd I makes it possible to fit the triplet levels of $np^2$ to the theory for these levels. The ratio of the intervals ${}^3P_1-{}^3P_0$ and ${}^3P_2-{}^3P_1$ depends only on the coupling parameter $\chi(=\zeta/5F_2)$. This ratio is expressed as

$$\frac{-5/2+5/2\,(1+2\chi/3+\chi^2)^{1/2}}{1+5\chi/4-(1-5\chi/6+25\chi^2/16)^{1/2}}\,.$$

The experimental values are 0.568 for Zn I and 0.672 for Cd I. Thus $\chi = 0.030$ for Zn I and $\chi = 0.131$ for Cd I. Using this value of $\chi$ with either observed interval, one can then calculate $F_2$ and hence $\zeta$ from the relationship $\chi = \zeta/5F_2$. The results for Zn I are $F_2 = 2812$ cm$^{-1}$, $\zeta = 422$ cm$^{-1}$; and those for Cd I are $F_2 = 1967$ cm$^{-1}$, $\zeta = 1283$ cm$^{-1}$. One may now make an extrapolation to Hg I, using the fact that $\zeta^{1/4}$ is approximately a linear function of the atomic number, $Z$. An estimate, $\zeta = 5000$ cm$^{-1}$, is obtained for the configuration $6p^2$ of Hg I. When this is combined with the known interval ${}^3P_1-{}^3P_0 = 3879$ cm$^{-1}$, $F_2$ becomes 1990 cm$^{-1}$. Thus $\chi = 0.503$ and the interval ratio $({}^3P_2-{}^3P_1)/({}^3P_1-{}^3P_0)$ becomes 0.888, from which the predicted position of $6p^2\ {}^3P_2$ is approximately 97,400 cm$^{-1}$, in fair agreement with the estimate of 96,500 cm$^{-1}$ made by Garton and Rajaratnam. A direct linear extrapolation of $\chi^{1/3}$ to Hg I gives the result $\chi = 0.632$ and leads to a prediction of 96,900 cm$^{-1}$ for the level $6p^2\ {}^3P_2$.

From Table 1, $6p^2\ {}^3P_0$ is at 90,097.$_2$ cm$^{-1}$ and $6p^2\ {}^3P_1$ is at 93,976.$_1$ cm$^{-1}$. The transition $6s6p\ {}^1P^\circ_1-6p^2\ {}^3P_2$ is to be expected near 43,350 cm$^{-1}$. There are several unclassified lines to be found on the plates between 42,850 and 43,850 cm$^{-1}$. These are listed in Table 2. There is no

Table 2. Unclassified Hg Lines

| Intensity | λ (Å) | σ (cm$^{-1}$) |
|---|---|---|
| 20 (?) | 2332.15 | 42865.7 |
| 50 *H* | 2326.87 | 42963.0 |
| 25 *b* | 2321.83 | 43056.2 |
| | 2311.96 | 43240.0 |
| 50 | 2306.15 | 43348.9 |
| 25 | 2305.22 | 43366.4 |
| 100 *b* | 2303.60 | 43396.9 |
| 50 | 2297.70 | 43508.4 |
| 400 | 2296.23 | 43536.2 |
| 25 | 2295.43 | 43551.4 |
| 75 | 2292.89 | 43599.6 |

way of choosing one of these lines as the transition sought. Indeed, there are several reasons for supposing the transition $6s6p\ ^1P^o_1-6p^2\ ^3P_2$ is absent. These are (1) the extreme weakness of the line $6s6p\ ^1P_1-6p^2\ ^3P_1$ (the corresponding line in Cd I was observed by Fukuda *et al.*[3] under the rather extreme conditions of 200 amp/cm$^2$; it is not included in other lists, although the line $6s6p\ ^1P^o_1-6p^2\ ^3P_0$ appears in several lists), (2) the absence of the corresponding line in Cd I even under the extreme conditions employed by Fukuda *et al.*, (3) the great haziness and weakness of the transitions $5s5p\ ^3P^o-5p^2\ ^3P_2$ in Cd I (ref 1), and the weakness or absence of the transition $6s6p\ ^3P^o-6p^2\ ^3P_2$ in Hg I (ref 1). If one assumes that the line at 1760 Å mentioned by Garton and Rajaratnam[1] is real, the line $6s6p\ ^1P^o_1-6p^2\ ^3P_2$ should be at 42,161 cm$^{-1}$; no line appears at this place on the plates measured by the author, although there is an unidentified line at 42,191 cm$^{-1}$.

The author is indebted to J. C. Albright for his assistance in taking the spectrograms used in this investigation.

[3]M. Fukuda, T. Kuyama, and Y. Uchida, *Sci. Papers Inst. Phys. Chem. Research (Tokyo)* **4**, 177 (1926).

## INFRARED SPECTRA OF THE DEUTERATED PHOSPHINE MOLECULES

H. W. Morgan P. A. Staats J. H. Goldstein[1]

During a recent study[2] of the isotopic ammonias, a technique was developed to allow recording of the infrared spectra of individual isotopic species in an equilibrium mixture. This technique has now been used for a study of the three deuterated phosphines, $PD_3$, $PHD_2$, and $PH_2D$.

Phosphine was generated by the action of water on calcium phosphide.[3] Equilibrium mixtures of phosphines containing varying amounts of deuterium and hydrogen were prepared by mixing known amounts of $H_2O$ and $D_2O$ prior to reaction with the phosphide. Purification of the phosphine was effected by fractional distillation. The infrared spectra were recorded on a double-beam Perkin-Elmer spectrometer equipped with LiF, NaCl, and CsBr prisms.

Since phosphine and ammonia behave somewhat similarly, the techniques previously described[2] for the ammonias were used for the phosphines and will not be described here. The phosphines were found to equilibrate much more slowly than the ammonias, but this did not interfere with the method of compensation. Figure 1 shows the spectra of the individual species $PH_2D$ and $PHD_2$, compared with the spectrum obtained from an equilibrium mixture.

Isotopic substitution in the molecules of $C_{3v}$ symmetry splits the two doubly degenerate modes into two pairs of frequencies, two each of the $A'$ and of the $A''$ species, symmetric and asymmetric with respect to the plane of symmetry. These were identified with the aid of group correlation tables[4] and the noncrossing rule. The numbering of fundamentals used here follows that of Reding and Hornig[5] and of Burgess,[6] and makes it possible to group together the physically similar vibrations.

Frequency measurements were obtained on all fundamentals except the $\nu_3$ asymmetric fundamental of $PH_2D$. It is believed that this fundamental lies so close to the stronger $\nu_1$ symmetric fundamental that it could not be observed with the prism resolution available.

A normal coordinate analysis has been performed, in which a simple valence-force potential was assumed. Lack of overtone frequencies has prevented determination of the zero-order frequencies.

[1]Consultant, Emory University, Atlanta, Georgia.

[2]H. W. Morgan, P. A. Staats, and J. H. Goldstein, *Phys. Semiann. Prog. Rep. Sept. 10, 1957*, ORNL-2430, p 96.

[3]Supplied by Rocky Mountain Research, Inc., Denver, Colorado.

[4]E. B. Wilson, Jr., J. C. Decius, and P. C. Cross, *Molecular Vibrations*, McGraw-Hill, New York, 1955.

[5]F. P. Reding and D. F. Hornig, *J. Chem. Phys.* **19**, 594 (1951).

[6]J. S. Burgess, *Phys. Rev.* **76**, 1267 (1949).

Because of the convenience in computation it was decided that compensation for anharmonicity would be introduced by the use of "spectroscopic masses" as suggested by Kilpatrick and Pitzer.[7] In this manner, anharmonicity corrections were applied separately to each symmetry species. The frequencies were computed in the usual manner by using the Wilson FG matrix technique on the Oracle.

[7] J. E. Kilpatrick and K. S. Pitzer, *J. Research Natl. Bur. Standards* 38, 191 (1947).

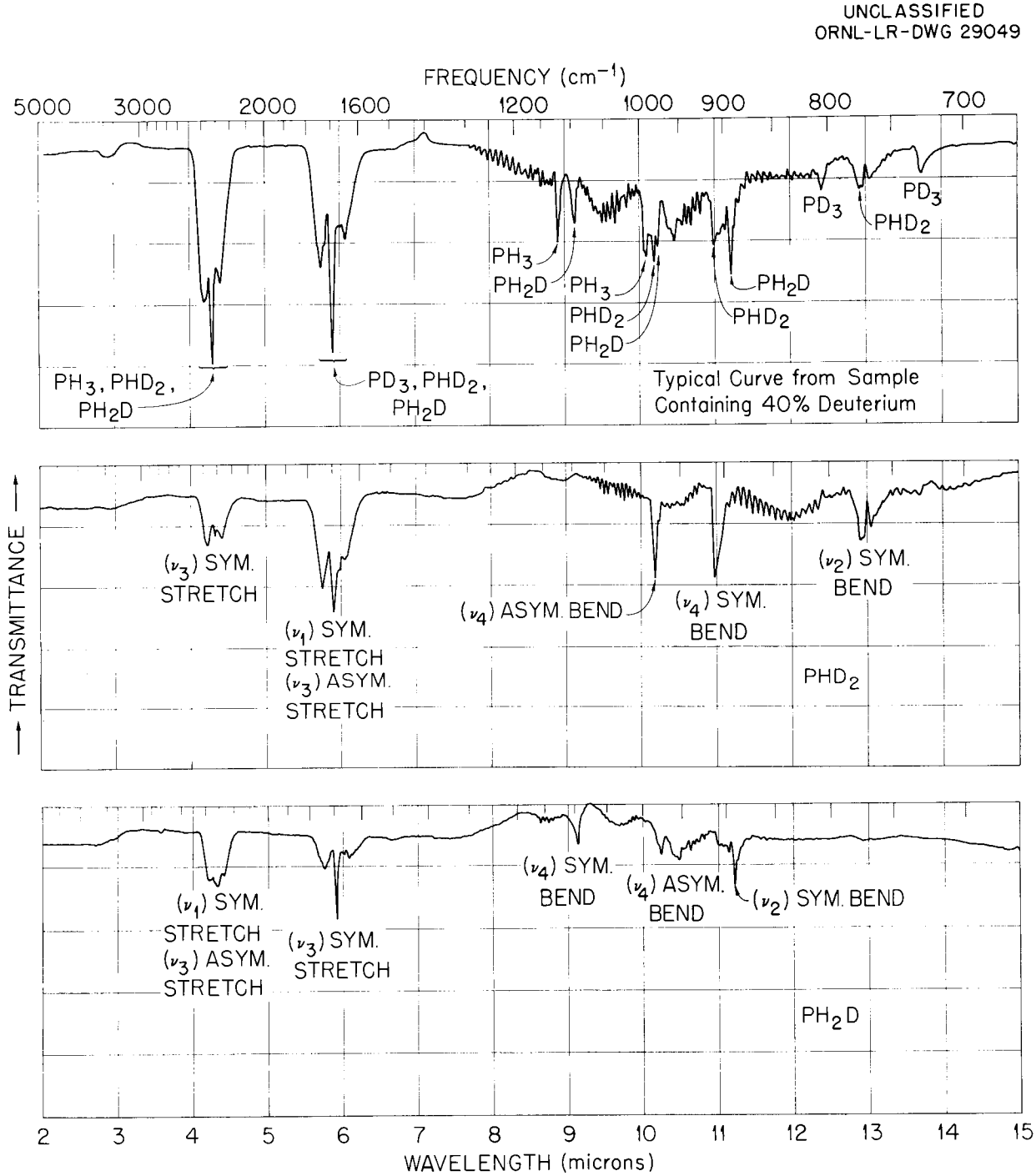


**Fig. 1. Infrared Spectra of the Deuterated Phosphines.**

Table 1 presents a comparison of the experimental and calculated frequencies. The calculated frequencies were computed by using a set of force constants computed from the experimental data on $PH_3$ obtained at grating resolution by McConaghie and Nielsen.[8] Table 1 also illustrates sharply the advantages of the multiple-cell technique. For example, note that 1691 $cm^{-1}$ has been listed as the $\nu_3$ vibration for $PD_3$, and also for the $\nu_3 A''$ vibration of $PHD_2$. In previous unpublished grating studies on $PD_3$, Ward and Nielsen listed 1691 $cm^{-1}$ as being probable for the $\nu_3$ of $PD_3$, but they were uncertain of the purity. Without the present technique, one could not be certain that $\nu_3 A''$ for $PHD_2$ was also 1691 $cm^{-1}$. Similarly, the $\nu_1$ symmetric vibration, 2332 $cm^{-1}$, for $PH_2D$ could not have been found in the presence of both the $\nu_1$ and $\nu_3$ of $PH_3$.

It is worthy to mention that the calculated frequencies agree quite well with the experimental values. In an earlier study of the isotopic ammonias,[2] good agreement was also obtained between the calculated and experimental frequencies. These facts support the assumption that the simple valence force field used here provides an adequate approach to normal coordinate problems in these molecules.

It is of interest to compare the force constants of ammonia and phosphine as calculated from their infrared spectra,[9] shown in Table 2. The force constants for ammonia are based upon recent grating measurements of the fundamental frequencies made by Plyler and Benedict.[10] Also presented

[8] V. M. McConaghie and H. H. Nielsen, *Proc. Natl. Acad. Sci. U.S.* **34**, 455 (1948).

[9] G. Herzberg, *Infrared and Raman Spectra*, p 176, Van Nostrand, New York, 1945.

[10] Private communication.

**Table 2. Summary of Force Constants of Phosphine and Ammonia ($10^5$ dynes/cm)**

| | $PH_3$ | | $NH_3$ |
|---|---|---|---|
| | ORNL | Weston and Sirvetz* | (ORNL) |
| $K_1$ | 3.1109 | 3.112 | 6.429 |
| $K_1'$ | 0.0003 | | −0.0067 |
| $K_\delta/l^2$ | 0.3339 | 0.324 | 0.5376 |
| $K_\delta'/l^2$ | −0.0211 | −0.0213 | −0.0775 |

*J. Chem. Phys.* **20**, 1820 (1952).

**Table 1. Summary of Observed and Calculated Frequencies of the Deuterated Phosphine Molecules**

| | $\nu_1$ | $\nu_2$ | $\nu_3$ | | $\nu_4$ | |
|---|---|---|---|---|---|---|
| $PH_3$ | | | | | | |
| Observed* | 2323 | 990 | 2328 | | 1121 | |
| Calculated | 2322 | 990 | 2328 | | 1121 | |
| $PH_2D$ | | | | | | |
| Observed | 2332 | 890 | 1687 $A'$ | | 1093 $A'$ | 975 $A''$ |
| Calculated | 2326 | 891 | 1678 $A'$ | 2326 $A''$ | 1097 $A'$ | 971 $A''$ |
| $PHD_2$ | | | | | | |
| Observed | 1683 ± 2 | 767 | 2310 $A'$ | 1691 $A''$ | 909 $A'$ | 980 $A''$ |
| Calculated | 1678 | 767 | 2326 $A'$ | 1684 $A''$ | 912 $A'$ | 981 $A''$ |
| $PD_3$ | | | | | | |
| Observed | 1680 | 727 | 1691 | | 804 | |
| Calculated | 1675 | 725 | 1684 | | 804 | |

*V. M. McConaghie and H. H. Nielsen, *Proc. Natl. Acad. Sci. U.S.* **34**, 455 (1948).

for comparison are the force constants for phosphine calculated by Weston and Sirvetz.[11] The decrease in the stretching and bending force constants reflects the lower bond energy in phosphine.

[11]R. E. Weston, Jr., and M. H. Sirvetz, *J. Chem. Phys.* 20, 1820 (1952).

The appreciably slower rate of isotopic exchange shown by phosphine arises not from the difference in bond energy but from the difference in the ionic character of the bond. Thus the stronger, more ionic $NH_3$ exchanges rapidly, while the more covalent $PH_3$ molecule exchanges slowly.

## COMPILATION OF DATA ON SOME SPECTRA OF THORIUM

G. W. Charles

A compilation of data on the spectra of Th IV, Th III, Th II, and Th I has been completed,[1] bringing together for the first time all the available data on these spectra. Principal sources of the data were published papers on Th IV (refs 2 and 3), Th III (ref 4), and Th II (refs 5–8); unpublished line lists and Zeeman data of Th II classified lines from P. F. A. Klinkenberg; unpublished line lists from the MIT card file on thorium and from the M.S. theses of Fred,[9] Ference,[10] and Bowersox[11] submitted to the University of Chicago; unpublished Zeeman data from MIT; as well as published[12] and unpublished data of Stukenbroeker and McNally on the isotope shift between lines of $Th^{232}$ and those of $Th^{230}$.

The principal features of the compilation are as follows:

1. Twelve energy levels[13] and 24 classified lines of Th IV were taken from the literature.

2. Also taken from the literature were 79 energy levels and 319 classified lines of Th III.

3. For Th II, 162 odd levels and 190 even levels were compiled, of which 15 odd levels and 30 even levels, obtained from Schuurmans and Klinkenberg, have not been published previously. The $g$ values not previously published are listed for 16 odd levels and for 27 even levels, of which the $g$ values of 10 odd levels and of 14 even levels have been determined by the writer from unpublished MIT Zeeman data. Improved $g$ values, determined in the same manner, are listed for 11 odd levels and for 9 even levels.

4. More than 2860 classified lines with Zeeman effects and isotope shifts are listed for Th II. All expected combinations of the known energy levels of Th II were calculated, and the list was compared with a list of observed lines. The resulting list of classified lines is considerably more extensive than the only published list[4] of about 1200 lines or Klinkenberg's unpublished list of about 1900 lines.

5. Fifty-six energy levels and 138 classified lines are listed for Th I.

6. Zeeman data are included for 216 unclassified Th II lines and for 91 Th I lines.

7. Data on isotope shifts of 49 unclassified lines are compiled.

[1]G. W. Charles, *A Compilation of Data on Some Spectra of Thorium*, ORNL-2319 (in press).

[2]P. F. A. Klinkenberg and R. J. Lang, *Physica* 15, 774 (1949).

[3]P. F. A. Klinkenberg, *Physica* 16, 185 (1950).

[4]P. F. A. Klinkenberg, *Physica* 16, 618 (1950).

[5]J. R. McNally, Jr., G. R. Harrison, and H. B. Park, *J. Opt. Soc. Am.* 32, 334 (1942).

[6]T. L. de Bruin, Ph. Schuurmans, and P. F. A. Klinkenberg, *Z. Physik* 121, 667 (1943).

[7]T. L. de Bruin, P. F. A. Klinkenberg, and Ph. Schuurmans, *Z. Physik* 122, 23 (1944).

[8]J. R. McNally, Jr., *J. Opt. Soc. Am.* 35, 390 (1945).

[9]M. Fred, M.S. Thesis, University of Chicago, 1934.

[10]M. Ference, Jr., M.S. Thesis, University of Chicago, 1934.

[11]R. B. Bowersox, M.S. Thesis, University of Chicago, 1934.

[12]G. L. Stukenbroeker and J. R. McNally, Jr., *J. Opt. Soc. Am.* 43, 36 (1953).

[13]The $g$ values for nine of these levels have been calculated by the writer from published Zeeman patterns.

An evaluation of the status of our present knowledge of thorium spectra has been made. It is concluded that no significant extension of Th IV or Th III can be made without new observations. Some extension of Th II seems possible with available data. Further theoretical study[14] is needed on the configuration assignments of known Th II levels. The knowledge of Th I is concluded to be in a very unsatisfactory condition, with more study needed on all phases of this spectrum.

[14]The configurations $6d^3$, $6d^2 7s$, and $6d7s^2$ have been treated by Y. Eisenberg, *Physica* 18, 177 (1952), while the configurations $5f7s^2$ and $5f6d7s$ have been treated by G. Racah (unpublished work).

## THE ROLE OF SPECTROSCOPY IN THERMONUCLEAR RESEARCH

J. R. McNally, Jr.

There are many difficult physical, metallurgical, chemical, and engineering problems presented in the development, design, and operation of a practical thermonuclear power device. Pertinent to the development and interpretation of thermonuclear systems is the ever-present problem of diagnostics. Spectroscopy is one of the most important tools for diagnostic studies. It is essentially an unperturbing probe that samples the system spatially and temporally. Some of the so-called "systems" parameters to be encountered by the spectroscopist and some of the promising spectroscopic methods of attack will be described. Some unusual and relatively new spectroscopic phenomena will be discussed to illustrate the potency of this method.

### SYSTEMS PARAMETERS

The following general boundary conditions show the tremendously broad scope of the problem insofar as the spectroscopist is concerned:

1. The gas density ranges from about $10^{10}$ particles/cm$^3$ for low-density plasmas up to about $10^{16}$ particles/cm$^3$.
2. The temperature of the system or of a particular class of particles may range from essentially room temperature to the $10^8$ °K of a true thermonuclear plasma.
3. The reaction mean free path of particles in a hot plasma is about 5000 miles; the collision mean free path in the same system may be of the order of a meter.
4. The pressure in the system ($p = nkT$) ranges from that of a cold low-density gas ($\sim 10^{-9}$ atm) to that of a hot, dense plasma, for which the pressure approaches 100 atm.
5. A hot plasma is essentially completely ionized; actual plasmas under study may be ionized to only a small degree.
6. Ionic velocities may range up to about $2 \times 10^8$ cm/sec, corresponding to ion energies of 100 kv; electron velocities may approach $10^{10}$ cm/sec.
7. Constraining magnetic fields will exist, either applied externally or brought about by the pinch effect resulting from ordered currents, and they may approach $10^5$ oersteds.
8. Electrostatic fields in an infinitely conducting plasma may be assumed small (i.e., $n_+ \cong n_-$) except near walls or plasma boundaries; however, transient effects resulting from near collisions between charged particles will contribute to strong local fields. Interionic fields of the order of several thousands of volts per centimeter may be encountered.
9. Bremsstrahlung radiation (visible, ultraviolet, and x-ray) becomes increasingly important at the elevated plasma temperatures.

It is obvious that essentially all phases of basic spectroscopic phenomena will play significant roles in the evaluation of plasma phenomena; the Doppler broadening due to random motion and Doppler shift due to ordered motions, Stark effect, Zeeman effect, forbidden transitions, continua, and all that they entail under strong perturbing influences must be understood and evaluated carefully in order to ascertain the true nature of the spectroscopic phenomena. In one sense, the spectroscopist has available a very unique multipurpose probe which can meet some of the demands of the thermonuclear physicist; on the other hand, he is beset by many conflicting phenomenological

processes. His system is far from idealized for any one measurement.

## GENERAL REMARKS

The low limits of sensitivity of the various spectroscopic techniques, as applied to the evaluation of important plasma properties, are listed in Table 1. These values are relatively conservative but, in general, are based on the assumption that in each instance no serious perturbing influences from causes other than the one under consideration exist and that moderately high resolution techniques of observation are available. If one were studying the Doppler broadening of hydrogen at the lower sensitivity limit ($\Delta\lambda_D/\lambda = 7 \times 10^{-5} \sqrt{T/M} = 1.2 \times 10^{-5}$), for example, the presence of an electric field strength of $10^3$ v/cm ($\Delta\lambda_E/\lambda = 1.7 \times 10^{-5}$ for $H_\alpha$) would make the measurement extremely difficult unless other means of suppressing the magnitude of electrostatic broadening were available (e.g., polarizers to eliminate outer Stark components except in the case of random local fields). Thus spectroscopic data may be obtained under such actual operating conditions as to vitiate the generally ideal conditions necessary to obtain the kind of sensitivity listed in Table 1. The different phenomena, the methods of measurement, and the limitations will be discussed separately.

## TEMPERATURE – GENERAL CONSIDERATIONS

The temperature of a gaseous discharge at low pressure, where the mean free path is of the order of the container size, may have little or no meaning. The greater bulk of neutral particles in the gas will have a velocity distribution corresponding essentially to the wall temperature, whereas the different ionic species may well have considerably different "temperatures." Inasmuch as we usually define temperature in terms of a Maxwell-Boltzmann distribution of velocities, each type of particle will have a different temperature, and in the case of anisotropic systems involving nonuniform electric or magnetic fields, each class of particle will have an entirely different "temperature" at different places in the system. In anisotropic systems one may, in fact, talk very loosely in terms of a temperature which is directional, inasmuch as the velocity distribution may be entirely different for various directions. The definition of temperature used here will be given by the usual relation

$$\bar{E} = \frac{3}{2} kT \quad , \tag{1}$$

where $\bar{E}$ is the average kinetic energy of a class of particles which have the same temperature; that is, the system is in temperature equilibrium or is thermalized.

In all subsequent discussions it should be understood that temperature is used only in the loose sense defined by Eq. 1 unless otherwise specified. Thus an ordered ionic drift motion may be said to have a "temperature" in the sense used here; however, in a thermonuclear plasma the required temperature of $10^8$ °K must be based on a thermalized or completely randomized type of motion for the positive ions.

**Table 1. Spectroscopic Sensitivity of Plasma Properties**

| Phenomenon | Technique | Approximate Low Limit of Sensitivity |
|---|---|---|
| Temperature | Doppler broadening | 300°K |
| Ordered motion | Doppler shift | $10^4$ cm/sec |
| Neutral particle density | Line shape | $10^{16}$ particles/cm$^3$ |
| Ion density | Interionic Stark effect | $10^{12}$ ions/cm$^3$ |
| | Series cutoff | $10^{12}$ ions/cm$^3$ |
| Ionization degree | Line ratios | 0% |
| Electric fields | Stark effect | 1000 v/cm |
| Magnetic fields | Zeeman effect | 1000 gauss |
| Electron energy | Line excitation | 2 v |

## ELECTRON TEMPERATURE

Electrons in a plasma may originate from ionization processes or by surface emission; the electrons may be produced with considerable excess energy or may be accelerated by the electric fields near the emitting surfaces. In any case the "young" electrons may have an entirely different energy distribution or temperature in the plasma from that of "well aged" electrons because of relatively slow degradation in elastic collision processes. Thus there may be two, or even more, temperature classes of electrons in the system.

Should the electrons be moving under the influence of an electric field of strength $\xi$, the electrons will have an energy of diffusion of order $\xi\lambda$, where $\lambda$, the mean free path for the electron, depends on the gas density, degree of ionization, and other parameters. The energy of thermal agitation superimposed on this energy of forced diffusion may well be smaller by a factor of the order of several hundred, as, for example, in a cathode sheath. Townsend defined a quantity $\eta$ to express this fact; that is, $KE = \frac{1}{2} mv^2 = \eta(\frac{3}{2} kT)$, where $T$ is the temperature equivalent of the thermal agitation.

Alfven[1] states that the electronic temperature becomes nearly equivalent to the gas temperature when

$$\lambda_e \xi = T_M \sqrt{\frac{m}{M}} \ .$$

Here, $\lambda_e$ is the electron mean free path in centimeters, $\xi$ is the accelerating field in volts per centimeter, and $T_M$ is the gas temperature in volts. Thus, in a field of only 1 v/cm and for hydrogen ions at 7730°K (1 v), the mean free path must be less than 200 $\mu$ in order for the gas and electronic temperatures to be approximately the same.

## DETERMINATION OF ELECTRON ENERGY

In low-pressure gases the excitation of the different atomic energy levels can be used to ascertain the upper energy limit of the electrons and, with some reservations, the energy distributions of the electrons in the plasma. These limiting factors include such items as the existence of metastable states which permit cumulative excitation processes. There is also a strong possibility of pileup of electrons of low energy because of the slow attenuation of electron energy by the elastic collision processes in low-pressure discharges, especially after the electron energy has degraded below the lowest excitation energy. Since the average fractional energy loss by an electron in an elastic collision with an atom or ion is of the order of $2m/M$, the number of such scattering collisions must in general be very large if the electron energy is to be degraded to a steady-state value. Conversely, the number of scattering collisions for an ion must also be very large if the ion is to be "heated" up to the electron temperature.

Inelastic collisions resulting in excitation, ionization, or dissociation can be used to measure the maximum electron energies, on the assumption that metastables are not involved and that single collisions are involved in the spectral excitation process. Carbon, nitrogen, and oxygen are frequent contaminants in gas discharges. Tables 2 and 3 illustrate the electron energies involved in the excitation of various important atomic energy states of oxygen and of carbon; appropriately useful spectrum lines involving these upper states are listed for correlation purposes (1 v = 8068 $cm^{-1}$). Use of the resonance lines is generally restricted to the vacuum ultraviolet region of the spectrum, although in all cases weaker lines in the visible and ultraviolet may be used. For example, if the C III line at $\lambda$ 4647 is observed, the electron energy must be at least 67.8 v in order for this line to be doubly ionized and excited (32.2 v above the C III ground state); however, if sufficient $C^{++}$ ions exist in the discharge such that excitation energy only is required, then electrons of at least 32.2 v must exist in the discharge.

The excitation of highly ionized atoms of high $Z$ can also be studied in the vacuum ultraviolet region, although there is always present the serious question as to how much inert gas impurity may be tolerable in a thermonuclear plasma because of the poisoning effects. The principal method of studying "partially stripped atoms" is by vacuum spectroscopic methods. The distribution of intensity in the spectra characteristic of the various stages of ionization is indicative of the mean temperature. Spectroscopic studies in the vacuum ultraviolet region have been made of hydrogen-like spectra through oxygen ($Z = 8$) and of helium-like spectra

[1] H. Alfven, *Cosmical Electrodynamics*, Clarendon Press, Oxford, 1950.

Table 2. Electron Energies Required to Excite Various States of Oxygen

| Atomic Species | Wavelength Excited (Å) | Excitation Energy (v) | Ionization Energy (v) | Total Ionization Energy (v) | Total Energy (v) |
|---|---|---|---|---|---|
| O I | 1302 | 7.68 | 0.00 | 0.00 | 7.68 |
| O II | 834 | 14.58 | 13.61 | 13.61 | 28.46 |
| O II | 539 | 22.99 | 13.61 | 13.61 | 36.60 |
| O III | 835 | 14.88 | 35.15 | 48.76 | 63.64 |
| O III | 374 | 33.17 | 35.15 | 48.76 | 81.93 |
| O IV | 790 | 15.73 | 54.94 | 103.70 | 119.43 |
| O IV | 239 | 52.00 | 54.94 | 103.70 | 155.70 |

Table 3. Electron Energies Required to Excite Various States of Carbon

| Atomic Species | Wavelength Excited (Å) | Excitation Energy (v) | Ionization Energy (v) | Total Ionization Energy (v) | Total Energy (v) |
|---|---|---|---|---|---|
| C I | 1657 | 7.49 | 0.00 | 0.00 | 7.49 |
| C I | 2478 | 7.68 | 0.00 | 0.00 | 7.68 |
| C II | 858 | 14.44 | 11.26 | 11.26 | 25.70 |
| C III | 977 | 12.69 | 24.38 | 35.64 | 48.33 |
| C IV | 1548 | 8.01 | 47.86 | 83.50 | 91.51 |

as far as aluminum ($Z = 13$); copper ($Z = 29$) has been studied with 18 electrons stripped, and tin ($Z = 50$) with 23 electrons removed.

Keller and Meyerott[2] have computed "stripping" data applicable in the range $10^6$ to $10^8$ °K for various densities of hydrogen and other gases. For iron ($Z = 26$) at $2.32 \times 10^6$ °K and for a gas density of $2.1 \times 10^{-4}$ $\mu g/cm^3$ (more than 75% of the gas being hydrogen), the occupation numbers for the electron shells have been computed by Keller and Meyerott to be 2.0 for $n = 1$, 7.2 for $n = 2$, and 2.4 for $n = 3$. Use of an inert gas such as krypton instead of iron would ensure some stripping down to an argon-like nucleus ($Z = 18$), or a neon-like nucleus ($Z = 10$) under the conditions of much lower densities.

[2]G. Keller and R. E. Meyerott, *The Ionization of Gas Mixtures in Stellar Interiors. II. The Average Number of Electrons Occupying Various Shells*, ANL-4856 (July 1952); see also, *The Ionization of Gas Mixtures in Stellar Interiors*, ANL-4771 (March 1952).

## DOPPLER BROADENING AND SHIFT

The simple Doppler effect on spectrum lines is well known. Random motion of the radiating atoms gives rise to a wavelength shift

$$\lambda_0 - \lambda_S = -\lambda_S \frac{v_S \cos\theta}{c} ,$$

where $v_S \cos\theta$ is the velocity component of the radiating atom along the line of observation and toward the observer, $\lambda_0$ is the wavelength observed, $\lambda_S$ is the wavelength at the source, and $c$ is the velocity of light. This effect is observed generally as a spectrum line broadening of half-width (for a Maxwellian distribution of velocities in the source) of

$$\Delta\lambda = 0.72 \times 10^{-6} \lambda_S \sqrt{\frac{T}{M}} ,$$

where $\Delta\lambda$ is the total line width of the half-intensity points, $T$ is the absolute temperature in degrees

Kelvin, and $M$ is the atomic weight of the radiating atom. The line shape for this case is given by the Gaussian expression

$$I = I_{max}\, e^{-\beta(\Delta\lambda/\lambda)} ,$$

where $\beta$ is $Mc^2/2kT$.

The complete relativistic effect has been treated by Ives[3] and observed by Ives and Stilwell[4] and later by Otting.[5] This complete Doppler effect includes a red shift of the spectrum lines due to the so-called "quadratic" or "transverse" Doppler effect at high velocities. The Doppler shift, including this second-order relativistic term, is for negligible observer motion:

$$\Delta\lambda = \lambda_S \left( -\frac{v_S}{c} \cos\phi + \frac{v_S^2}{2c^2} \right) .$$

In a disordered ion beam of protons having energies of 10 kv ($v_S = 1.4 \times 10^8$), the maximum first-order effect is about 0.005 $\lambda_S$ (about ±25 Å in the blue), while the second-order shift is only about $10^{-5}$ $\lambda_S$ (0.05 Å). Even for deuterons at 100 kv, the second-order effect is only about 0.1 Å. Thus, for all practical purposes in a thermonuclear plasma discharge, the first-order effect alone is significant.

The first-order Doppler shift of spectrum lines due to ordered motion of the radiating system has been observed readily in stellar spectra and in spectra emitted by fast-ion beams; however, only small shifts have been observed in conventional discharge sources. In low-current d-c discharges, very small line shifts (0.001 to 0.004 Å) have been observed in the case of ions which have been accelerated by the weak electric field in the discharge.[6] Unusually large Doppler shifts have been observed in the ORNL electromagnetic separator source arcs, the shifts corresponding to ordered ion motions of several volts of energy (see Fig. 1). The velocity of these ionic drifts ($\sim 2 \times 10^6$ cm/sec) is very closely the same as that in interstellar clouds.[7] It should be noted

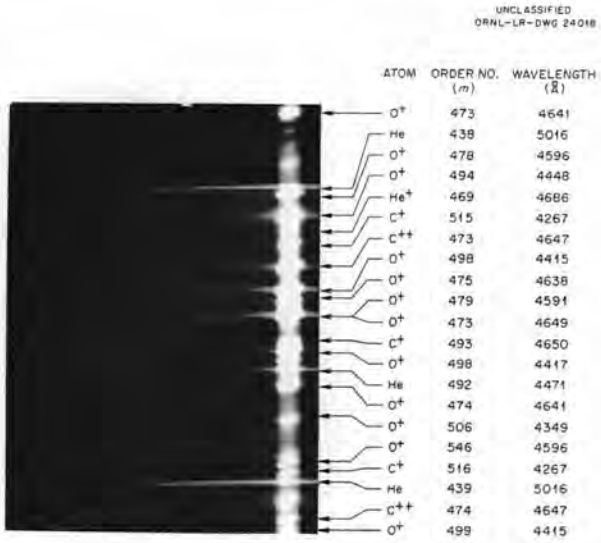


**Fig. 1. Doppler Shifts Due to Ordered Motion of Radiating Ions in the ORNL Electromagnetic Separator Ion Source Arcs.**

that in addition to the slant nature of the ionic spectrum lines, these lines show a marked broadening, indicating possibly a significantly large disordered velocity distribution superimposed on the drift motion of the ions. The spectra of neutral atoms show very slight additional line broadening and no measurable slant effect in these magnetically constrained axial arc sources. These effects are discussed in more detail in the next section.

## "SLANT" SPECTRA DUE TO ORDERED MOTION

Spectroscopic studies have been made of the high-intensity arc used in the large ORNL electromagnetic isotope separators or calutrons. The spectrum lines of ions and the recombination spectra of hydrogen ions show unusually marked broadening and a "slant line effect." This latter effect[8] is attributed to a Doppler shift due to the ordered rotation of ions about the arc column.

The discharge source under study consisted of an open-type calutron $J$ arc which operates as a PIG discharge[8] (see Figs. 2 and 3). Gas, in general, was fed into the filament region. Electrons from the tantalum filament ($K$), which was heated

[3] H. E. Ives, *J. Opt. Soc. Am.* 27, 389 (1937).

[4] H. E. Ives and G. R. Stilwell, *J. Opt. Soc. Am.* 28, 215 (1938).

[5] G. Otting, *Physik. Z.* 40, 681 (1939).

[6] S. E. Frisch and J. M. Kagan, *Zhur. Eksptl. i Teoret. Fiz.* 17, 577 (1947); also personal communication from K. W. Meisnner on smaller shifts observed in d-c operated $Kr^{84}$ and $Kr^{86}$ standard light sources (1957).

[7] E. Fermi, *Phys. Rev.* 75, 1169 (1949).

[8] J. R. McNally, Jr., and M. R. Skidmore, *Unusual Doppler Effects in Calutron Ion Sources*, paper F 3 presented at the Spectroscopy Symposium, Argonne National Laboratory, Chicago, 1956; *J. Opt. Soc. Am.* 47, 863 (1957).

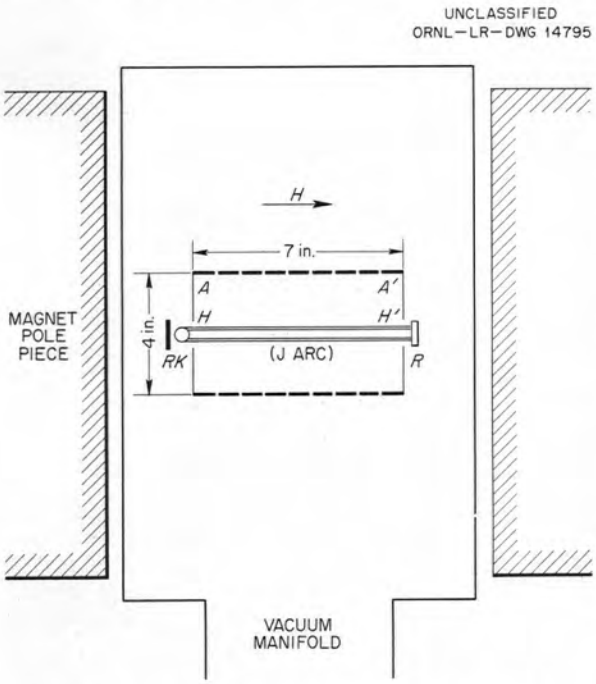


**Fig. 2. Diagram of the Modified Ion Source of the ORNL Electromagnetic Separator.**

by about 350 amp, were accelerated along the magnetic field to a graphite or copper anode plate ($A$) which contained a collimating hole ($H$) for the emergent $J$ arc. The $J$ arc was operated with a floating reflector ($R$) located behind a second anode plate ($A'$) containing a hole ($H'$) similar to the initial collimating hole. Operating parameters include accelerating voltages ($K$ to $A$) up to 200 v and total $J$ currents ($A$ to $K$) up to 20 amp. Pressure in the tank region was about 0.5 $\mu$, and in the $K$ region was an estimated 50 $\mu$. Similar results were obtained when the arc was operated at a total tank pressure ranging from 1 to 100 $\mu$, gas being leaked into the main body of the tank instead of into the filament region. A high-resolution, high-dispersion Bausch and Lomb echelle attachment was used for photographic recording, with exposure times varying from several seconds to several hours. The echelle spectrograph was used at high orders of interference according to the relation

$$2{,}195{,}000 \leqq m\lambda \leqq 2{,}204{,}000$$

Spectrum dispersion was $D = 318/m$ Å per millimeter, where $m$ is the order of interference. Since

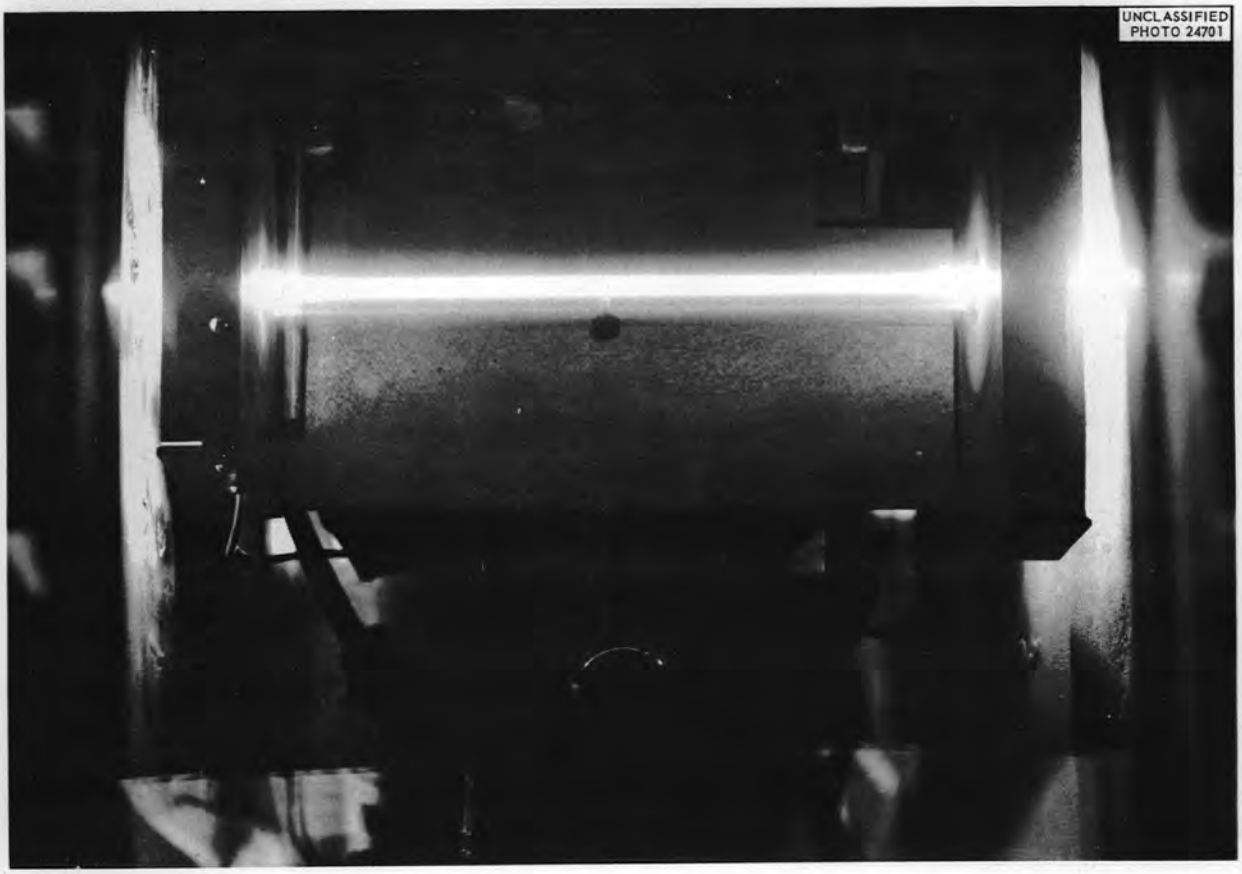


**Fig. 3. Photograph of the Arc in the Modified Ion Source of the ORNL Electromagnetic Separator.**

with the echelle attachment many orders of spectra overlap, it was necessary in some instances to select appropriate interference filters and emulsion sensitivities in order to eliminate line overlaps. Spectra studied included those of hydrogen, helium, carbon, nitrogen, and oxygen.

All the neutral atom lines studied were relatively sharp, being broadened slightly only by the Zeeman effect, interionic fields, Stark effect, and fine structure. Ionic lines revealed an unusual effect in the *J* arc core which included line broadening and a new effect which we call "slant effect" because of the slant appearance of the lines compared with the neutral lines. Hydrogen lines on overexposures showed similar effects on the wings of the parent line which we attribute to electron recombination due to charge exchange with neutral gas atoms. Experiments at fields up to 8000 gauss gave indicated $H^+$ energies of the order of 3 v (see Fig. 4). Ionized helium lines gave energies up to about 15 v (Fig. 1). The so-called "temperature" of these ions as obtained from line widths at the center corresponded to ionic velocities about half the velocity obtained from the slant measurements, but this may or may not be a significant difference. Maximum ionic velocities for all types of ions ($H^+$ in recombination, $He^+$, $C^{++}$, etc.) were in the region of $2 \times 10^6$ cm/sec. The Larmor radii for these ionic velocities in a magnetic field of 7000 oersteds are approximately 0.03, 0.11, and 0.26 cm.

The effects, both slant and broadening, increase with increasing current, increasing voltage, and decreasing pressure; however, since these parameters are interdependent, no direct correlation can be made. The slant and broadening effects are also dependent on the magnetic field strength, reversing when the field is reversed. Figure 5 shows the effect of increasing the magnetic field to about 20,000 gauss. It is believed that this

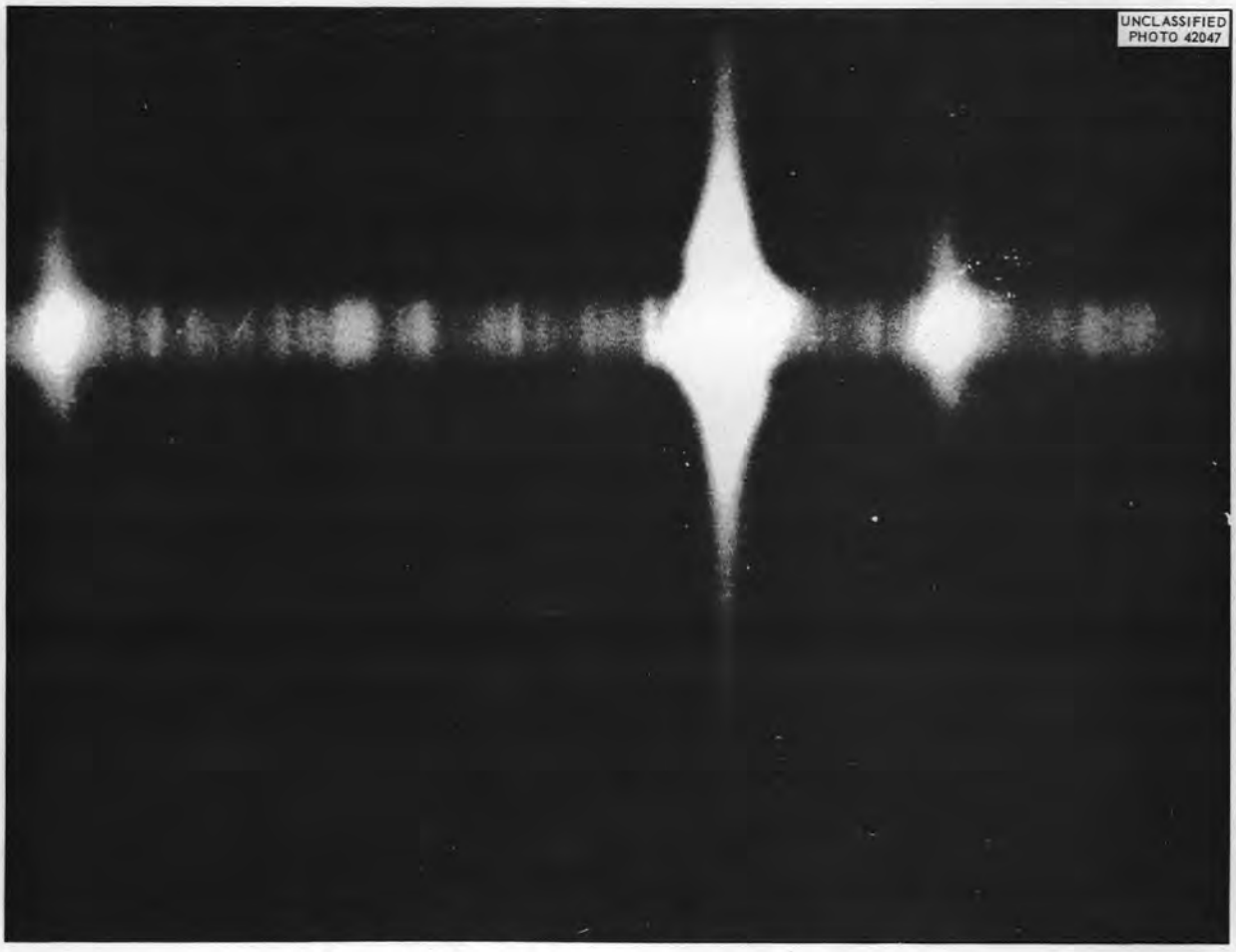


**Fig. 4. Slant Line Effect in the Spectrum of Hydrogen.**

UNCLASSIFIED
ORNL-LR-DWG 21580

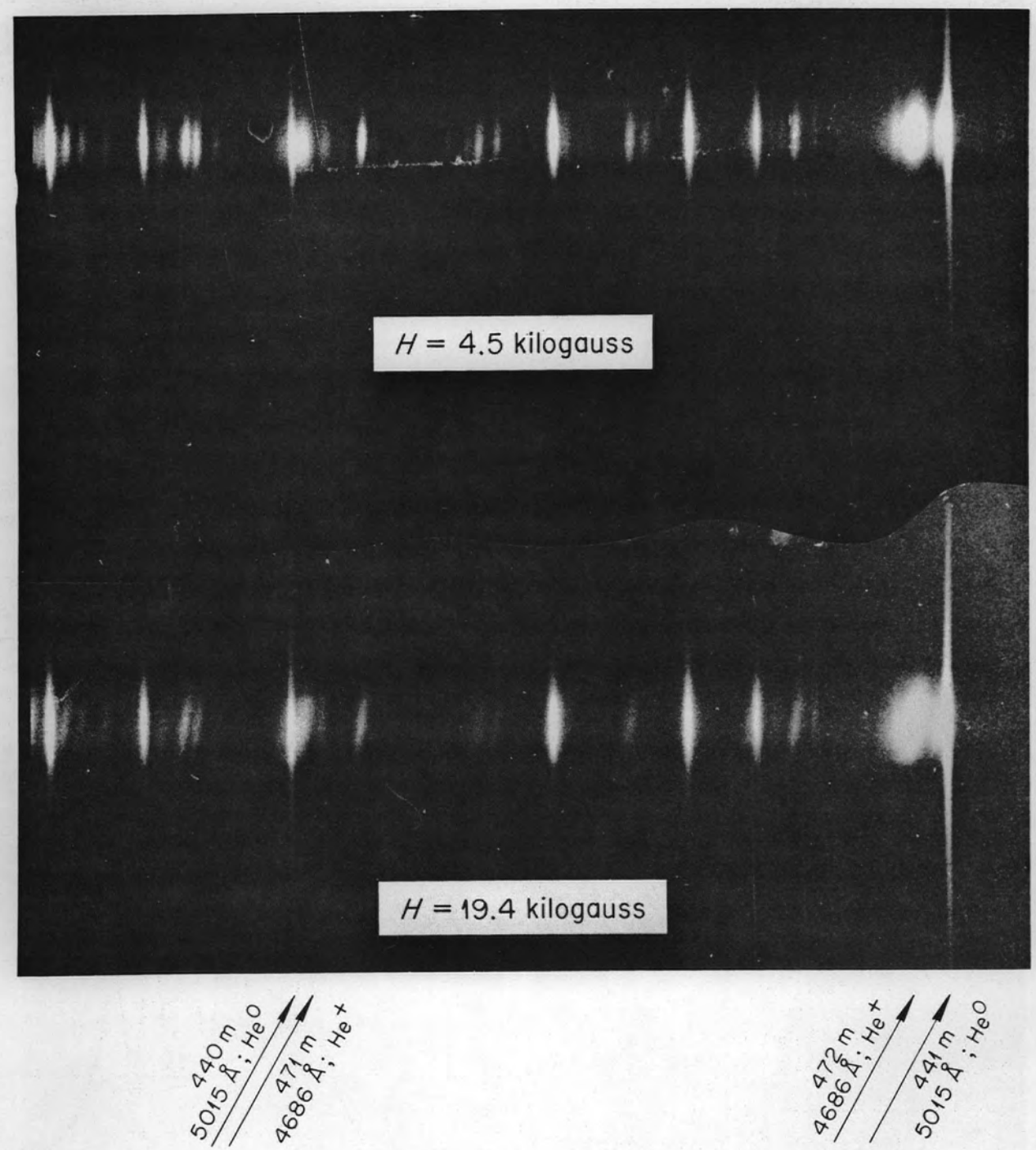


**Fig. 5. Photograph of Doppler Slant Effect in Ionic Spectrum Lines, Showing Dependence on Magnetic Field.**

slant effect is due to the existence of crossed electric and magnetic fields, the electric field being associated with an anode type of fall extending along the magnetic field lines. The radial $E$ field may be computed by the relation[9]

$$E = \frac{v_D H}{c} ,$$

where $v_D$ is the average drift velocity, approximately 0.5 esu or 150 v/cm.

## SELF-ABSORPTION AND PHOTOEXCITATION PROCESSES

The line absorption out of a continuum source of light may be expressed as

$$I_\nu = I_{0\nu}\, e^{-k_\nu x} , \tag{2}$$

where $k_\nu$ is the absorption coefficient at a given frequency, and $x$ is the distance the light beam travels through the gas. The absorption coefficient $k$ depends markedly on the frequency or wavelength in the neighborhood of the critical absorption, the density of the absorbing atoms, the relative population of the absorbing state, the natural or true shape of the absorption spectrum, and the superposed source shape of the absorbers. This last item depends on various perturbing influences which broaden the region of absorption and which may arise from Doppler, Stark, or other sources.

The integral of the absorption coefficient over the region of absorption is dependent only on the total number of absorbing atoms and is completely independent of all other physical processes contributing to the absorption line, provided that the emission contribution to the same line by excited atoms is negligible.[10] In the general case, we have

$$\int k\, d\nu = \frac{\lambda^2 g_2 N_1}{8\pi g_1 \tau} \left(1 - \frac{g_1}{g_2}\frac{N_2}{N_1}\right) ,$$

where $\lambda$ is the wavelength in centimeters, $\nu$ is the frequency, $\tau$ is the half life of the excited state, $g_1$ and $g_2$ are the statistical weights of the low and excited states, respectively, and $N_1$ and $N_2$ are the densities of atoms in the low and excited states, respectively. In low-temperature gases the second term on the right can be neglected. In terms of a classical oscillator of strength $f$, this integral of the absorption coefficient is also used in the form

$$\int k_\nu\, d\nu = \frac{\pi e^2 N_1 f}{mc} .$$

For small $k_\nu x$ and for $I_{0\nu}$ constant, Eq. 2 can be approximately rewritten as

$$I_{abs} = I_0 \frac{\pi e^2 N_1 f x}{mc} ,$$

where $I_{abs}$ is the integrated absorption

$$\int (I_0 - I_\nu)\, d\nu .$$

Thus, if the oscillator strength of a particular transition is known or can be calculated, the density $N_1$ may be determined.

Self-absorption by monatomic atoms is generally considered a plague insofar as the spectrochemist is concerned. Figure 6 shows a trace of self-absorption in an electrodeless discharge tube excited by about 20 w of power. The five-component structure of Hg 2537 appears as five minima on the figure. This indicates the unusually high degree of sensitivity to be expected for resonance absorption transitions.

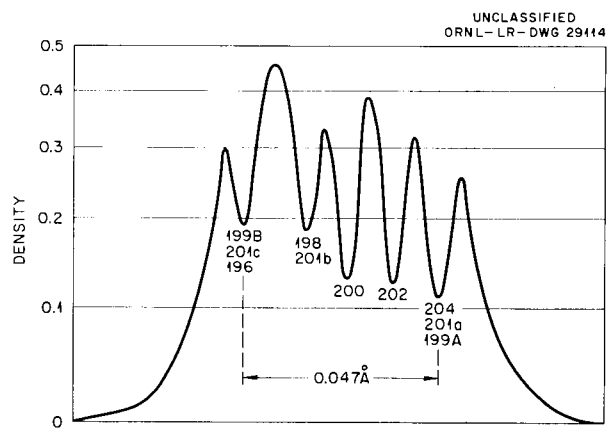


**Fig. 6. Self-absorption in the Hyperfine Components of the 2536-Å Resonance Line of Mercury.**

[9] H. Alfven, *Cosmical Electrodynamics*, Clarendon Press, Oxford, 1950.

[10] See, for example, A. C. G. Mitchell and M. W. Zemansky, *Resonance Radiation and Excited Atoms*, MacMillan, New York, 1934; see, also, E. Hinnov, *J. Opt. Soc. Am.* 47, 151 (1957); and E. Hinnov and H. Kohn, *J. Opt. Soc. Am.* 47, 156 (1957).

## ELECTRON DENSITY BY SERIES TERMINATION

The Bohr radius of the $n$th hydrogen orbit is

$$r = 0.528n^2 \times 10^{-8} \text{ cm} .$$

Bohr suggested that in a neutral gas the orbiting electron would be perturbed if the gas density approached $1/r^3$. Thus, for observing the tenth member of the Balmer series, this critical density would have to be about $15 \times 10^{18}$ particles/cm$^3$ or one-half an atmosphere of pressure. Actually Wood[11] found that the condition for extending the series was best met when the excitation was such as to give a positive column essentially devoid of molecular hydrogen. Other workers[12] have also observed that anomalous spectrum broadenings and shifts occur when the neutral gas density is such that the interparticle distance approaches the so-called "Bohr radius," the effects varying with different gases. In the case of hydrogen, Whiddington observed only four series lines at a pressure of 1 mm but obtained 20 members at a pressure of $10^{-3}$ mm. It is clear, however, that the evaluation of neutral density by this classical Bohr model does not give a unique explanation for the limiting of the hydrogen series, although series perturbations do occur.

Should the particles be ions, the perturbing Coulomb energy is about $15/r$, with $r$ in angstroms, or 0.3 v for $r = 50$ Å. Such a perturbation, amounting to a Stark electric field strength of 600,000 v/cm, would smear out such states into practically a continuum. Even at densities of about $10^{15}$ electrons/cm$^3$, $r = 1000$ Å, the first-order Stark effect for $H_\alpha$ (due to perturbations of order 1500 v/cm) would give rise to significant line broadening. Eventually the lines disappear into the continuum. The Inglis-Teller relation,[13] which has been verified by Mohler,[14] gives

$$N_e = \frac{10^{23}}{n_m^{7.5}} ,$$

where $n_m$ is the maximum orbit number observed. This relation is quantitatively determined by plotting the log of the line-to-line background intensity ratio against the log of the quantum number and extrapolating to zero intensity ratio (i.e., $I_{\text{line}} = 0$). Since this condition can be observed quite readily by inspection, a rough estimate of electron density may be obtained (see Table 4). Accurate quantitative results may be obtained by detailed evaluation of the Mohler plot. The ion and electron densities are essentially the same in this density region.

**Table 4. Limiting Excitation States and Lines of Hydrogen vs Electron Densities**

| $N_e$ (cm$^{-3}$) | $n_m$ | λ (Å)* |
|---|---|---|
| $5 \times 10^{17}$ | 5 | 4340.47 |
| $2.3 \times 10^{17}$ | 6 | 4101.74 |
| $4.6 \times 10^{16}$ | 7 | 3970.07 |
| $1.7 \times 10^{16}$ | 8 | 3889.06 |
| $6.9 \times 10^{15}$ | 9 | 3835.40 |
| $3.2 \times 10^{15}$ | 10 | 3797.91 |
| $1.6 \times 10^{15}$ | 11 | 3770.06 |
| $8.1 \times 10^{14}$ | 12 | 3750.15 |
| $4.4 \times 10^{14}$ | 13 | 3734.37 |
| $2.5 \times 10^{14}$ | 14 | 3721.95 |
| $1.5 \times 10^{14}$ | 15 | 3711.98 |
| $9.3 \times 10^{13}$ | 16 | 3703.86 |
| $5.9 \times 10^{13}$ | 17 | 3697.15 |
| $3.9 \times 10^{13}$ | 18 | 3691.55 |
| $2.5 \times 10^{13}$ | 19 | 3686.83 |
| $1.7 \times 10^{13}$ | 20 | 3682.82 |
| $1.2 \times 10^{13}$ | 21 | 3679.35 |
| $0.9 \times 10^{13}$ | 22 | 3676.34 |

*Deuterium lines are shifted to the violet by approximately λ/3672 and tritium lines by λ/5508.

## RECOMBINATION, BREMSSTRAHLUNG, AND CHARGE EXCITATION RADIATION

Recombination, in the broad sense, means the process whereby the charge state of an ion is decreased by the acquisition of an electron from the plasma electron sea or by charge exchange

[11] R. W. Wood, *Proc. Roy. Soc.* (*London*) **97A**, 455 (1920).

[12] N. Tsi-Zé and C. Shang-Yi, *Phys. Rev.* **51**, 567 (1937); H. Margenau and W. W. Watson, *Revs. Modern Phys.* **8**, 22 (1936).

[13] D. R. Inglis and E. Teller, *M. N.* **98**, 694 (1938); also, *Astrophys. J.* **90**, 439 (1939).

[14] F. L. Mohler, *Astrophys. J.* **90**, 429 (1939).

involving another atom. In the restricted sense it means only the former process, in which case the total charge (positive and negative) in the plasma is reduced by a factor of 2. Bremsstrahlung radiation pertains to the so-called "free-free" photon transitions in which an electron is decelerated by a heavy ion, and the momentum and energy, including those of the photon, are conserved in the resulting three-"body" system. Similarly, electron capture by ionized molecules may occur with subsequent dissociation of the molecule.

The actual phenomenon of charge exchange by relatively fast ions (several volts) has been observed spectroscopically in high-density arc streams, as discussed previously. The ions radiate spectra with Doppler shifts appropriate to the ion motion immediately prior to capturing the electron. The neutrals remember what they were doing as ions just before the charge exchange event occurred.

The bremsstrahlung power radiated from a plasma of electron density $n_i$ depends on the electron energy. Obviously, in a free-free transition the electron cannot radiate more energy than its kinetic energy. In fact, the radiation spectrum is sensibly flat on a frequency scale out to this maximum energy. The total radiated power is

$$P = 1.3 \times 10^{-32} n_i^2 \sqrt{V} \ .$$

where $n_i$ is the electron density in $cm^{-3}$, $V$ is the electron temperature in volts, and $P$ is the power in $w/cm^3$. Ninety per cent of this radiation occurs in the wavelength region from $\lambda = 12{,}395/V$ to $1{,}239.5/V$. Thus, if $V = 10^4$ v, essentially all the radiation is x rays.

Recombination cross sections are small, especially for plasmas containing fast electrons. Even in hydrogen at a temperature of only 1 ev, the recombination cross section is $2 \times 10^{-21}$ $cm^2$, a value which compares more with nuclear interaction cross sections than with atomic ones.

## COLLISION BROADENING OF SPECTRUM LINES

The treatment of collision broadening of spectrum lines is usually considered from either of two limiting aspects. The Holtzmark theory involves a statistical approach, whereas the Lorentz theory is an impulse type of approach. In the former the atom is considered to be continuously under the influence of a perturbing force during the radiation process, and the radiated frequency is represented as a probability distribution about some mean value. The impact theory assumes that the radiated wave train is disturbed instantaneously so that a phase change occurs, and the independent wave trains are then treated by using a Fourier analysis. The impact theory gives rise to broadening effects near the line center, whereas the statistical theory contribution is mainly in the wings of the line. There have been numerous recent reviews of the earlier theories, notably by Sobelman,[15] Kolb,[16] Breene,[17] and Aller.[18] Major contributors to the early theories were Lorentz, Lenz, Weisskopf, Jablonski, and Lindholm in the case of the impact theory, and Holtzmark and Margenau in the statistical case. Attempts such as the one of Kolb to join the two theories have not been entirely successful because of the approximations necessary to the calculations. A generalized relation for the intensity distribution of pressure-boradened spectrum lines is of the form

$$I = \frac{I_0 N v \sigma_r}{\pi \left[(\nu - \nu_0 - N v \sigma_i)^2 + (N v \sigma_r)^2\right]^2} \ ,$$

where $\sigma = \sigma_r + i\sigma_i$ is the collision cross section, and $Nv\sigma$ is the number of collisions per second $(=1/\tau)$. For the $1/r^4$ type of interaction forces (quadratic Stark effect) $\sigma_r/\sigma_i = 0.58$, whereas for the $1/r^6$ interactions (van der Waal's forces), $\sigma_r/\sigma_i = 1.4$. The quantity $Nv\sigma_i$ represents an actual line shift such as might be caused by fast ions or electrons or by the quadratic Stark effect. For hydrogen-like interactions or ion-ion interactions which are of the $1/r^2$ type, the above theory of collisional broadening breaks down. The Holtzmark theory is applicable to hydrogen and helium for $1/r^2$ interactions.

In the case of a superimposed electric field, the Balmer $H_\alpha$ line splits into five major components,

---

[15] I. I. Sobelman, *Uspekhi Fiz. Nauk* 54, 550 (1954).

[16] A. C. Kolb, *Theory of Hydrogen Line Broadening in High-Temperature Partially Ionized Gases*, AFOSR-TN-57-8 (March 1957).

[17] R. G. Breene, Jr., *The Shift and Shape of Spectral Lines*, AFCRC-TR-55-214 (September 1955), available from U.S. Dept. of Commerce; also, *Revs. Modern Phys.* 29, 94 (1957).

[18] L. H. Aller, *Astrophysics; the Atmospheres of the Sun and Stars*, Ronald Press Co., New York, 1953.

the maximum separation between strong components being approximately

$$\Delta T\ (\mathrm{cm}^{-1}) = 25 \times 10^{-5} F \ ,$$

where $F$ is in volts per centimeter. Thus, at $10^4$ v/cm, the $H_\alpha$ line has components 2.5 $\mathrm{cm}^{-1}$ apart which can readily be observed. The author has measured fields as low as 3000 v/cm in the dark space of the hollow cathode source by using the $H_\beta$ line. The higher-series members are split to a degree which goes approximately as $(n - 1)^2$. Nonuniform electric fields of this order of magnitude would show a line broadening of this same magnitude. The nonuniform fields due to ionic concentrations may be determined from the Stark broadening of the Balmer lines by using Holtzmark's theory. The width of different hydrogen lines broadened by a uniform potential gradient is given below, where $F$ is in kv/cm:

| Line | $\Delta\lambda/F$ (Å) |
|---|---|
| $H_\alpha$ | 0.11 |
| $H_\beta$ | 0.28 |
| $H_\gamma$ | 0.43 |
| $H_\delta$ | 0.61 |

This line broadening of hydrogen due to the linear Stark effect may also be used to measure ion densities (when Doppler and Zeeman effects are negligible). Ordinary ionic broadening of hydrogen lines by the interatomic Stark fields is proportional to $(n_+)^{2/3}$. Shown below are representative values for $H_\beta$:

| $n_+$ ($\mathrm{cm}^{-3}$) | $\Delta\lambda$ (Å) |
|---|---|
| $10^{10}$ | 0.0006 |
| $10^{11}$ | 0.0028 |
| $10^{12}$ | 0.013 |
| $10^{13}$ | 0.06 |
| $10^{14}$ | 0.28 |
| $10^{15}$ | 1.3 |
| $10^{16}$ | 6 |
| $10^{17}$ | 28 |
| $10^{18}$ | 130 |

## ZEEMAN EFFECT

Most, if not all, thermonuclear scientists are convinced that hot plasmas must be held off the container walls by magnetic fields in order to reduce evaporation and sputtering of the solid container material into the plasma and to confine the high-temperature gases. The magnetic splitting of an atomic state, neglecting for simplicity the nuclear hyperfine contribution, is given by

$$\Delta\sigma = \frac{\Delta W}{hc} = m_J g \frac{eH}{4\pi mc^2} \ ,$$

where $m_J$ is the magnetic quantum number $(J \geqq m_J \geqq -J)$, $g$ is the Landé $g$ factor, and $H$ is the magnetic field in oersteds. Introducing the physical constants we have

$$\Delta\sigma = 4.67 \times 10^{-5} m_J g H \ .$$

Thus, for $m_J = g = 1$ and $H = 25{,}000$ oersteds, the magnetic splitting of the components is $\pm 1.17$ $\mathrm{cm}^{-1}$ or about $\pm 0.19$ Å at 4000 Å. Optical polarizers can be set to pass only the $\pi$ components and will reduce, in general, the actual line width from 0.38 Å to a small value, depending on the quantum complexity of the particular line.

# ZEEMAN DATA REDUCTION. PART I

K. L. Vander Sluis

The availability of several unique tools applicable to a Zeeman program has led to a new approach to the general problem of classification of atomic spectra. The improved quality of spectrograms obtained when the advantages of high-resolution electrodeless discharge tubes, a stable medium-strength (33,000-oersted) magnetic field, and the high-resolution echelle spectrograph are combined has been demonstrated.[1-3] It was also demonstrated that, when data from these spectrograms were given full use by application of least-squares calculation, the resulting Landé $g$ factors that could be computed routinely were two orders of magnitude more precise than the results of other workers in the field.

The Landé $g$ factor is the ratio of the magnetic moment to the mechanical moment of the atom in a given energy state, and as such is a number descriptive of that energy state. Landé $g$ factors, which were reliable to a few per cent, were useful in the search for energy levels in the atom, but only in a qualitative sense. The increase in precision by two orders of magnitude, however, makes feasible the use of the Landé $g$ factor as a quantitative description of the energy level. A second quantitative measure of the energy level obtainable from the Zeeman spectrogram is the value of the total angular momentum quantum number ($J$). The combination ($J,g$) then forms an almost unique identification of an atomic energy level.

The disadvantages introduced by the Zeeman approach to classification of atomic energy levels are the increased number of observations that have to be made and the time expended in computing and arranging the results into a meaningful order. It is the purpose of this report to describe a method which has eliminated the second disadvantage by use of the Oracle in all phases of computation and data handling.

The application of the number combinations ($J,g$) to the problem of setting up the energy-level system is a simple deductive process. If the radiating atom is placed in a weak magnetic field, each transition will become a set of transitions which comprise the Zeeman pattern. From this pattern the values of the total angular momenta $J$ and the Landé $g$ factors[4] can be computed for both the energy levels involved in the transition of energy $\nu$. After completion of these calculations for a number of transitions, the information pertaining to a given energy level may be extracted by searching through the results for all transitions which contain the ($J,g$) combination describing the desired energy level. In this manner a new list may be formed which consists of the ($J,g$) of a level common to a set of transitions $\nu_i$ [and the corresponding $(J,g)_i$ levels which terminate these transitions] for each of the combinations that occur. This is then a listing of proposed energy levels identified by ($J,g$); and with each proposed energy level is a sublisting of possible transitions $\nu_i$ which terminate on the corresponding levels $(J,g)_i$.

Oracle routines which will perform the above operations have been completed and checked. The Oracle is supplied with the parameters which relate distance measurements on a spectrogram to wavelengths of light and with the set of distance measurements of the observed spectrum lines. With this information the machine will in one continuous operation compute by least squares the Landé $g$ factors and store the results on magnetic tape. Upon completion of these calculations the list of results is ordered by energy of transition $\nu$. This allows multiple observations of a given transition to be grouped and reduced to a single

[1] P. M. Griffin and K. L. Vander Sluis, *Stable Isotope Research and Production Semiann. Prog. Rep. May 20, 1955*, ORNL-1908, p 7; *Nov. 20, 1955*, ORNL-2208, p 3; K. L. Vander Sluis, P. M. Griffin, and J. H. Vander Sluis, *Nov. 20, 1955*, ORNL-2208, p 6.

[2] P. M. Griffin and K. L. Vander Sluis, *The Application of Electrodeless Discharge Sources and the Echelle Spectrograph to Zeeman Spectroscopy*, paper presented at the Meeting of the Optical Society of America, Pittsburgh, Pennsylvania, October 6–8, 1955.

[3] P. M. Griffin and K. L. Vander Sluis, *Application of New Techniques to Zeeman Spectroscopy*, paper presented at the Spectroscopy Symposium, Argonne National Laboratory, February 15–17, 1956.

[4] K. L. Vander Sluis, *J. Opt. Soc. Am.* **46**, 605 (1956).

weighted mean observation of the Landé $g$ factors and transition energy $\nu$. Continuing, the machine then orders the averaged list by the $(J,g)$ combinations so that the information pertaining to each level is grouped together. Calculation times for these operations, of course, vary somewhat with each specific case but can be given approximately as follows:

| | |
|---|---|
| Landé $g$ factor calculation and storage | 2.1 sec/pattern |
| Ordering results by $\nu$ | 1000 groups/min |
| Reduction of multiple observations | 500 groups/min |
| Ordering results by $(J,g)$ | 600 groups/min |

There are, of course, auxiliary routines included which allow a monitoring output of results at any stage and the deletion or insertion of information on the list as well as other functions necessary for keeping an ordered list. The key routine which allows the data to be treated in terms of a complete list rather than as individual Zeeman-pattern results is the sorting routine written by Vander Sluis.[5]

Part II of this problem is concerned with confirming the possibility of the transitions listed in Part I. The confirmation requires that the Ritz combination principle, in addition to the $(J,g)$ relationships, be satisfied. The process of confirming the transitions will result in the meshing of the $(J,g)$ sublists into an energy-level system.

[5] J. H. Vander Sluis, Mathematics Panel Information Meeting, 1957.

## SPHERICAL ELECTROSTATIC SPIN ROTATOR FOR ELECTRON POLARIZATION MEASUREMENTS

H. B. Willard A. Galonsky H. O. Cohn N. H. Lazar

In order to observe an asymmetry in Mott scattering of beta particles from gold, it is necessary to convert the longitudinal spin of the electron into a transverse spin.[1] This has been done by bending the electron path through 136 deg with the electric field in a 1-cm gap between two spherical aluminum plates of mean radius 25 cm.

The plates are shown in Fig. 1. At the left-hand entrance to the plates is a beryllium can containing the radioactive source and a brass fitting with a small aperture. The three vertical pieces between the plates are Lucite strips with slots (not visible in this picture) to collimate the electron beam through the spin rotator.

The 624-kev $Cs^{137}$ $K$ electrons are transmitted when the plates are charged to ±17.5 kv. As shown in Fig. 2, the resolution is sufficient to separate the $K$ and $L$ lines. With a ±6-deg azimuthal acceptance angle at the source, the transmission is $5 \times 10^{-5}$ at this energy.

Because of relativistic effects there is no radial focusing, but in the direction of the expected scattering asymmetry (up-down) the image of a 1.5-mm source is ~3 mm wide at half maximum. Electrons which are scattered from the plates (and possibly depolarized) are not focused and appear as tails on the intensity distribution of the image. By inserting Lucite apertures between the plates, the ratio of peak-to-tail intensity for a $P^{32}$ source has been made ~100.

The importance of collimation in reducing the relative amount of scattered electrons in the emergent beam is illustrated in Fig. 3. Most of this reduction is accomplished with the Lucite aperture nearest the source. The dashed curve was obtained with an additional brass aperture placed 2½ in. from the gold scattering foil. It is concluded that, with the present collimation and $P^{32}$ source, about 2% of the beam striking the gold is not focused and may arise from scattering in the plates and aberrations caused by edge effects in the spin rotator.

Figure 4 shows the scattering apparatus: essentially a gold foil and two 1¼ × 0.14 in. anthracene counters 3.6 in. from the gold at angles of 135 deg with respect to the incident beam. Measurements thus far on $P^{32}$ at 0.63 Mev

[1] H. A. Tolhoek, *Revs. Modern Phys.* 28, 277 (1956).

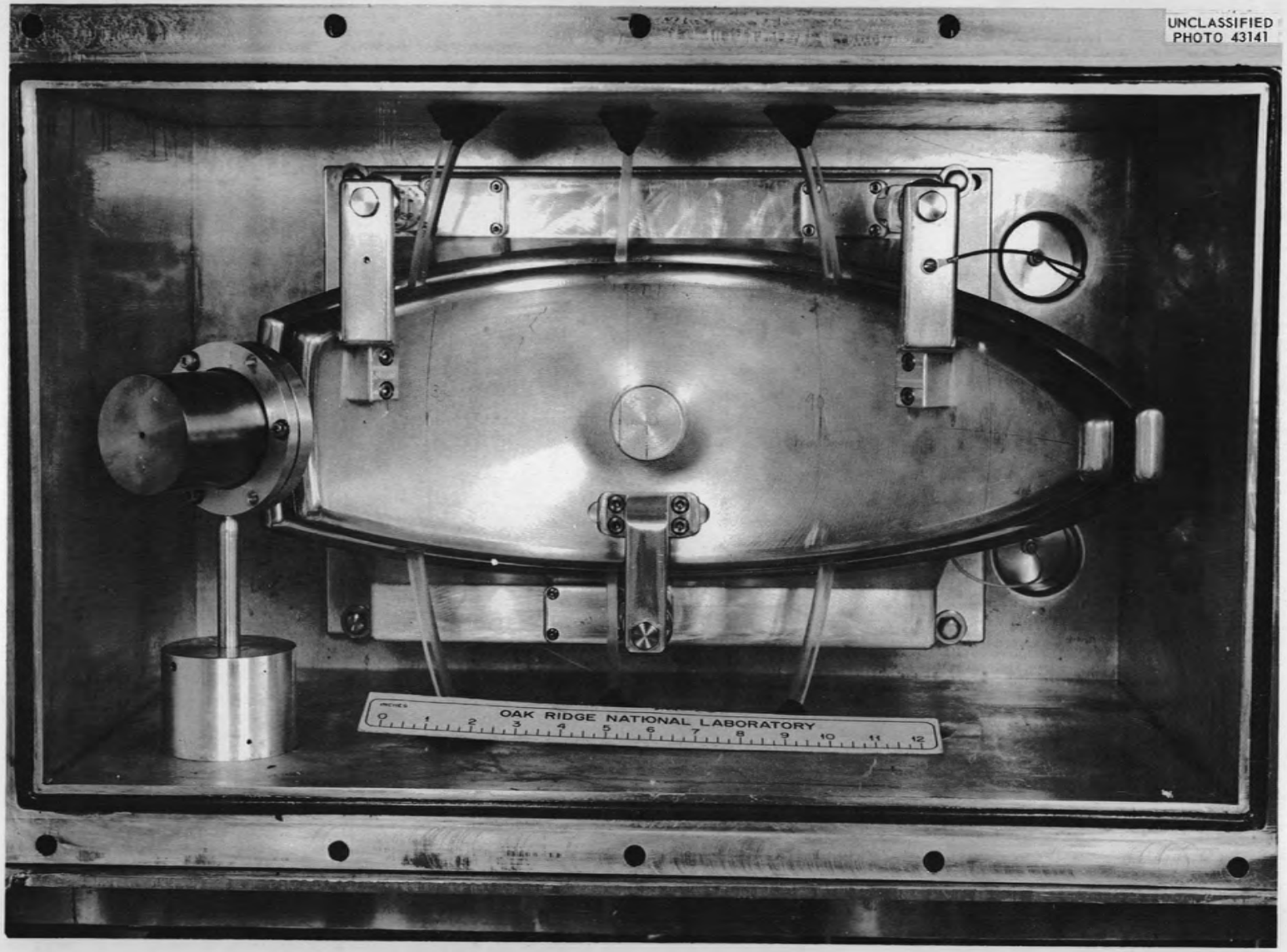


Fig. 1. Photograph of the Spin Rotator. The radioactive source is in the beryllium can at the left.

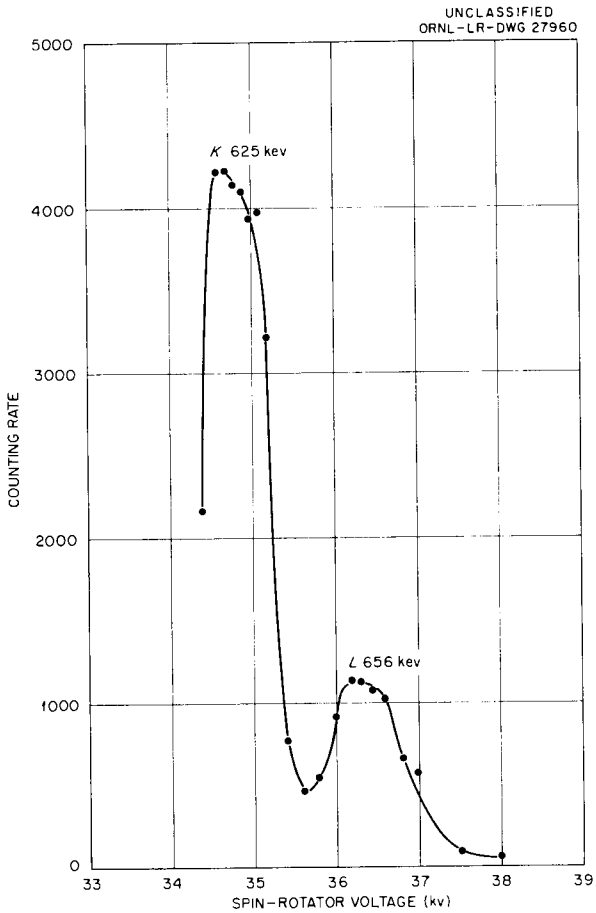


**Fig. 2. Energy Calibration and Resolution of the Spin Rotator as Measured with Conversion Electrons of $Cs^{137}$.**

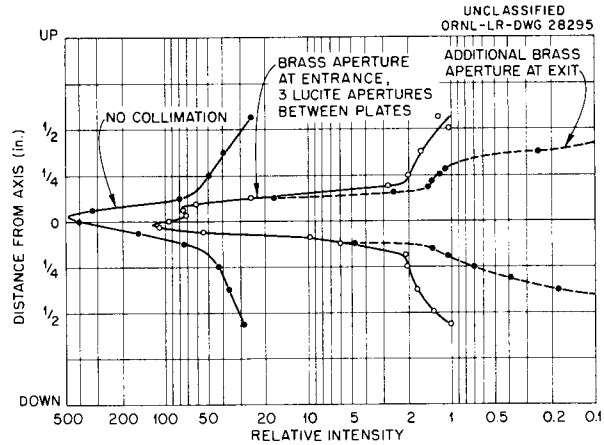


**Fig. 3. Improvement of Beam Purity by Collimation. These data were obtained by scanning across the beam with a small brass aperture and an anthracene scintillation spectrometer.**

have yielded up-down asymmetries (omitting small corrections of 0.87 ± 0.03 for 7.4-mg/cm$^2$ gold and 0.71 ± 0.03 for 2.0-mg/cm$^2$ gold. As may be seen from Fig. 5, 0.47 is the ratio expected if the initial longitudinal polarization is $v/c$.

This work is being performed in collaboration with A. R. Brosi and B. H. Ketelle of the Chemistry Division. J. W. Johnson of the Instrumentation and Controls Division is responsible for much of the detailed design of the equipment.

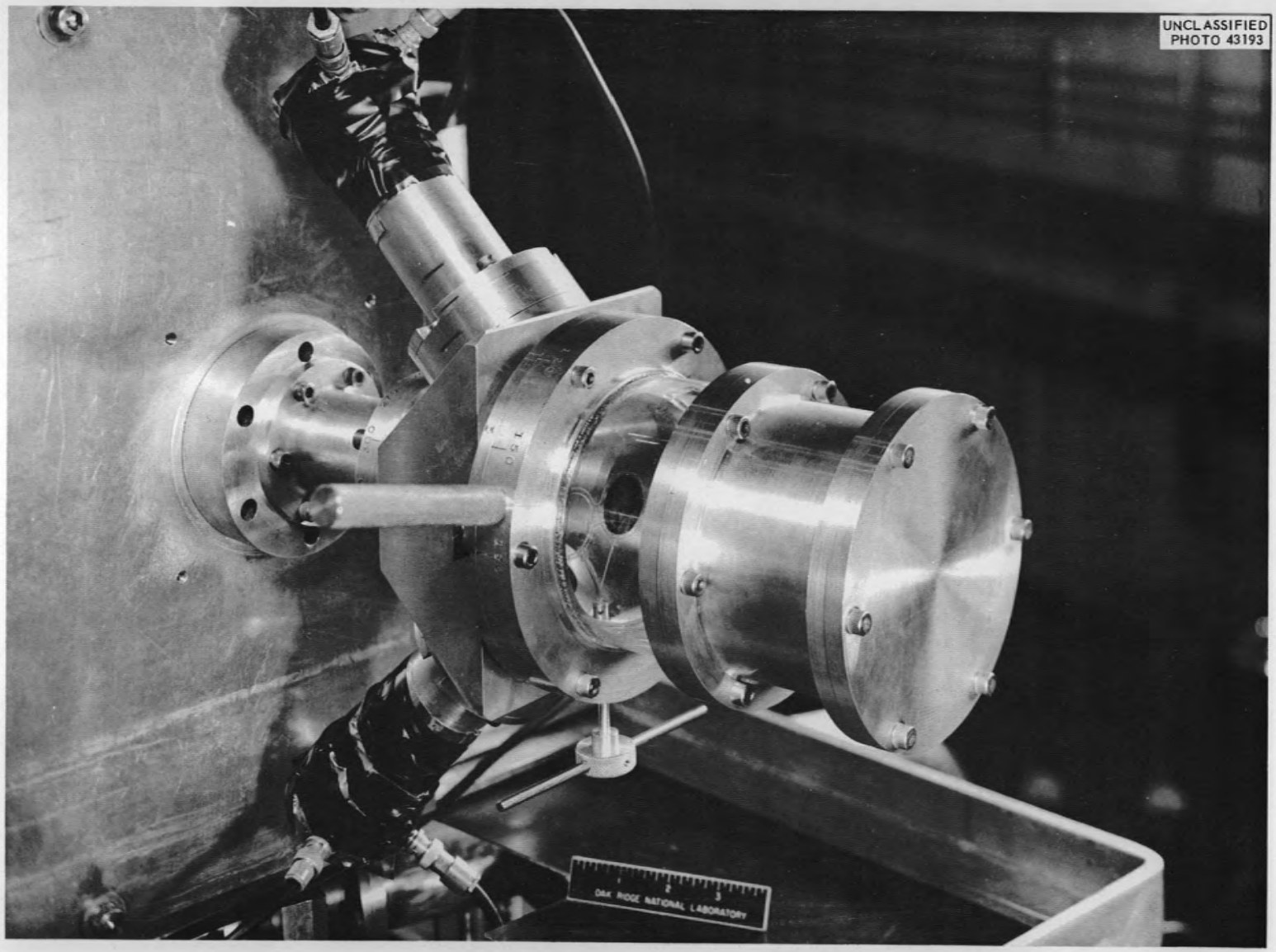


Fig. 4. Photograph of the Scattering Apparatus.

UNCLASSIFIED
ORNL-LR-DWG 27961

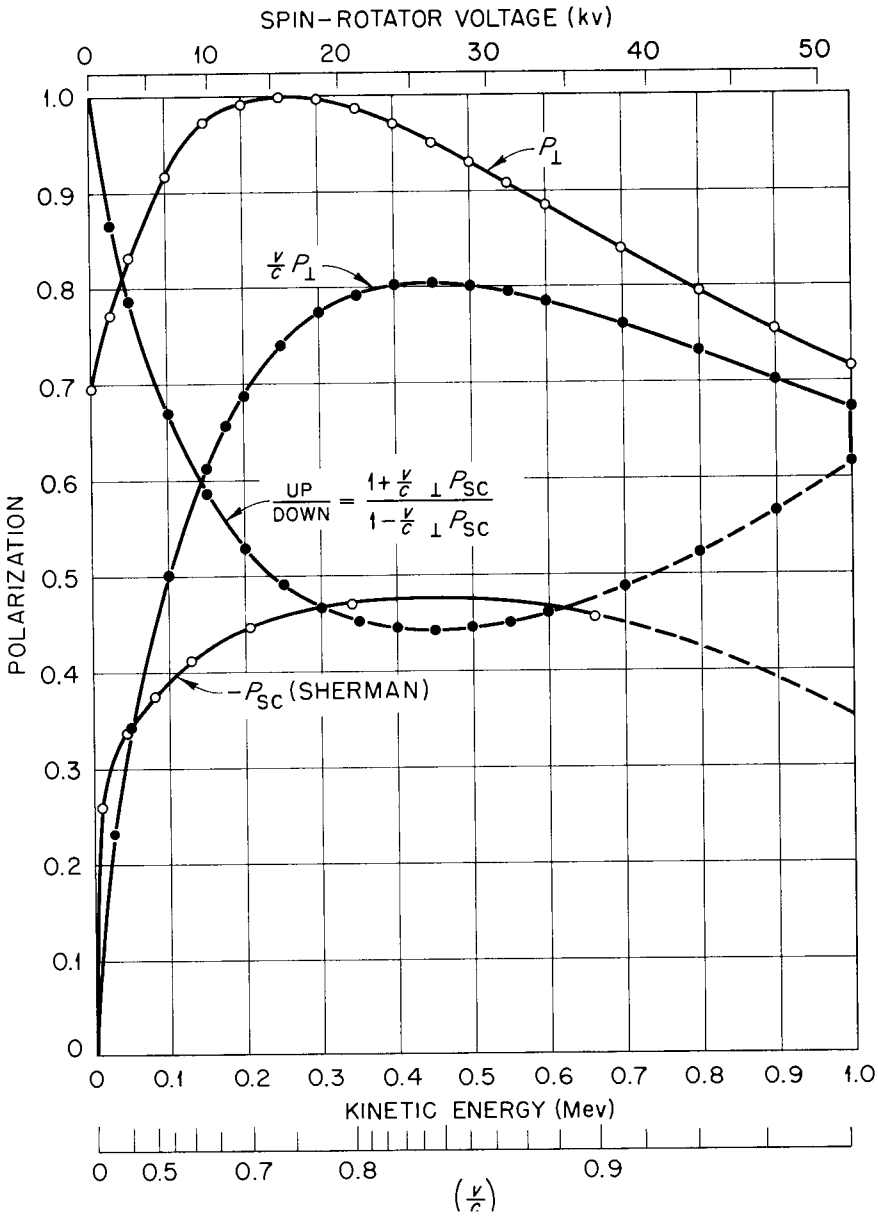


**Fig. 5. Polarization Properties of the Spin Rotator as a Function of Electron Energy.** $P_\perp$ is the fractional transverse polarization the spin rotator imparts to an electron with an initial longitudinal polarization of 1; $(v/c)P_\perp$ is the transverse polarization of an electron with initial longitudinal polarization of only $v/c$; $P_{sc}$ (Sherman) is a calculation by N. Sherman, *Phys. Rev.* **103**, 1601 (1956) of the polarization produced by scattering unpolarized electrons from gold through an angle of 135 deg; the up-down asymmetry is then

$$\frac{1 + (v/c)\,P_\perp\,P_{sc}}{1 - (v/c)\,P_\perp\,P_{sc}}$$

if the electron has an initial longitudinal polarization of $v/c$.

## BROAD-AREA GERMANIUM *p-n* JUNCTION COUNTERS

J. W. T. Dabbs F. J. Walter L. D. Roberts

Germanium (*p-n*) surface barriers, similar to those first used by Mayer and Gossick,[1] have been found suitable for use as both alpha-particle and fission-fragment counters at liquid-nitrogen and at liquid-helium temperatures. A typical counter (Figs. 1 and 2) is prepared from a wafer of germanium cut from a large single crystal. This wafer, about ½ mm thick by about 1 $cm^2$ in area, is etched to remove surface damage caused by the cutting, and the two faces are then coated with a thin (on the order of 1000 Å) layer of gold. No effort has been made thus far to produce a surface barrier that is good at room temperature. At liquid-nitrogen temperatures and below, however, the electrical resistance at ~1 v is found to be very high, and, since the germanium intrinsic resistance is still relatively low at 77°K, it is inferred that a barrier is formed.

With about 1 v applied to the barrier, pulses of about 0.5 mv have been obtained for 4.8-Mev alpha particles. The resolution under optimum conditions was found to be 4% at 77°K (Fig. 3). Correspondingly larger pulses are obtained for fission fragments up to ~100 Mev, and Fig. 4 shows these results obtained at 4.2°K. Approximate proportionality between pulse height and energy was found. No effects attributable to radiation damage have been observed from a bombardment of about $10^{11}$ alpha particles.

[1] J. Mayer and B. Gossick, *Rev. Sci. Instr.* 27, 407 (1956).

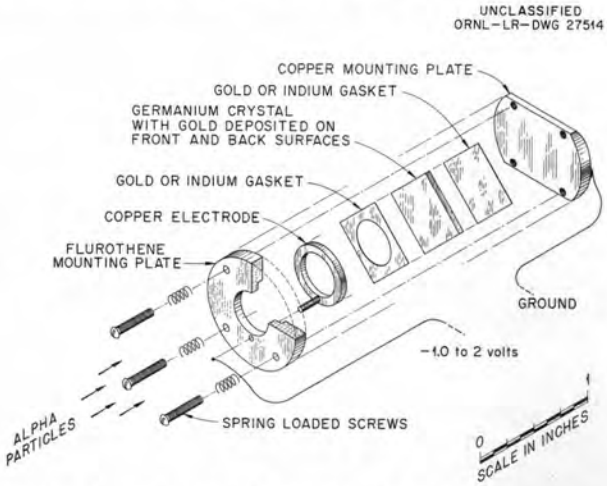


**Fig. 2. Construction Details of a Germanium Conduction Counter.**

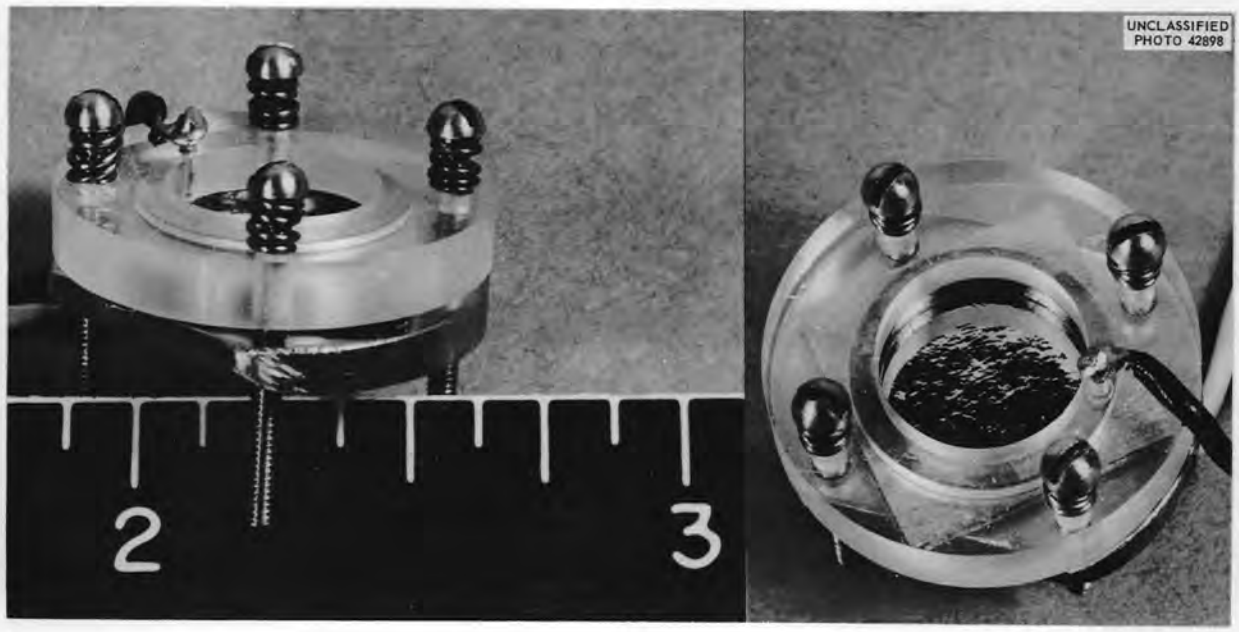


**Fig. 1. Germanium Conduction Counter.**

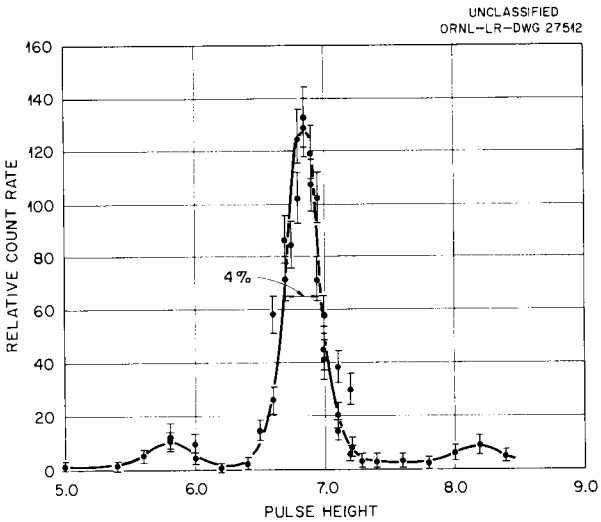


**Fig. 3. Count Rate as a Function of Pulse Height for *n-p* Germanium Surface-Barrier Counter at 77°K.** The main peak is due to $U^{233}$ (4.82 Mev) alpha particles, and the side peaks are due to impurities.

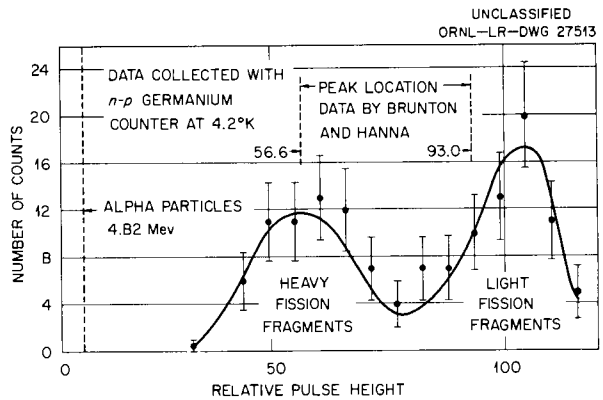


**Fig. 4. Pulse-Height Distribution of $U^{233}$ Alpha Particles and Thermal Fission Fragments.**

A possible mechanism for the counter operation may be as follows: The thickness of the barrier layer is presumably of the same order of magnitude as the range of the alpha particles or fission fragments. An electron-hole pair is formed in the crystal for each 3 ev of energy lost by the energetic particle,[2] thus yielding about $1.6 \times 10^5$ pairs for a 4.8-Mev alpha particle. The voltage gradient in the barrier is presumably of the order of 1000 v/cm, and with the very high electron and hole mobilities found at low temperatures, the collection time would be expected to be $10^{-10}$ to $10^{-11}$ sec. The 0.5-mv pulse height found for 5-Mev alpha particles suggests an effective capacitance of the order of 1000 $\mu\mu$f, a value not inconsistent with the assumed barrier thickness and the germanium dielectric constant.

When the counter is first cooled to liquid-helium temperature, the pulse height is double that found at 77°K. This increased pulse voltage is then found to decay to approximately the 77°K value in about 1 to 2 hr. This effect, as well as the apparently high effective capacitance at helium temperatures, is not yet understood.

[2] K. G. McKay, *Phys. Rev.* 84, 829 (1951).

# SOME EVALUATIONS OF A NEW HIGH-INTENSITY ION SOURCE

C. D. Moak J. W. Johnson
R. F. King H. E. Banta

The Duo-Plasmatron, a new ion source developed in Germany by Von Ardenne, has been described recently in a new book on mass spectrography and electron microscopy.[1] Some rather interesting features of this source prompted us to evaluate its characteristics in a high-voltage accelerator arrangement. The features are as follows:

1. A magnetic mirror with a very high mirror ratio is used to reflux the discharge electrons many times through a constricted region focused on the extraction aperture.
2. The plasma is concentrated over an aperture in the region just above the magnetic mirror.
3. The most intense part of the plasma is allowed to protrude through a very small aperture into the accelerator itself. In this way, space-charge spreading in the aperture is entirely avoided.
4. Just inside the accelerator tube, extremely strong fields in a high-perveance Pierce-gun structure are used to hold the beam together and accelerate the particles away from the plasma boundary.

A perspective drawing of the Duo-Plasmatron source is shown in Fig. 1. The gap of the magnetic-mirror field is located just above the small exit aperture at the bottom. The upper pole piece runs at approximately 30 v with respect to cathode. The lower end of the source containing the aperture runs at approximately 150 v with respect to cathode. Filament temperature is adjusted for arc currents of 1 to 5 amp. The magnet coil consists of 1840 turns of No. 24 enameled wire. Typical operating current is 0.8 amp. The aperture insert is made of tungsten so as to withstand the high temperature due to bombardment of the tip by the intense arc which centers over the aperture.

The Duo-Plasmatron and its power supplies are isolated at the terminal potential of a small 0- to 50-kv accelerator. Just under the source at very close spacing (4 mm) is the grounded extractor-accelerator electrode. Below the extractor is an electrostatic Einzel lens-focusing assembly followed by a magnetic mass analyzer and a biased, water-cooled, Faraday cage collector cup.

The initial operation of the source was tried with an aperture diameter of 0.032 in., somewhat smaller than the 0.039-in. (1 mm) apertures used by Von Ardenne. The source operation appeared quite normal, but the ion output was so great that the accelerator power supply was held down to very small voltages by the large beam current. A 0.025-in. aperture, then a 0.015-in., and finally a 0.005-in. aperture were tried before a beam of controllable size was achieved. With the 0.005-in. aperture, beam currents of 2 to 3 ma were accelerated, focused, and analyzed. Thus on a small scale we were able to verify the results that von Ardenne found by using 1-mm apertures. According to von Ardenne, up to 0.3 amp of protons can be accelerated from a 1-mm aperture at arc currents of 1 to 2 amp,

UNCLASSIFIED
ORNL-LR-DWG 27493

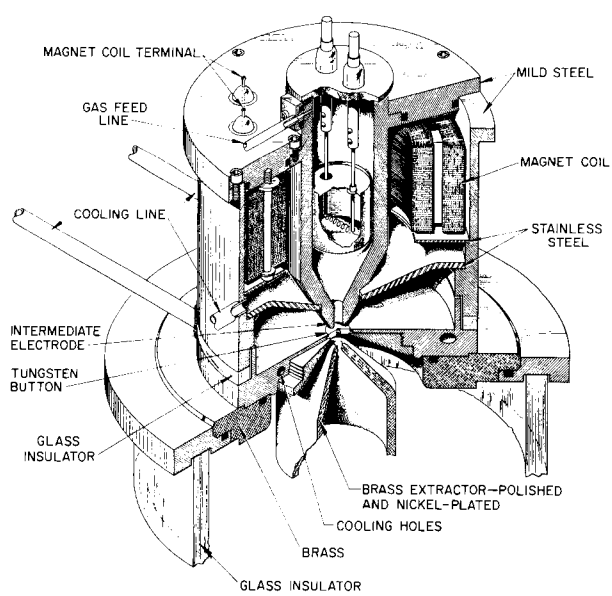


**Fig. 1. Duo-Plasmatron Ion Source.**

[1] M. von Ardenne, *Tabellen der Elektronenphysik, Ionenphysik und Übermikroskopie*, Deutscher Verlag der Wissenschaften, Berlin, 1956.

and, under pulsed operation at arc currents up to 8 amp, 1 amp of protons can be achieved in such an arrangement. Compared with the best conventional ion sources, the performance would appear as follows:

| | |
|---|---|
| Gas consumption | Gas efficiency of the Duo-Plasmatron is nearly 100% |
| Ion energy spread | 5 to 8 ev, comparable to other modern sources |
| Usable life | ~100 hr for each filament; filament life is short because of sputtering in the discharge; the Duo-Plasmatron would compare unfavorably with some nonfilamentary types of source, depending upon the application |
| Maximum beam current density | 125 amp/cm$^2$; the highest current densities achieved by any other sources known to the authors is 2 amp/cm$^2$; it is here that the Duo-Plasmatron excels the conventional types |

From the above tabulation it can be seen that the real advance in this field shows up best when beam current densities are compared for various sources. As is well known in optics, the brightness of the source cannot be exceeded at any image, regardless of the efficiency of the optical system placed in between (assuming equal initial and final indices of refraction). An analogous situation holds in the field of accelerator optics. It can be seen that when an ion source is developed which is some 50 times brighter than previously existing sources, re-evaluations of existing limitations in accelerator work are in order. The pulsed-beam Van de Graaff machine for neutron time-of-flight work is a typical case in point. Other cases in other fields have been pointed out by von Ardenne himself.

A new pulser arrangement is being built around the Duo-Plasmatron ion source for the ORNL 3-Mv Van de Graaff accelerator. The new source and pulser are designed to deliver a peak current of 10 ma with a gas consumption of only 4 atm cc/hr. With a 1% duty cycle, this would correspond to an average target current of 100 $\mu$a. It is hoped that faster pulsing will bring the duty cycle to 0.1%, giving a tenfold decrease in pulse duration and an average target current of 10 $\mu$a. At a 1-Mc/sec repetition rate this would correspond to pulses of proton current 1 m$\mu$sec in duration and having a peak value of 10 ma. The average current of 10 $\mu$a would be a fivefold increase over present currents, and part of this intensity increase could be used to extend the flight paths for further resolution improvements. It appears that, if the brighter source can be reliably run in a Van de Graaff terminal, a considerable improvement can be made in the performance of the neutron time-of-flight pulsing apparatus.

## CHARGE SPECTROMETRY

A. H. Snell F. Pleasonton

Several major revisions have been made in the apparatus used in obtaining the previously reported charge spectra of various radioactive isotopes of the rare gases A, Kr, and Xe. As a result of these changes the following improvements are noted:

1. We now have a wider latitude in the choice of gases to examine. All materials used in assembling the "howitzer" (which collects and focuses the ions into the beam for magnetic analysis) and its vacuum housing, or "source volume," may now be heated to at least 100°C, thus reducing the unrefrigerated base pressure from $10^{-5}$ to $1.5 \times 10^{-6}$ mm Hg. Many gases that would condense on a cold trap are, therefore, no longer excluded as possible source materials.

2. Ions with low $e/m$ values may now be collected more efficiently. This has been achieved by installing new coils on the magnet, together with an appropriate power supply for them. The previous limitation of about 2250 gauss in field strength has now been raised by a factor of 3, allowing an increase in efficiency of collecting the ions of low $e/m$ by a factor of about 9, which is particularly beneficial in studying spectra where the ions of low charge are of relatively weak intensity.

3. The resolution of the spectrometer is now 1.9% instead of 2.6%, as measured by peak width at half-maximum intensity. This is a consequence of changing the entrance aperture from a ½-in.-dia hole to a slot about ¼ in. wide by ½ in. high, and tailoring the exit aperture to match the shape of the image as observed on film exposed in the magnet's focal plane.

4. Both positive and negative ions may be detected. Provisions now exist for accelerating ions of either charge, after analysis, to energies suitable for detection with a secondary electron multiplier. They also permit varying of the accelerating potentials inversely as the charge of the ions in order to eliminate possible differences in focusing the ions onto the first dynode of the multiplier. A re-examination of the $Xe^{133}$-$Cs^{133}$ charge spectrum seems to indicate that this introduces modifications of a few per cent, particularly in the measured intensities of ions of low charge.

## PUBLICATIONS


Barnett, C. F., and H. K. Reynolds, "Charge Exchange Cross Sections of Hydrogen Particles in Gases at High Energies," *Phys. Rev.* **109**, 355 (1958).

Barnett, C. F., and P. M. Stier, "Charge Exchange Cross Sections for Helium Ions in Gases," *Phys. Rev.* **109**, 385 (1958).

Beard, D. B., and M. E. Rose, "Circular Polarization Detection of Gamma Rays," *Phys. Rev.* **108**, 164 (1957).

Fowler, J. L., and H. O. Cohn, "Oxygen Differential Neutron Scattering and Phenomenological Nuclear Potentials," *Phys. Rev.* **109**, 89 (1958).

Good, W. M., J. H. Neiler, and J. H. Gibbons, "Neutron Total Cross Sections in the kev Region by Fast Time-of-Flight Measurements," *Phys. Rev.* **109**, 926 (1958).

Green, A. E. S., and A. H. Snell, "An Internal Conversion Coefficient for the Outermost Electron Shell in Xenon," *Proc. Roy. Soc. London* **242A**, 400–402 (1957).

Harris, C. C., P. R. Bell, and J. E. Francis, "An Aural Count Rate Indicator," *Nucleonics* **15**(9), 152–54 (1957).

Harvey, J. A., and D. J. Hughes, "Spacings of Nuclear Energy Levels," *Phys. Rev.* **109**, 471 (1958).

Johnson, C. H., J. P. Judish, and C. W. Snyder, "Focusing Procedures for Electrostatic Accelerators," *Rev. Sci. Instr.* **28**, 942 (1957).

Macklin, R. L., "Graphite Sphere Neutron Detector," *Nuclear Instr.* **1**, 335–39 (1957).

Macklin, R. L., and J. H. Gibbons, "A Study of the $T(p,n)He^3$ and $Li^7(p,n)Be^7$ Reactions," *Phys. Rev.* **109**, 105 (1958).

McGowan, F. K., and P. H. Stelson, "Internal Conversion Coefficients for Pure E2 and Mixed E2+M1 Transitions," *Phys. Rev.* **107**, 1674–80 (1957).

McGowan, F. K., and P. H. Stelson, "Yields, Angular Distributions and Polarization of Gamma Rays from Coulomb Excitation," *Phys. Rev.* **109**, 901 (1958).

McNally, J. R., Jr., "On the Purity of Mercury-198 Produced by Neutron Irradiation of Gold-197," *J. Opt. Soc. Am.* **47**, 1032 (1957).

McNally, J. R., Jr., and M. R. Skidmore, "Doppler Slant Lines Observed in an Axial Discharge in a Magnetic Field," *J. Opt. Soc. Am.* **47**, 863 (1957).

Morgan, H. W., P. A. Staats, and J. H. Goldstein, "Infrared Spectra of $N^{15}H_3$ and $N^{15}H_4^+$," *J. Chem. Phys.* **27**, 1212 (1957).

Morgan, H. W., P. A. Staats, and J. H. Goldstein, "Infrared Spectrum of $NT_4Cl$," *J. Chem. Phys.* **27**, 1212 (1957).

Newson, H. W., R. M. Williamson, K. W. Jones, J. H. Gibbons, and H. Marshak, "$Li^7(p,n)$, $(p,p'\gamma)$ and $(p,\gamma)$ Reactions Near Neutron Threshold," *Phys. Rev.* **108**, 1294 (1957).

Rose, M. E., "The Statistical Tensors for Oriented Nuclei," *Phys. Rev.* **108**, 362 (1957).

Snell, A. H., F. Pleasonton, and H. E. Leming, "Molecular Dissociation Following Radioactive Decay: Tritium Hydride," *J. Inorg. & Nuclear Chem.* **5**, 112 (1957).

Stolovy, A., and J. A. Harvey, "Radiation Widths of Levels in Nuclei Near Closed Shells," *Phys. Rev.* **108**, 353 (1957).

Wills, J. E., Jr., J. K. Bair, H. O. Cohn, and H. B. Willard, "Scattering of Fast Neutrons from $C^{12}$ and $F^{19}$," *Phys. Rev.* **109**, 891 (1958).

Worsham, J. E., Jr., M. K. Wilkinson, and C. G. Shull, "Neutron-Diffraction Observations on the Palladium-Hydrogen and Palladium-Deuterium Systems," *J. Phys. and Chem. Solids* **3**, 303 (1957).

## PAPERS PRESENTED AT SCIENTIFIC AND TECHNICAL MEETINGS

*Reactor Physics Conference, Phillips Petroleum Co., Sun Valley, Idaho, September 23–26, 1957*

R. L. Macklin, "Capture Cross Sections Near 25 kev."

*Molecular Beam Conference, Brookhaven National Laboratory, November 1–2, 1957*

J. E. Sherwood, "Spin of Iodine-128."

*Pittsburgh Diffraction Conference, Pittsburgh, Pennsylvania, November 6–8, 1957*

W. C. Koehler, E. O. Wollan, M. K. Wilkinson, and H. R. Child, "Antiferromagnetic Structure and Related Magnetic Field Studies of $MnBr_2$."

M. K. Wilkinson, J. W. Cable, E. O. Wollan, and W. C. Koehler, "Investigations of the Two Antiferromagnetic Structures of $MnCl_2$."

*International Conference of European Atomic Energy Society – Colloquium on Exponential and Critical Experiments, Mol, Belgium, November 5, 1957*

E. C. Campbell and P. H. Stelson, "Study of Diffusing and Multiplying Media with a Pulsed Neutron Source."

*American Physical Society Meeting, St. Louis, Missouri, November 29–30, 1957*

J. E. Sherwood, "Nuclear Spin of $I^{128}$."

*American Physical Society Meeting, Stanford, California, December 19–21, 1957*

M. E. Rose, "Finite Size Effects in Internal Conversion."

*Annual Meeting of the American Association for the Advancement of Science, Indianapolis, Indiana, December 27–28, 1957*

J. R. McNally, Jr. (invited paper), "The Role of Spectroscopy in Thermonuclear Research."

*Scintillation Counter Symposium, Washington, D.C., January 27–31, 1958*

N. H. Lazar, "Analysis of Gamma Ray Scintillation Spectra for Quantitative Photon Intensities."

*American Physical Society Meeting, New York, New York, January 29–February 1, 1958*

W. C. Koehler (invited paper), "Single Crystal Neutron Diffraction Studies of Antiferromagnetism at Low Temperatures with Applied Magnetic Field."

P. H. Stelson (invited paper), "Level Positions and Transition Rates from Coulomb Excitation."

M. K. Wilkinson (invited paper), "Antiferromagnetic Structures and Related Domain Properties as Studied by Neutron Diffraction Techniques at Low Temperatures."

E. L. Church, M. E. Rose, and J. Weneser, "Electric-Monopole Directional-Correlational Experiments."

H. O. Cohn and J. L. Fowler, "Resonances in the Total Neutron Cross Section of Neon."

J. W. T. Dabbs, L. D. Roberts, and G. W. Parker, "Fission of Oriented Nuclei and the Bohr Model."

M. M. Gordon and T. A. Welton, "The 8/4 Resonance and Beam Extraction from the AVF Cyclotron."

N. H. Lazar and W. S. Lyon, "Experimental *L*-Shell Fluorescence Yields."

R. L. Macklin and J. H. Gibbons, "$(p,n)$ Reactions in Light Nuclei: I and II."

G. W. Parker, L. D. Roberts, and J. W. T. Dabbs, "Anisotropy of $\alpha$-Particle Emission from Oriented $U^{235}$ Nuclei."

F. Pleasonton and A. H. Snell, "Molecular Dissociation Following Beta Decay in $CH_3T$."

L. D. Roberts, J. W. T. Dabbs, and G. W. Parker, "Anisotropy of Fission Fragments from Oriented $U^{233}$ Nuclei."

H. W. Schmitt, "Cross Section for the $S^{32}(n,\alpha)Si^{29}$ Reaction as a Function of Energy."

A. H. Snell and F. Pleasonton, "Charge Spectrometry for $Xe^{133}$."

T. A. Welton, "Relativistic Quantum Mechanics with a Momentum Cut-Off."

T. A. Welton, "Resonant Inflection in Alternating Gradient Synchrotrons."

H. B. Willard, J. K. Bair, and H. O. Cohn, "Total Neutron Cross Sections of $C^{12}$ and $C^{13}$."

---

## ANNOUNCEMENTS

Additions to the Physics Division staff during this period were as follows: D. G. Maeder, from the Physikalisches Institute in Zurich, Switzerland, is on temporary appointment, working with the Scintillation Spectrometry and Instrument Development Group. C. N. Inskeep transferred from the Instrument Department to the Physics Division's High Voltage Group. S. H. Hanauer, of the Instrumentation and Controls Division, is on loan to the Physics Division, where he is conducting research for his Ph.D. thesis with the Low-Temperature Group.

Transfers and Terminations: The following members of the Spectroscopy Group transferred to the Analytical Chemistry Division during this period: Z. Combs, H. W. Dunn, J. J. Mundzak, and J. A. Norris. Members of the Scintillation Spectrometry and Instrument Development Group who transferred to the Thermonuclear Experimental Division included R. C. Davis, O. Eason, J. E. Francis, R. R. Hall, D. P. Hamblen, C. C. Harris, and G. G. Kelley. J. Schenck terminated his employment with the Laboratory during this period. He was formerly with the Scintillation Spectrometry and Instrument Development Group.

*INTERNAL DISTRIBUTION*

1. C. E. Center
2. Biology Library
3. Health Physics Library
4-6. Central Research Library
7. Reactor Experimental Engineering Library
8-19. Laboratory Records Department
20. Laboratory Records, ORNL R.C.
21. A. M. Weinberg
22. L. B. Emlet (K-25)
23. J. P. Murray (Y-12)
24. J. A. Swartout
25. E. H. Taylor
26. E. D. Shipley
27. J. L. Fowler
28. M. L. Nelson
29. A. H. Snell
30. A. Hollaender
31. K. Z. Morgan
32. F. L. Culler
33. M. T. Kelley
34. D. Phillips
35. E. O. Wollan
36. D. W. Cardwell
37. A. S. Householder
38. L. D. Roberts
39. R. B. Briggs
40. R. N. Lyon
41. W. C. Koehler
42. E. P. Blizard
43. M. E. Rose
44. G. E. Boyd
45. W. H. Sullivan
46. R. W. Stoughton
47. C. E. Winters
48. W. H. Jordan
49. E. C. Campbell
50. D. S. Billington
51. M. A. Bredig
52. R. S. Livingston
53. C. P. Keim
54. F. C. Maienschein
55. C. E. Clifford
56. R. C. Block
57. C. D. Susano
58. C. J. Borkowski
59. M. J. Skinner
60. M. K. Wilkinson
61. J. W. Cable
62. P. M. Reyling
63. G. deSaussure
64. W. M. Good
65. G. C. Williams
66. F. K. McGowan
67. R. W. Johnson
68. J. R. McNally, Jr.
69. J. L. Gabbard
70. R. A. Charpie
71. G. G. Slaughter
72. Eugene Guth
73. R. W. Peelle
74. P. R. Bell
75. G. G. Kelley
76. C. C. Harris
77. H. G. MacPherson
78. P. H. Stelson
79. J. E. Sherwood
80. W. Zobel
81. R. B. Murray
82. H. B. Willard
83. J. Schenck
84. J. H. Neiler
85. J. A. Harvey
86. C. F. Barnett
87. N. H. Lazar
88. R. R. Dickison
89. A. Simon
90. J. H. Gibbons
91. J. J. Pinajian
92. S. Bernstein
93. F. Pleasonton
94. C. A. Preskitt
95. E. P. Wigner (consultant)
96. H. A. Bethe (consultant)
97. E. Creutz (consultant)
98. L. P. Smith (consultant)
99. R. L. Thornton (consultant)
100. R. F. Christy (consultant)
101. M. Goldhaber (consultant)
102. T. Lauritsen (consultant)
103. J. A. Wheeler (consultant)
104. N. F. Ramsey (consultant)
105. W. R. Brode (consultant)
106. ORNL – Y-12 Technical Library, Document Reference Section

## *EXTERNAL DISTRIBUTION*

107-191. Given external distribution

192-795. Given distribution as shown in TID-4500 (13th ed. rev.) under Physics and Mathematics category (75 copies – OTS)